D5.6 24 Month Progress Report

GA number: 815058
Project acronym: FLIPASED
Project title: FLIGHT PHASE ADAPTIVE AERO-SERVOELASTIC AIRCRAFT DESIGN METHODS

Funding Scheme: H2020 **ID:** MG-3-1-2018
Latest version of Annex I: 1.1 released on 12/04/2019
Start date of project: 01/09/2019 **Duration:** 40 Months

Lead Beneficiary for this deliverable:	SZTAKI
Author(s): Bálint Vanek, Virág Bodor, Thiemo Kier, Charles Poussot-Vassal, Christian Rössler	
Last modified: 11/11/2021	**Status:** Delivered
Due date: 30/09/2021	

Project coordinator name and organisation: Bálint Vanek, SZTAKI
Tel. and email: +36 1 279 6113 vanek@sztaki.hu
Project website: flipased.eu

Dissemination Level:		
CO	Confidential, only for members of the consortium (including the Commission Services)	
PU	Public	X

"This document is part of a project that has received funding from the European Union's Horizon 2020 research and innovation programme under grant agreement No 815058."

Glossary

BP	Back-up Pilot
CG	Centre of Gravity
DLR-SR	Institute of System Dynamics and Control (SR), DLR
ECU	Engine Control Unit
EDL	Engineering Data Link
EDMO	Special Airport Oberpfaffenhofen
FBG	Fibre Bragg Grating sensor
FLEXOP	Flutter Free Flight Envelope Expansion for Economical Performance Improvement
FM	Flight Manual
FTC	Flight Test Card
FTE	Flight Test Engineer
FTM	Flight Test Manager
FTO	Flight Test Operator
GCS	Ground Control Station
GPS	Global Positioning System
LiPo	Lithium polymer battery
MAV Link	Micro Air Vehicle Link
ONERA	Office National d'Etudes et de Recherches Aérospatiales (The French Aerospace Lab)
PIC	Pilot-in-Command
RWY	Runway
SZTAKI	Institute for Computer Science and Control
TOW	Take-off Weight
TUD	Technical Univerity of Delft
TUM	Technical University of Munich
UAV	Unmanned aerial vehicle
ASE	Aero-servo-elasticity
GLA	Gust Load Alleviation
MLA	Maneuver Load Alleviation

Table of Contents

1 Summary for Publication

1.1 Summary of the context and overall objectives of the project

Flight Phase Adaptive Aero-Servo-Elastic Aircraft Design Methods (FliPASED) opens a complete new dimension for the integrated aircraft design. Coupling between aeroelasticity, gust response, flight control methods, instrumentation and certification aspects is not exploited in current aircraft design. A common set of models, coupled with joint requirements enable a multidisciplinary-optimized design for the entire aircraft, leading to more optimized overall performance. The concept of exploiting coupling between disciplines will take advantage of tools developed by the partners in former projects.

The main objectives of the project aim at tightly coupled multi-objective optimization of advanced, active controlled wing designs through the integration of a collaborative design tool chain. More than 10% fuel efficiency improvement, and 20% reduction in peak amplitude of the gust response, as well as a 50% reduction of number of distinct models used during the development and certification process are set as project goals. Through the integration of all discipline tools from aerodynamics, structural design, aeroelastic simulation and control design in one integrated tool chain an active, condition optimized wing design becomes feasible, enabling enhanced performance at lower weight and cost. The project will raise the efficiency of a currently separately existing development toolchains, by advanced multidisciplinary and collaborative capabilities for whole aircraft along its life cycle. It will develop methods and tools for very accurate flexible-mode modelling and flexible aircraft control synthesis, in the context of reliable implementation of the avionics system, taking into consideration the fault detection and reconfiguration. The accuracy of developed tools and methods will be validated on a safe and affordable experimental platform, and results will be shared along with design requirements and standardized interfaces in an open source approach.

1.2 Work performed from the beginning of the project to the end of the period covered by the report and main results achieved so far

Work has been performed in three technical and one management work packages, while minor preparatory work was also done on the non-active work package (WP4) about scale-up. These work items were the following:

- Setup of requirements incl. open data process,
- Definition of collaborative work process including interfaces between disciplines & selection of collaborative work tools
- Reference model definition
- Enhancement and maturation of (single discipline) tools towards robustness
- Demonstrator overall and component level improvements

- Setup of integrated tool framework (inc. design of control functions)
- Model refinement using GVT data & flight tests
- Setup of a collaborative (remote) workflow for many sub-problems

WP1

The demonstrator MDO workflow with interfaces and requirements were set-up.

The wing and demonstrator actuation and sensing concept was reviewed to account for the increased need of sensing and larger number of actuators coupled with the main objectives of demonstration.

Also, the requirements were reviewed to show clear benefits for a/c MDO design, where different advanced functions must work together in the design phase and their improvement potential has to be quantified.

WP2

The demonstrator MDO workflow with interfaces and requirements were adopted and the individual tools were given a common RCE/CPACS interface.

Building and intergrating methods/tools was successfully consolidated.

- Overall model setup
  - Parametric CAD model
  - Finite element model
  - Model condensation
- Model step
  - LTI (reduced) model construction
  - LPV (reduced) model construction
- Control design
  - Flight controller
  - Load controllers (MLA and GLA)
  - Flutter controller
- Analysis
  - LTI Performance evaluation

WP3

The demonstrator is instrumented and prepared for flight testing.

1. **Sensor concept refined**
   - Sensing concept for new wings
   - V-tail IMUs
   - Aeroprobe and IMU repositioning
   - Thrust measurement
2. Demonstrator wing design: -3 planing and back up Plan
3. Demonstrator component upgrades:
   - On board computer 2
   - Open MCT (Flutterometer)
   - Antenna Upgrade
   - Landing gear improvements and testing

- Power wiring

4. Flight test specification and system identification
5. Flight testing
    - Extensive ground taxi campaign for low speed handling improvement
    - Alternative location at Cochstedt and the respective EASA SORA application process prepared

WP4

The scale-up workflow and performance objectives are formally defined, and the baseline model (D150) have been investigated. Preparatory work started to share the model with partners responsible for different disciplines.

WP5

The demonstrator MDO workflow with interfaces and requirements were set-up.

Setup of the project management and collaborative environment for the project is complete. Publicatios and exploitation is tracked and managed within the consortium.

The consortium established collaborative tools for project management (Nextcloud + Agantty), software development (Git), document editing (Overleaf). Moreover, the collaborative work process also involves common hardware development tools - a common hardware-in-the-loop platform. The partner contributions within the common MDO toolchain are all implemented and tested using the RCE environment.

1.3 Progress beyond the state of the art and expected potential impact (including the socio-economic impact and the wider societal implications of the project so far)

The collaborative design framework with low-medium fidelity aerodynamics including drag estimate and control design related aspects is significantly beyond state of art. There are several difficulties with respect to integrating modelling (with different number of flaps) and control synthesis into an automated workflow, what was sucesfully tackled by the consortium.

The demonstrator development also includes several instrumentation and avionics related components what are unique in such small scale demonstrators (thrust measurement system, telemetry and onboard computing capabilities). The common software and hardware development approach, using shared models and simulation environment is also unique and provides significant advantage against other organizations. The operational modal analysis method, what was only available in extensively instrumented commercial aircraft test programmes is also implemented in embedded onboard FCC.

Model reduction, control design, worst-case analysis and fault detection methods are also published in premier journals and conferences in the field, hence they are highly advanced and provide a potential for industry partners to gain socio-economic impact.

2 Explanation of the work carried out by the beneficiaries and Overview of the progress (Technical Report 1)

Objectives

Current efficiency and performance improvement measures are mainly single discipline driven in aviation (e.g. fuselage stretches, new engines, wing tip devices). Secondary effects are rather rarely explored, in order to reduce risks of higher interdependencies of detrimental effects (e.g. large winglets leading to increased loads in the outer wings, making the aircraft more roll sensitive to crosswind (especially during take-off and landing), leading to a possible reduction of the critical flutter speed. The main objectives of the project aim at developing multi-objective optimization of advanced, active controlled wing designs through a collaborative design tool chain complemented by an open data approach. Publicly sharing important and actual (flight) test data and project results will facilitate the adoption of standardized methods, tools and interfaces. Since Universities, Academic Institutes, and SMEs lack the knowledge of global picture about a complex Multidisciplinary Project, like the overall design of a commercial transport aircraft, their access to specific data and measurements seriously limits their global impact on the aircraft design research and development trends. Active, flight condition optimized wing design becomes feasible through the integration of tools into an integrated tool chain from disciplines of aerodynamics, structural design, aeroelastic simulation and control design. This enables enhanced performance at lower weight and thus cost, which provides benefits for short, medium and long term as incremental improvement over existing designs:

- design stage: reduced design life-cycle with better understanding of model based multidisciplinary aspects and the associated certification aspects via standardization of models and interfaces, by building-up and validating a tightly-coupled (aero-structure-flight control) design tool chain (based on previous public funded projects, e.g. LuFo ViTAM) → *addressed by developing a common tool interface structure via CPACS and executed by RCE*
- short term: improved gust response, lower loads, lower control effort, improved passenger comfort, active load control being a key element for the ultimate goal of a 1g wing design (reduced margins, reduced safety factors leading to minimum wing weight) → *active load reduction control laws (and their methodology) are developed and their simulations are already performed to initially assess their benefits*
- medium term: fuel efficiency improvement by wing shape optimization at different phases of flight, taking into account different wing configuration, fuel mass and height/dynamic pressure, hence departing from the static approach of being optimal for one single flight configuration → *drag reduction control laws need models of the x directional forces acting on the wing and fuselage, what is under study and development within the project*
- long term: active control of wing reduces fatigue loads, hence the structure sizing can be less conservative, since impact on the structure can be kept under strict control

with advanced finite element models and novel sensors, which are monitored and processed by model based and data-driven methods → *operational modal analysis methods, constantly monitoring the structural (servoelastic) properties of the wing are under implementation within the flight control computer of the demonstrator*

The European Commission through its Strategic Research and Innovation Agendas has formulated a high number of requirements for the next generation of aircrafts. For example, 1.5% annual fuel efficiency improvement, or flights arriving within 1 minute of the planned arrival time regardless of weather conditions (which necessitates the ability to better route the aircraft, in addition to be more gust and turbulence resistant, tackled by one of the targets of the FLiPASED project to demonstrate 20% reduction in peak amplitude of gust response compared to the reference aircraft), as well as "progress from the current patchwork approach, with local virtual testing and certification, to a federated approach" which is closely coupled with another target of the proposal, to show a 50% reduction of number of distinct models used during the development and certification process. In order to meet all these expectations, the aircraft components (airframe structures, aerodynamics, propulsion, avionics, control) have to be optimized to suit various design objectives and have to be integrated into a reliable, consistent system, where every component works in tight coupling with the others. These new design goals make it necessary to revise the existing design workflow, invent new design methods and methodologies and advance the design process. Since multidisciplinary methods are opening up previously unviable design alternatives, certification approaches have to be adapted, what can be catalysed only by projects capable of demonstrating the safety, maturity and performance of new approaches in a way proposed by FLiPASED.

1. Currently, the aircraft components (airframe, avionics, and control) are designed almost separately by different expert teams working only in loose cooperation. While first steps of a stronger integration between aerodynamics and structural design have been already taken, the required high level of optimality can only be achieved through tight cooperation. Therefore, efficient design chains have to be developed, which provide continuous flow of relevant information among the partners and enable fast design iteration cycles that converge to required aircraft architecture. To improve the cooperation of the design teams it is necessary to:

- clarify the requirements and underlying rules of cooperative design principles → *a common ASE requirement set and performance objectives are formulated for the MDO process by all expert teams*
- formulate the relevant information (e.g. specification of data and communication structures) relevant to the involved partners → *a common data standard for information exchange is adopted within the consortium*
- automate the information generation process in order to speed up the communication between the partners. (Parametric model generation, automated controller construction, fast analysis tools, data analytics, etc.) → *the information flow automation is in good progress, but still not fully assembled due to IT restrictions at partners.*

2. The present aircraft design methods do not exploit the coupling between aeroelasticity, gust response, flight control methods, instrumentation and certification. The required

performance improvement cannot be reached without taking into consideration and/or exploiting these interactions. New methods, algorithms have to be developed that are able to consider these coupling in the design process. (Flexible modelling, wing shape control, sensor data feedback, safety critical operation) → *several new tools have been developed and enhanced to study the aero-servo-elastic interactions of different building blocks (including wing shape optimization for drag, drag modelling, model order reduction for design, parametric model generation).*

3. The latest results of scientific research on the field of control, information processing and system modelling can be applied to further improve the design procedure: big data analysis, data-driven control, sensor and actuator selection methods, model reduction and collaborative framework elements. → *The early results of the project are already published in premier conferences and journals in the aeronautics field, and big data analysis methods are already in research stage in collaboration with machine learning and big data experts.*

The goal of this project is to develop an advanced design toolchain and novel methods for constructing a demonstrator aircraft that satisfies the key requirements defined for the future aerial vehicles. The simulation based virtual design and assessment of a highly coupled, actively controlled aero-structure will be complemented with extensive test data generated with the flexible wing demonstrator aircraft established in the EU FLEXOP project. Providing extensive ground and flight testing data will support the tool chain validation as well as providing the international research community real life test cases to check and improve their models and methods.

The following 3 main research objectives are proposed:

1. Raise the efficiency of a currently separately existing **wing design, flight controls and avionics development toolchains** by advanced multidisciplinary and collaborative capabilities for overall aircraft designs along their life cycle [28]. According to preliminary flight test result by NASA, optimization algorithms and actively shaping the wing found trim configurations that required approximately 3 percent less fuel flow than utilizing baseline trim conditions at the same flight condition (*Peak-Seeking Optimization of Trim for Reduced Fuel Consumption: Architecture and Performance Predictions: J. Schaefer and N.A. Brown*), if using advanced flight control augmentation. Key component to this goal is to treat all flight control surfaces uniformly with the consequence of certification aspects still utilizing the multi-functional capabilities to actively control a wide range of conditions of the aircraft. → *Preliminary results of FLiPASED show 17% induced drag reduction at off-nominal flight conditions for the demonstrator with using 16 flaps per wing.*
2. Develop methods and tools for very accurate **flexible-mode modelling** and **flexible aircraft control** synthesis, in the context of **reliable** implementation of the **avionics** system, taking into consideration the fault detection, isolation and reconfiguration mechanism in failure cases. It is expected that better sensing and advanced control methods can lead to 15% reduction in peak amplitude of the gust response (*Introduction to Aircraft Aeroelasticity and Loads: J.R. Wright, J.E. Cooper*). Special emphasis will be made on recommending standardized methods and tools across design and certification teams to significantly reduce the number of different mathematical models (50% reduction is sought) leading to more efficient engineering and management effort via better capturing the synergies between multiple

disciplines. Through intelligent implementation of reduced order models in the design process also massive reaction time reductions of complex simulations and models are expected. → *Modelling is already significantly improved w.r.t. state-of-art low/medium fidelity aeroelastic methods by introducing a standard workflow to include GVT data via tuning beams in the FEM model and also via drag modelling using near field, far field and 3D panel based calculation. The flexible aircraft control methods include GLA, MLA, flutter control at the moment as well as FDI of actuators. All flight control laws are developed with onboard implementation in mind.*

3. **Validate** the accuracy of developed tools and methods on a **safe and affordable experimental platform**, developed in a prior H2020 project (FLEXOP), which will also lead to demonstration of the interdisciplinary development cycle. This will facilitate the **interaction** of structures, flight controls and avionics disciplines. Gust response prediction and mitigation, active wing morphing for fuel consumption reduction and flight envelope assessment in the event of failures will be tested using the existing ground and flight infrastructure of the partners, with a new set of optimised wings and custom sensor and actuator arrangement. It is foreseen that significant cost can be saved by only manufacturing an advanced set of flexible, aeroelastically tailored wings (supported by shape and loads monitoring) and re-using main components from FLEXOP. In combination with the existing wings sets of the FLEXOP project the overall design space of active flexible wing enabled capabilities will be efficiently expanded, providing a broader and more robust insight into the underlying design and control principles, along the lines of ACARE Action area 2.4 (Secure continued and focused investment). The platform, with its rich sensor and actuator set will also generate vast amount of data, which on the one hand will be handled by Big-Data analytics inside the project and on the other hand will be available through the open data approach for the research and industrial community. → *The demonstrator is significantly improved both in terms of safety (ground controllability) and instrumentation (onboard sensing and data processing). Preliminary flight envelope analysis already discovered the most promising configurations and flight points.*

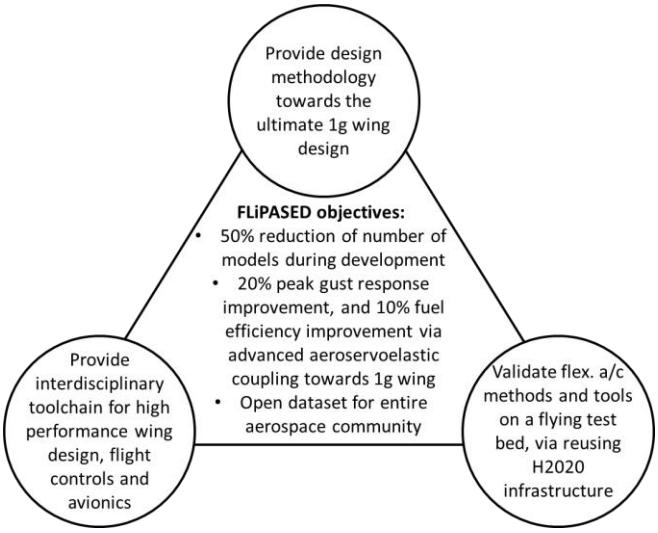

Figure 2.1. Objectives and relation to Work Programme

Flight Phase Adaptive Aero-Servo-Elastic Aircraft Design Methods (FliPASED) thus opens a complete new dimension for the integrated **aircraft** design. It is planned to demonstrate the

performance claims in a **scale-up** task. As baseline reference for this scale-up task a *High Fidelity Flexible Aircraft Benchmark* will be defined in coordination with the industrial advisory board and used as the reference during the project. The resulting derivative aircraft will have a more flexible wing, with tailoring modifications in the wing structure designed for lower safety factor, which is enabled by advanced avionics and flight control architecture, leading to better gust response at lower structural weight. Objectives for this derivative are more than **10% fuel efficiency improvement**, and **20% reduction in peak amplitude of the gust response** compared to the reference aircraft, as well as a **50% reduction of number of distinct models used during the development and certification process** using incremental improvements, in comparison with the development of a new aircraft with same performance features. The excellence of the project partners in the aforementioned topics have been demonstrated in several European industrial and research programs, and the scope of the projects is limited to reach its goals within 40 months. The industrial relevance of the project will be further enhanced by a strong industrial advisory group, who will facilitate the exchange of information between the project and key OEMs in aviation industry.

2.1 Explanation of the work carried per WP- Work Package 1

This section explains the work carried out in WP1 during the reporting period giving details of the work carried out by each beneficiary involved. As such, WP1 (Recommendations capture and attainment) focuses on derivation of key requirements for the aircraft categories under investigation as well as the interconnection of design tool and the relevant data acquisition and analytics methods and process.

2.1.1 Objectives and activities

The main objective of this work package is to address the complete integrated avionic process including aircraft shape, sensors and actuator locations and detailed control design. The purpose is to set up an integrated collaborative framework and tool-chain for the design of a new passively and actively controlled flexible wing-based aircraft, in a safer and more reliable context. The purpose of the activity is to end-up with an enhanced and fastened maturation process tool to quickly reach high maturity levels through digital-based methods and tools.

- Detailed design of control functions
- Enhancement and maturation of (single discipline) tools
- Setup of integrated tool framework
- Establish integrated, collaborative design tool chain
- Re-Design of FLEXOP -1 Wing established (Validation)
- Design of new advanced active controlled wing
- Establish redundancy based methods for enhanced safety and reliability

2.1.2 Starting point and approach

The two main starting points for this WP are the existing demonstrator design (inherited from FLEXOP), what has to be accommodated into the improved design toolchain, and the existing tools, standards and available scale-up aircraft models of the partners.

The approach consists of assembling the main specifications and criteria what must be demonstrated during the flight tests of the demonstrator and from these specifications the required hardware and software modifications and improved data processing workflow have to be developed in an incremental fashion.

On the other side, the limitations of the current demonstrator has to be established (like low Mach number, lack of wind tunnel and complex CFD testing). Based on these limitations the scale-up study also has to limit its scope, to be aligned with the tools and methods developed by partners.

Besides the existing tools the partners have to agree also on the common standards and workflow, what is highly facilitated by DLR's experience with MDO tools and the related CPACS data interchange language.

2.1.3 Efforts and achieved results, name involved contractors

The main effort in WP1 was to set-up the tasks and responsibilities for the MDO workflow. This involved breaking down the conceptual design of the demonstrator into design steps and assign a responsible partner within the consortium to each one of them. This involved creating clear performance objectives and agreement on the data sharing format (CPACS). The overall workflow will be executed on a distributed cluster of workstations, scheduled by RCE environment.

Figure 2.2 Demonstrator workflow

Agreement on tools and adoption of them within the collaborative work process (RCE, CPACS, NASTRAN, Matlab, Python, Tixi, Tiegl, Nextcloud, Overleaf, etc.) was natural, but required longer time since IT infrastructure was inaccessible for long time due to the pandemic.

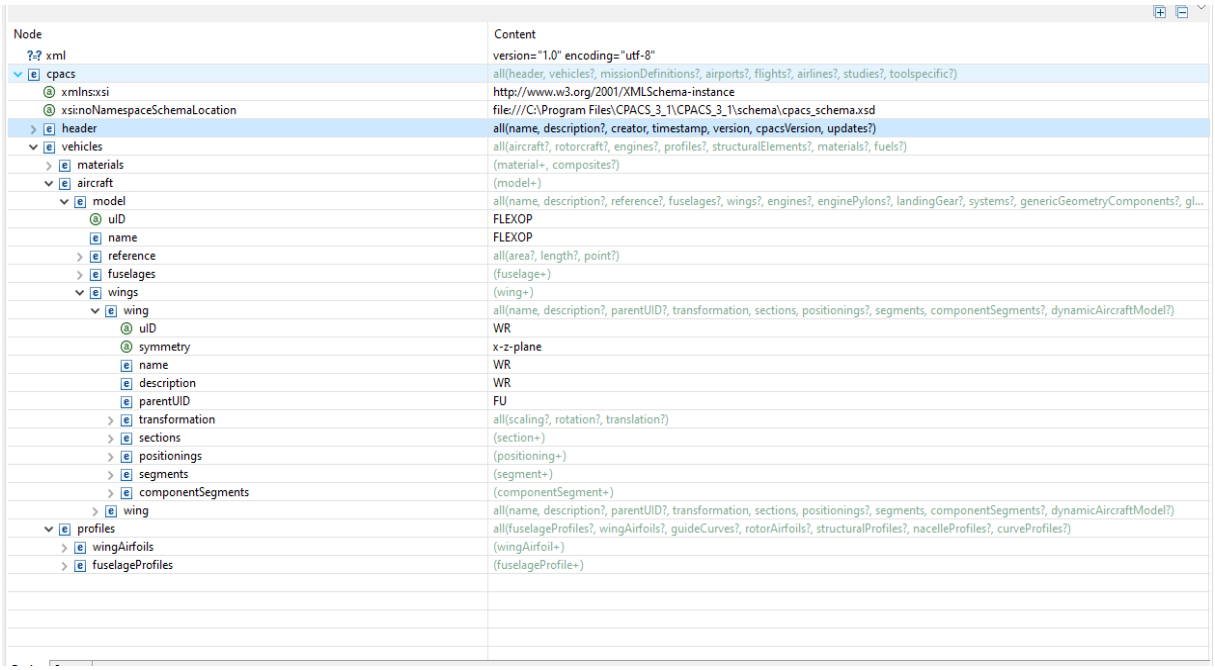

Node	Content
?-? xml	version="1.0" encoding="utf-8"
cpacs	all(header, vehicles?, missionDefinitions?, airports?, flights?, airlines?, studies?, toolspecific?)
xmlns:xsi	http://www.w3.org/2001/XMLSchema-instance
xsi:noNamespaceSchemaLocation	file:///C:\Program Files\CPACS_3_1\CPACS_3_1\schema\cpacs_schema.xsd
header	all(name, description?, creator, timestamp, version, cpacsVersion, updates?)
vehicles	all(aircraft?, rotorcraft?, engines?, profiles?, structuralElements?, materials?, fuels?)
materials	(material+, composites?)
aircraft	(model+)
model	all(name, description?, reference?, fuselages?, wings?, engines?, enginePylons?, landingGear?, systems?, genericGeometryComponents?, gl...
uID	FLEXOP
name	FLEXOP
reference	all(area?, length?, point?)
fuselages	(fuselage+)
wings	(wing+)
wing	all(name, description?, parentUID?, transformation, sections, positionings?, segments, componentSegments?, dynamicAircraftModel?)
uID	WR
symmetry	x-z-plane
name	WR
description	WR
parentUID	FU
transformation	all(scaling?, rotation?, translation?)
sections	(section+)
positionings	(positioning+)
segments	(segment+)
componentSegments	(componentSegment+)
wing	all(name, description?, parentUID?, transformation, sections, positionings?, segments, componentSegments?, dynamicAircraftModel?)
profiles	all(fuselageProfiles?, wingAirfoils?, guideCurves?, rotorAirfoils?, structuralProfiles?, nacelleProfiles?, curveProfiles?)
wingAirfoils	(wingAirfoil+)
fuselageProfiles	(fuselageProfile+)

Figure 2.3 Visual representation of the XML based CPACS file describing the FLiPASED demonstrator

Roles within the workflow are the following:

1. CPACS basic description generation is performed by DLR using Matlab based tools, with visualization aids from Tixi/Tiegl
2. The aero-structural block is handled by TUM with the help of DLR
    a. Aircraft external and internal (structural) geometry is generated with the Phyton based CAD tools made by TUM, leading to parametric description of the wing – with 3 different versions of distinct flap numbers: 4, 8, 16 per wing.
    b. The FEM model is generated automatically in NASTRAN by the tools of DLR-AE
    c. The aero model is based on standard VLM/DLM methods, but the teams of DLR, TUM and SZTAKI are working on increasing the fidelity of induced drag prediction to include its effect in drag reduction control law development
3. Model integration is done in Matlab by DLR-SR based on the standardized components coming from the aero-structural blocks
4. Loads analysis is performed by the tools developed at DLR-AE, which is a mere check in the demonstrator workflow but will be fed back to the FEM/Structural sizing in the scale-up.
5. The various control design related components are assembled in the workflow int one functional block, overseen by ONERA. This block includes several functional sub-components:
    a. Model order reduction (ONERA & SZTAKI)
    b. Baseline controller synthesis (SZTAKI)

c. Maneuver load alleviation (ONERA)
d. Gust load alleviation (DLR-SR)
e. Flutter control (SZTAKi & DLR)
f. Drag reduction control (SZTAKI)
g. Stability and HQ assessment (SZTAKI)

6. The overall aeros-servo-elastic system is analysed and performance is calculated in the Mission Analysis block, led by DLR-SR.

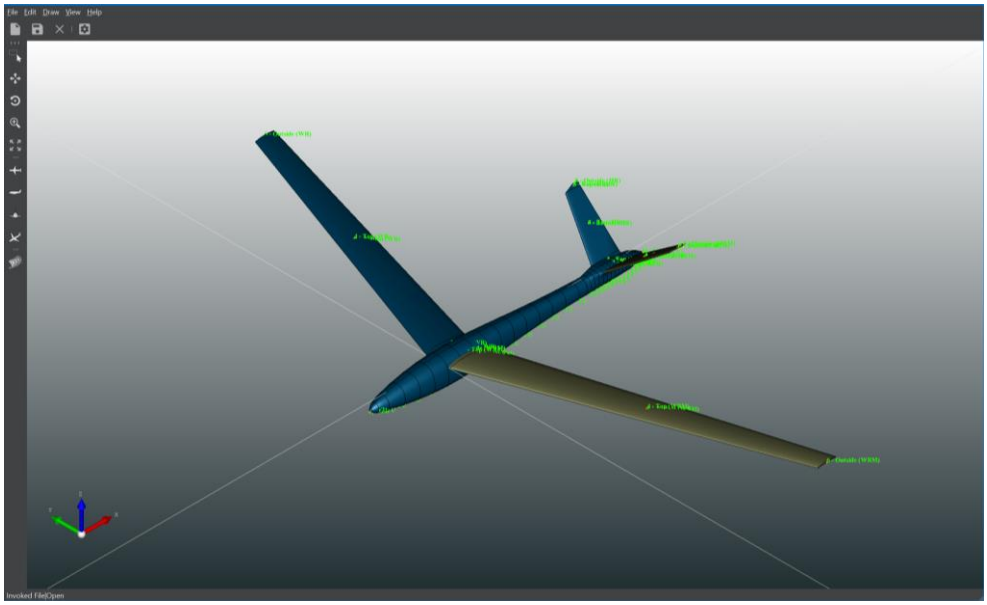

Figure 2.4 Screenshot of FLiPASED CPACS File with TiGL Vizualization library

An objective function was also carefully selected for the demonstrator workflow to provide focus for the optimization – we aim to maximize the weighted sum of open-loop vs. closed-loop difference in drag, flutter speed, maneuver load, and gust load. This would provide the benefit of being able to demonstrate the highest contrast between open-loop performance vs. closed-loop performance. A wing/demonstrator designed in this way would be flown with control laws switched off and the performance recorded, then the control laws would be turned on one by one and the increase in performance would be assessed.

Figure 2.5 Optimization cost function and design parameters

Within the reporting period a number of changes have been proposed to improve the conceptual design of sensor layout and actuation system of the wing (3), and the improvements made and proposed on the fuselage based on operational experience.

During integration and operation of the aircraft the operation team found a couple of design related problems which either made the operation unsafe like the landing gear, or give too harsh boundary for critical function implementation like the lack of digital remote control interface on the RX-MUX units. Along with that, some additional changes were already

made to improve the existing functionality like secondary on board computer, and further changes are proposed to have even increased functionality like electrical power measurement or High bandwidth telemetry system. The deliverable D1.1 introduce these changes in more depth.

The wing (3) sensor layout and actuation system has been also revides and a number of improvments have been proposed and implemented. Along with the inertial measurement units used on previous wings other sensor layout concepts are proposed. On flight control and actuator system side, a CAN bus based actuator system is proposed. Along with that a detailed comparison is given between the proposed design and the system used on previous wings during the legacy FLEXOP project.

The experiences and detailed study on the servo health monitoring system currently used in the -0, -1 and -2 wings have been also revised and improvements have been proposed to increase servo deflection measurements for better system identification.

The main contributions of the team are:

- Collecting the main changes proposed in the fusealge, compared to original design documents

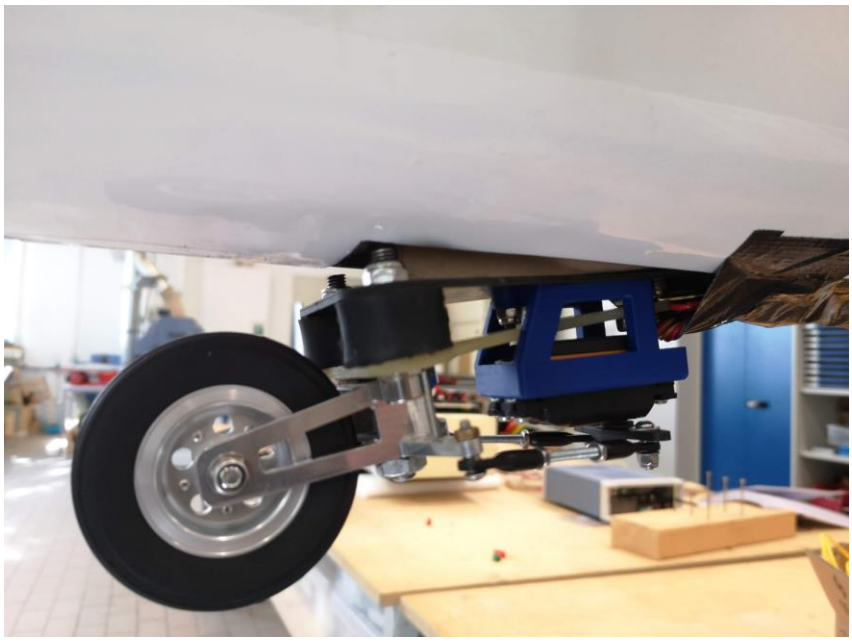

Figure 2.6 modified steerable landing gear

- Providing an updated sensor layout concepts for wing (3).

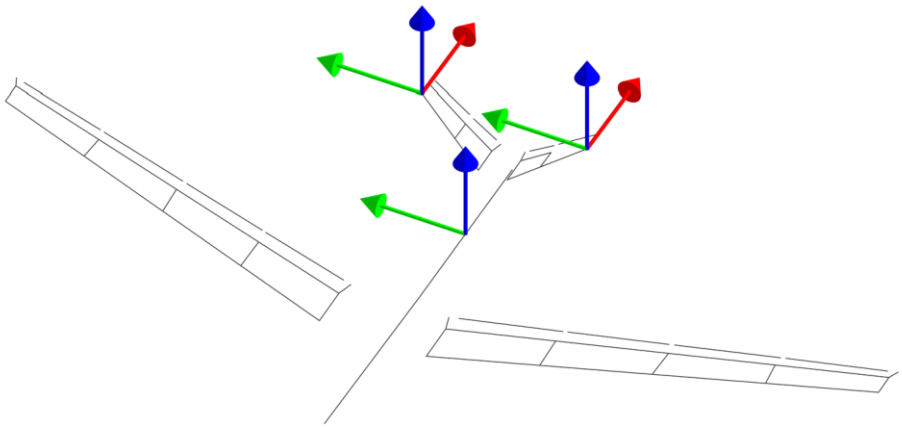

Figure 2.7 Improved onboard IMU locations for tail flexible motion detection

- Providing an actuator system concept for wing (3).
- Showing a detailed analysis of the previously used servo health monitoring tools system.

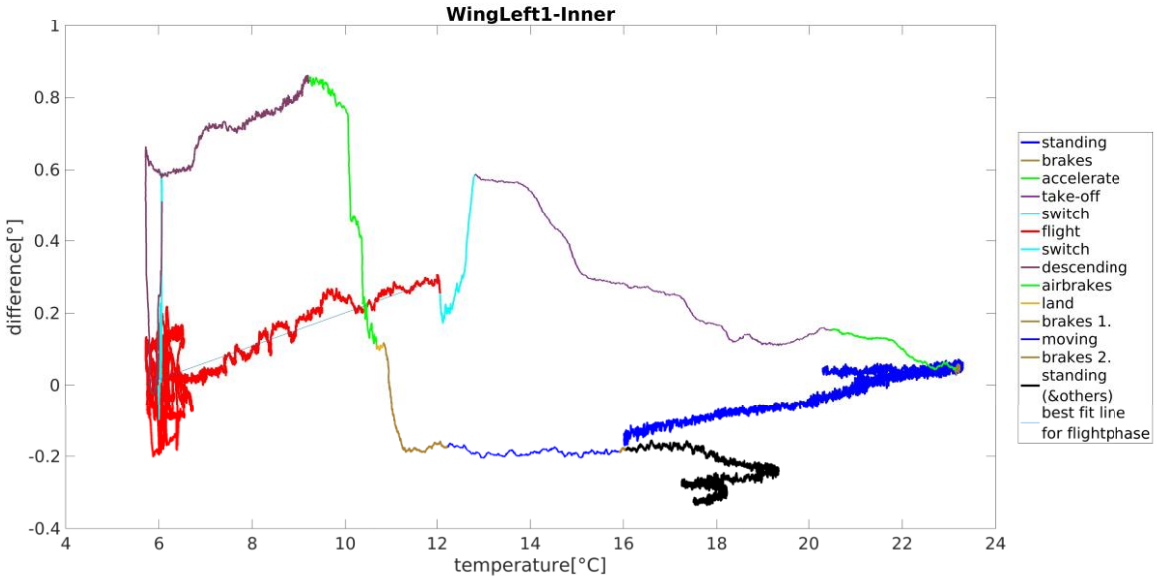

Figure 2.8 Temperature and flight state related calibration of servo deflection feedback

On the overall MDO design loop front to set up a collaborative design toolchain for an advanced, actively flight condition optimized wing design, requirements for the MDO toolchain need to be captured first. Deliverable D1.2 captured the outcomes of activities conducted for the requirement capture and serves as the top-level guideline for the subsequent MDO implementation.

The tasks conducted within the period related to setting up the overall collaborative MDO toolchain have been the following:

The objectives of the MDO toolchain and derived requirements were discussed and agreed among the partners. Two sorts of requirements are specified because of the different objectives for demonstrator wing design and commercial transport aircraft wing design.

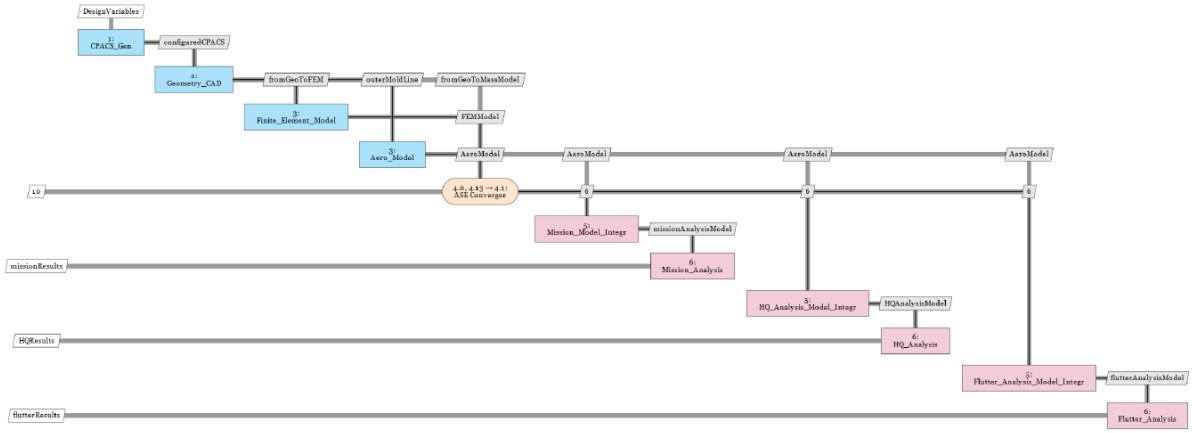

Figure 2.9 MDO worklflow in XDSM format with collapsed 'ASE converger'

The context of the consortium's activities related to the industry standard MDO toolchains were studied. Based on prior project results and experience the MDO toolchain structure is captured by MDAx, which is developed by DLR to support the ideation phase of MDO. The functions of individual blocks are specified and their interconnection has been iterated among the partners. An introduction of the integration framework RCE is given here.

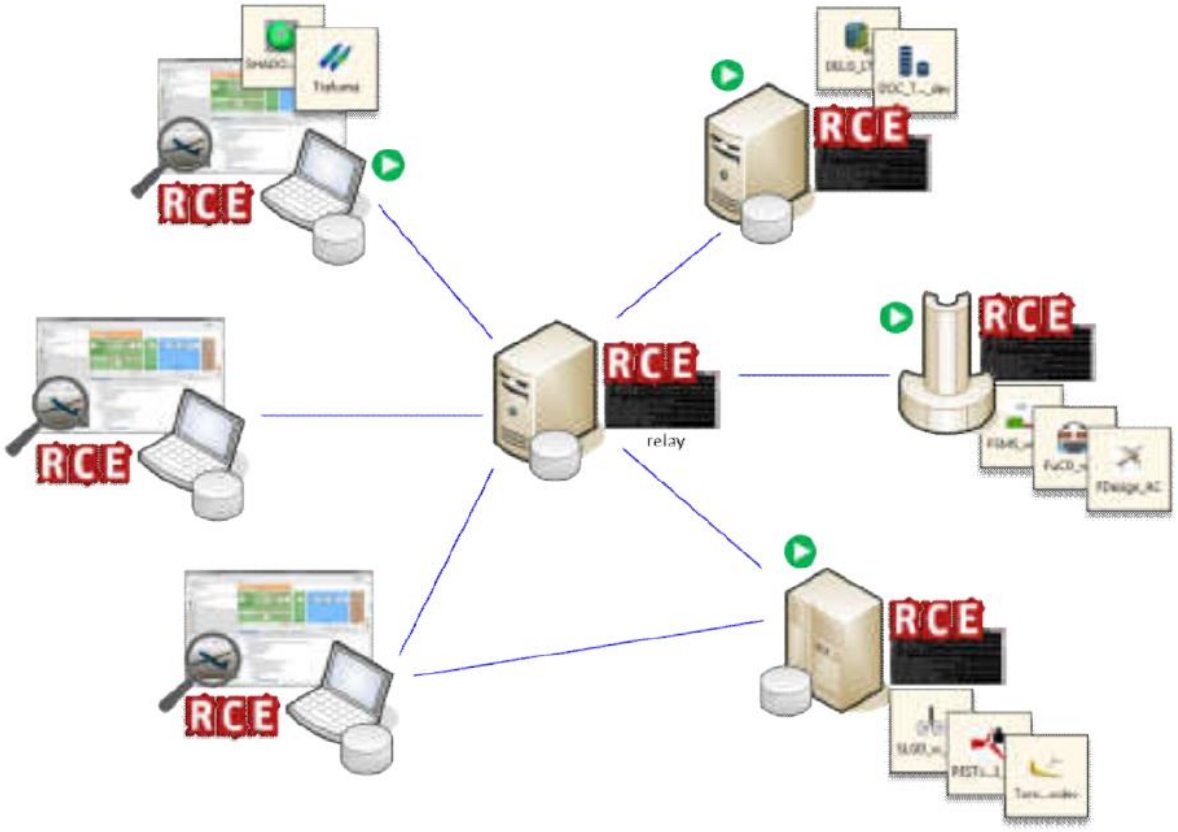

Figure 2.10 Distributed RCE workflow

The definition of interfaces of connected blocks in MDO toolchain required significant effort, due to the multidisciplinary nature of the project and due to the need that each block has to be 'human intervention free', to avoid lengthy hand tuning of parameters by experts within the MDO iteration loops. An introduction to CPACS, which is agreed by the consortium to serve as the standard interface medium, is also given here.

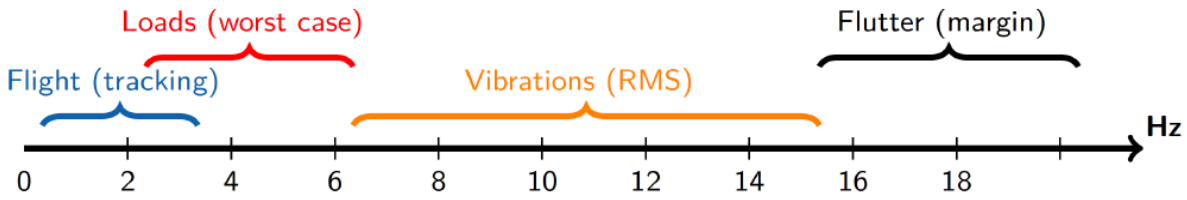

Figure 2.11 Frequency grid of the physical phenomena occurring over an aircraft. Ranges and values are different from an aircraft to an other.

The MDO toolchain has been singnificantly improved. On one hand, a simple example was set up to test the communication and data exchange between the partners. TUM, DLR-SR and SZTAKI succsessfully established connection on their locally running computers and after the task execution the data was sent to the corresponding partner. On the other hand,

specific details for the interfaces and data types between partners were layed out. The details are presented in D1.4. Based on these two steps the MDO tools are currently being integrated into the RCE framewrok by each partner and in parallel the interface specifications and data exchanges are being evaluated. An example of the model integration and simulation is given in the figure below.

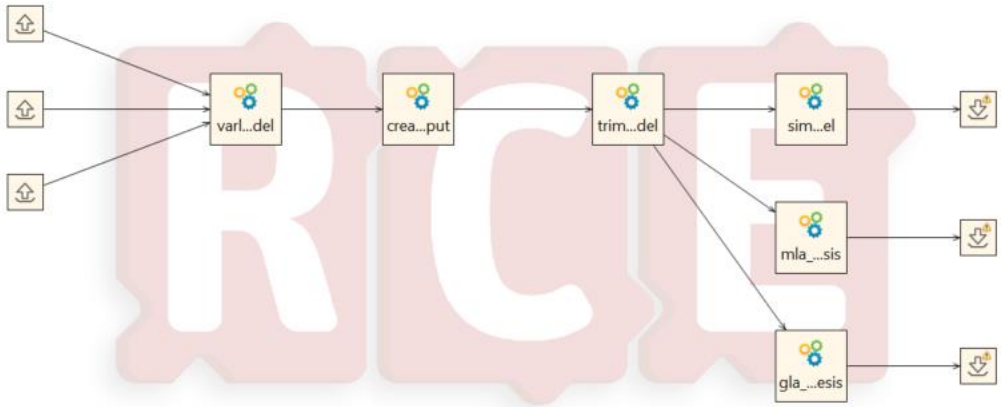

Figure 2.122 RCE workflow for the aeroelastic model generation and simulation.

From the perspective of the RCE workflow, the input to the NASTRAN aeroelastic model generation block are the following.

1. *CPACS.xml* - containing the most recent aircraft CPACS dataset
2. *wingFE* directory - directory containing the FE and DLM models of the wing, generated by TUM
3. *principal_angle_shifts_{1, 2}* float variables - outer-level optimization variables that define the prinicipal angle with respect to which the laminates in the upper and lower skin are oriented

The wing models are generated by the preceding block following an established numbering scheme for the entire aircraft, together with defined interfaces for assembly with the fuselage and empennage models.

This ensures that different configurations of the wing model are compatible with the existing fuselage and empennage models, generated based on FLEXOP data. The input wing model to this RCE block has a defined file-folder hierarchy as shown in Figure 2.13.

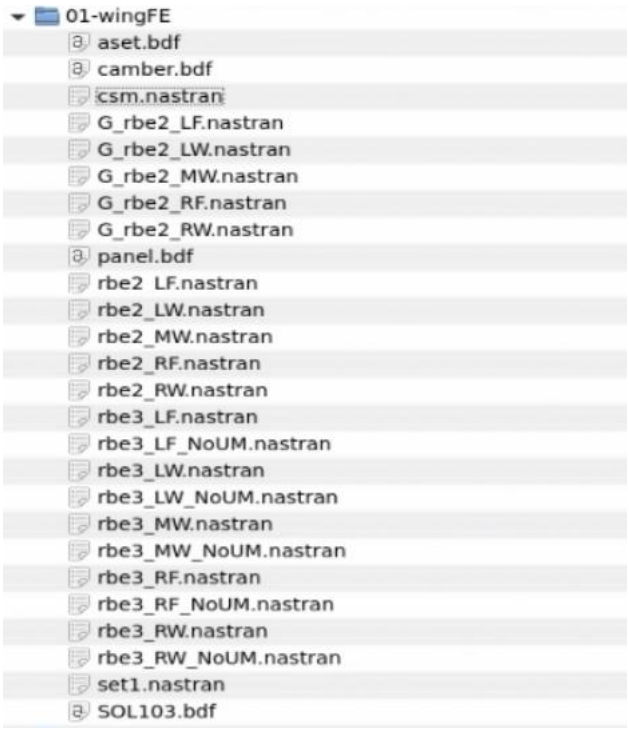

Figure 2.13 Defined folder-file architecture for wing models from TUM

The NASTRAN aeroelastic model integration block primarily performs the following tasks.

1. Create a modified wing FE model by rotating the existing laminate definitions on the upper and lower skins according to the input variables *principal_angle_shifts_{1, 2}*
2. Assemble the aerodynamic model of the aircraft by merging the panel definitions, spline sets and the camber correction entries for the wing, fuselage and empennage
3. Run pre-defined NASTRAN decks corresponding to modal, aeroelastic, flutter analyses and a static Guyan reduction
4. Aggregate the output data, including mass and stiffness matrices, and pre-defined aerodynamic bulk data into the output directory

The outputs from this block include two directories and the CPACS dataset as shown in Figure 2.14.

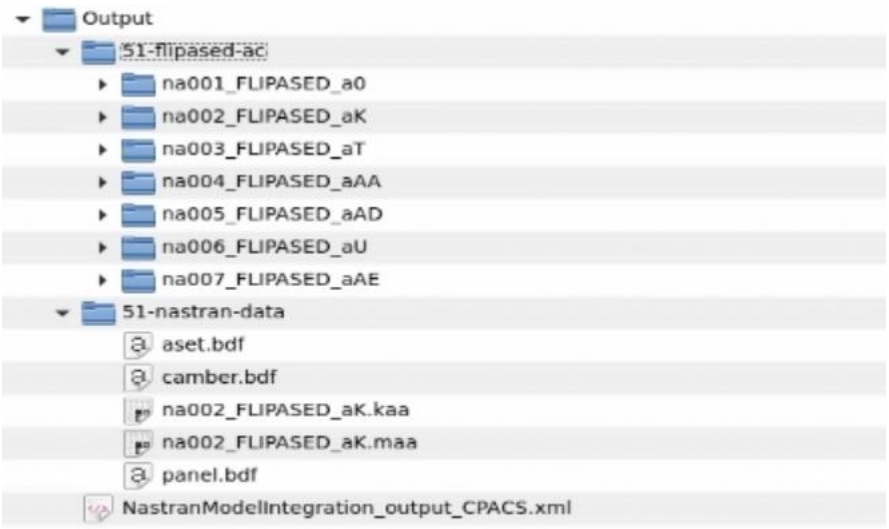

Figure 2.14 Defined folder-file architecture of NASTRAN aeroelastic models to DLR-SR

1. *51-nastran-data* directory - contains the outputs required by the next partner in the RCE workflow, DLR-SR in this case. Files include the mass and stiffness matrices, aerodynamic bulk data - panel definition and camber correction, and other outputs needed for the tools downstream.
2. *51-flipased-ac* directory - contains different NASTRAN solution decks for various analyses in order to aid in debugging.
3. output CPACS dataset - for the demonstrator workflow, the CPACS dataset is not altered during the execution of the tool. For the scale-up workflow, information from analyses such as structural weight, thickness and material properties of the various structural entities can be appended.

The aeroelastic model generation and simulation workflow implemented in RCE is given in Figure 2.12. The workflow is executed from the left to the right. All the corresponding functions are executed in Matlab. The result of each individual block is saved in a Matlab struct. First the aerodynamic, structural and spline grid information as well as mass and stiffness matrices are provided to the first block called "varloads model". VarLoads is a tool created in Matlab for defining flexible aircraft models by e.g. setting-up aerodynamic influence coefficient matrices and performing an eigen value analysis of the aircraft structure. The results are passed on to the block "create model input". The data is then downsized and provided in a specific form, so it can be used with the Simulink simulation environment. In the block "trim lin model" the simulation environment is initialised and also linearized. It is possible to adapt the simulation environment based on various parameters, that have to be defined. First of all the model order is selected by deciding on a model with unsteady aerodynamics or steady aerodynamics, flexible dynamics or rigid dynamics. Furthermore, dynamics coming from sensors, actuators, airbrakes and the engine can be switch on or off. Dependent on the simulation to be performed or the type of controller to be synthesized gust inputs and load outputs can be added. Finally the operating point for which the aircraft model should be trimmed and linearized has to be selected by defining the indicated airspeed, the

barometric height, the roll angle and others. Subsequent to the block "trim lin model" the model can be simulated with the block "sim model" by means of the trim results. It creates a time series for dedicated inputs commanded to the control surfaces, the engine rotational speed and so on.

In accordance with the workflow in Figure 2.12, after the "trim lin model" block has finished, the synthesis of the various controllers follows. The linearised state-space systems offer the opportunity to synthesize linear controllers. Here it is shown for a maneouvre load alleviation controller block "mla control synthesis" and a gust load alleviation controller block "gla control synthesis". Both seek to reduce the wing root bending moment corresponding to manoeuvres and gust encounter. Their structure is predefined with specified inputs and outputs. The pitch angle and rate, the commanded and real vertical acceleration are needed for the manoeuvre load alleviation controller. Based on these measurements it calculates the necessary aileron and elevator deflections. The gust load alleviation controller takes the pitch rate, the vertical acceleration in the fuselage and on both wing tips as an input. It likewise provides aileron and elevator deflections. Both controllers are synthesized based on the structured H_infinity synthesis method with a full order model including unsteady aerodynamics, gust inputs and load outputs. Before the synthesis takes place, the order of the state-space model of the aircraft is reduced removing irrelevant dynamics. As an objective function for the MLA and GLA controller the weighted transfer function from gust input to wing root bending moment has to be reduced.

Output of the RCE blocks are state-space models of the controllers. More controller types, like an active flutter suppression controller, could be synthesized subsequent to the "trim lin model" block as well. The resulting controller state-space systems can then be fed to a closed loop model in order to analyse the overall aircraft performance.

The other group of tasks carried out is the advanced modeling of the induced drag for different flight phases of the aircraft. This requires fluid-structure interaction in order to capture the effect of the elastic deformation of the aircraft on the overall drag. The aerodynamic modeling was set up in PANUKL (see figure bellow).

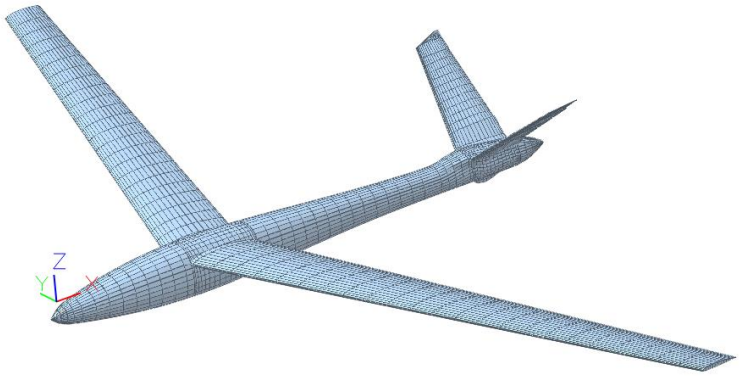

Figure 2.153 Aerodynamic panel generation in PANUKL.

The initial computation is done based on the jig-shape of the aircraft and the resulting pressure coefficients are then appied to the structural dynamics model via splining. An example of the elastically deformed aerodynamics panels are shown in the figure below.

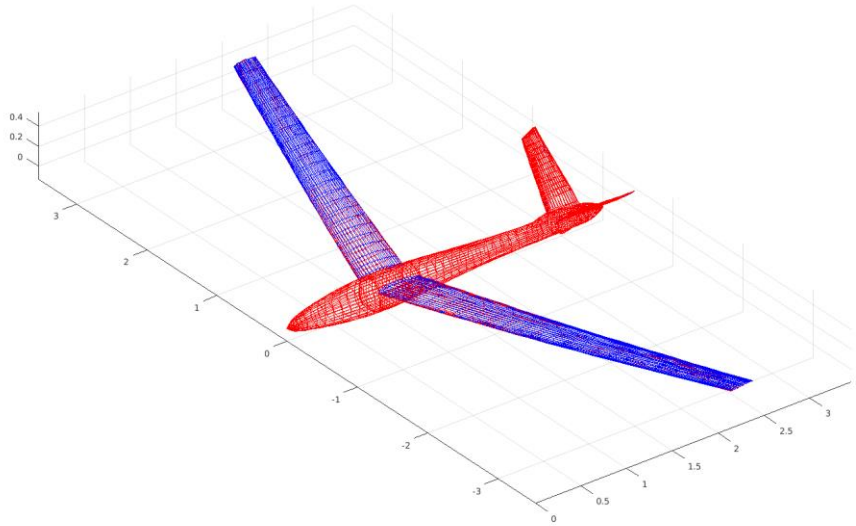

Figure 2.164 The underformed (red) and deformed (blue) aerodynamics panels.

An algorithm is set up in Matlab in order to compute the trim angle of attack, elevator deflection and elastic deformation. The algorithm can be run as a batch to compute drag values for various flight conditions (airspeeds) but it can also be used to calculate drag forces if not only the elevators are used for trimming but also the ailerons on the wing. With the ailerons it is possible to achieve different elastic deformations in the wings and the aim is to

generate drag models in order to set optimal wing deformations for different flight phases of the aircraft. The Matlab/PANUKL intergation is shown in the figure bellow.

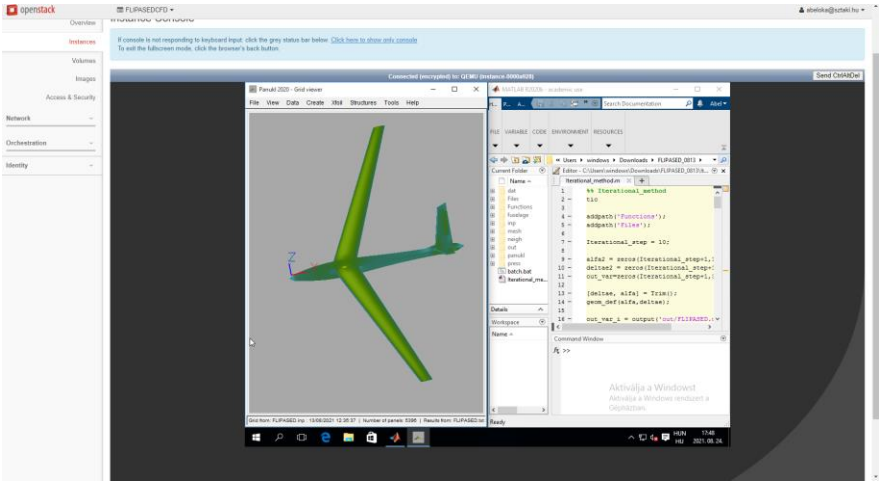

Figure 2.175 Matlab/PANUKL integration.

2.1.4 Deviations, their reason, impact on the project and corrective actions

The project is heavily impacted by the COVID related restrictions, what are even more striking in WP1, since both the hands-on work on the demonstrator must be postponed several times and the supporting teams of DLR and SZTAKI were only able to be on site at TUM for a very limited time.

On the other hand, this facilitated the need of online collaborative tools and methods. What has been established on several fronts: the teams are using common software development repositories using the SZTAKI hosted Gitlab site. The teams also collaborated more closely on developing tools compatible with the CPACS/RCE framework, what can be integrated into the workflow remotely.

Task 1.1: Requirements Capture is mostly done, but on-site brainstorming sessions would highly facilitate the discussions. The team adopted a weekly webex session where dedicated sessions are devoted to requirement capture.

Task 1.2 A/C Reference Model Definition – the team selected a suitable aircraft benchmark, the D150, which is well known and understood by DLR and its limitations are set, to limit the scope of the consortium. The deliverable related to this task (D1.5) was delivered late, but the actual work and decision within the consortium was done on time, and this does not have impact on the critical path of the project.

Task 1.3 Collaborative Work Process Definition – based on the CPACS and RCE standards the work process is defined but there is significant delay in the integration of these blocks,

since many partners are permanently at home office, where they cannot access the company's main computer infrastructure.

2.2 Explanation of the work carried per WP- Work Package 2

2.2.1 Objectives and activities

Within Work Package 2, the driving objective is to address the feedback control functions construction. The main objective of the WP is to develop a bundle of functions allowing designing the control functions in an automated manner, in order to be included in the global Multi Disciplinary Optimisation (MDO) process. This MDO being the central objective of FLiPASED, the proposed process should fit this frame and should not involve that much external user intervention. This is why we aim at providing a strong attention in constructing systematic approach. This WP involves three research groups, the DLR, ONERA and SZTAKI.

As a sub-objective, one seeks for the development and maturation of tools used for structural, aerodynamic and aeroelastic designs. The second sub-objective set concerns the development and integration of tools such as control, detection and estimation synthesis into the MDO toolchain.

2.2.2 Starting point and approach

Overall control big picture

The MDO loop presented above in the report considers the construction of dynamical models of the aircraft, sensors and actuators. These models, together with objectives and performance specifications are the starting point of the control design. Generally, aircraft manufacturers control design workflow follows what we can call a frequency grid approach. This approach consists in designing different controllers, through a frequency guideline. Each of them then address a « single » phenomena an aircraft is faced during its operation. Within the overall MDO process philosophy, and in this WP, we aim at following this very same approach. With reference to below figure, one may notice that different phenomena (flight, loads...) usually occurs at different frequencies. These frequencies are dependent on the geometry and structure of the aircraft, and in the considered case, one may expect even more blending in the phenomena. This sequential control structure will be kept in mind in the WP2 flow to stick to industrial and practical expectations.

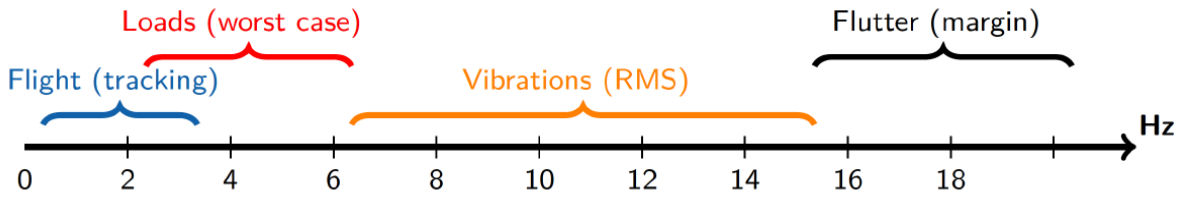

Frequency grid of the physical phenomena occurring over an aircraft.
Ranges and values are different from an aircraft / geometry to an other

At the present stage, flight, manoeuver and gust load, and flutter controllers were considered and a preliminary control architecture has been deployed. Without entering into many details, this is then

presented in the following section. Moreover, as an undistinguishable point, model approximation and analysis are also considered in these tasks.

Connection between the MDO unicorns with FLEXOP

From the modelling point of view, the initial starting point was the geometrical, structural and aerodynamic model of wing -1 which is the legacy of FLEXOP project.

In order to achieve a fully automated MDO toolchain, a parametrized geometrical model is the cornerstone of the whole toolchain. All the downstream FE-Model and aerodynamic model would be built upon it. Based on the available wing -1 Catia model, it would be parametrized with wing planform parameters (sweep angle, span and taper ratio), structural layout parameters (spar position, jig twist) and control surfaces design parameters (flap position). To have a better drag reduction effects with control surfaces deflection, the number of flaps is increased. It will give more freedom for control law designer. To add drag estimation functionality to the toolchain, a suitable aerodynamic solver needs to be chosen and coupled with Nastran.

There are lot of different tools involved in the model generation process. To avoid the human intervention in the MDO toolchain, interface between software needs to be defined specific and all the human operation needs to be programmed or recorded in Macro. Besides, component model of aircraft would be delivered separately by partners and would be assembled eventually. To automatize this process, detailed interface definition was carried out among partners.

From the control design point of view, the starting point is from previous research projects, especially FLEXOP. These methods and algorithms need to be adopted to the MDO toolchain, which requires a special attention. For example, the control oriented modeling involves some heuristic steps. These steps need to remain robust for model variation due to the MDO optimization. A possible way for such adaptation is the automatic evaluation of the accuracy of the resulting low order model and automatic increase in the states for the low order model to maintain sufficient accuracy. In case of the control design blocks, the control performance specifications need to be adopted to the MDO toolchain in a way that they can be automatically relaxed in case no feasible controller can be found.

2.2.3 Efforts and achieved results, name involved contractors

Dynamical high complexity model construction for MLA, GLA and flutter (TUM)

Catia model of wing -1 is reconstructed with parametrized platform and structural layout. To increase the number of flaps, three different configuration sets of flaps (4 flaps, 8 flaps and 16 flaps) were modelled in Catia. The current CAD model is fully capable of handling the design parameters. The geometrical modelling process is automated with the Catia macro language. Structure of wing -1 was modelled in HyperMesh. All the model generation operation was programmed with HyperMesh native macro language TCL. Currently the geometrical and structural modelling tools are integrated in the RCE framework and works automatically without human intervention.

The aerodynamic modelling tool for aeroelastic analysis is developed with PyNastran. It is implemented with a CPACS interface to ease the data input and has a default Nastran output. The tool is also integrated into RCE.

The aerodynamic solver for drag estimation would be finally integrated into MDO toolchain, which make a high request for the calculation speed. So several VLM-based aerodynamic tools are investigated for instance AVL, PyTornado and VSPAERO. And CFD simulations are carried out with StarCCM+ and SU2 to provide the baseline for comparison. Up to writing the final decision of aerodynamic solver is not made. The comparison of different aerodynamic solver is still in progress. This model serves as a baseline for what follows

After elaborated comparison of different solvers, AVL was chosen to be integrated into toolchain. AVL is well validated with experiment results. The calculation speed of AVL is also an advantage. The integrated trim routine also save some development efforts. The batch mode and rather simple geometry definition of AVL back up the selection.

A CPACS-AVL wrapper is implemented to create an AVL model based on CPACS data fast and automatic. The interface between AVL and Nastran is established to transfer the aerodynamic loads to Nastran structure model and regenerate AVL model based on deformed wing model in Nastran. The coupling between AVL and Nastran is realized by aeroelastic splining. The all the sub-block AVL, Nastran, aeroelastic splining are being integrated into a loop to model the induced drag taking aeroelasticity into account. Up to writing the loop is not finalized, further tuning is needed to improve the convergence speed.

In order to improve the accuracy of structure model order reduction, more elaborated model order reduction method was investigated, for instance Improved Reduced System (IRS). The investigation shows the IRS method can improve the accuracy of reduced model. It can be integrated into RCE framework later on.

NASTRAN aeroelastic model integration (DLR)

The structural FE model of the wing is obtained from the CAD-FEM toolset at TUM. This wing model is integrated to the fuselage and empennage based on aeroelastic models generated during FLEXOP at DLR-AE. These latter were generated using an in-house model generator ModGen.

In order to smoothen this integration, an interface between the models is set up. This is in the form of a document describing a numbering scheme for the different cards present in the models, for each component. Additionally, connection points between the components, for instance, between the fuselage and wings is also specified, such that iterations of the wing models can always be integrated to the aircraft model without any changes or adaptations necessary.

For the sake of completion, a brief summary of the fuselage and empennage models are presented below.

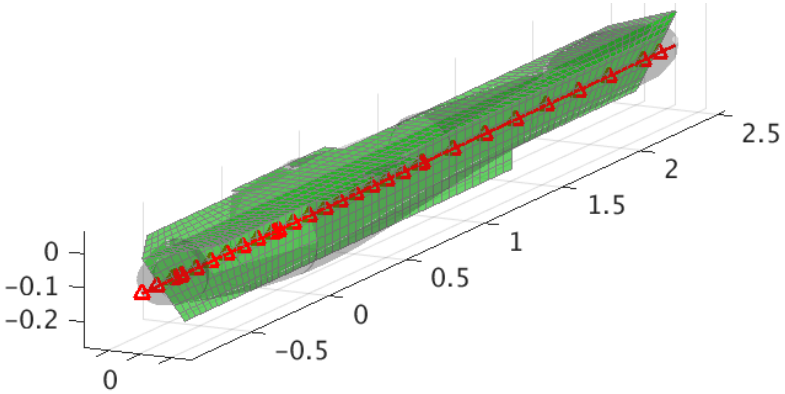

Figure 2.18: Fuselage DLM, hull, beam model Fuselage

FE model - fuselage hull is modelled as equivalent beam elements (CBEAM in MSC.NASTRAN) (Figure 2.18)

DLM model - a cruciform T-arrangement for the aerodynamic panels concentrated point masses for non-structural components interface - provisions for connection with the wings and empennage

Empennage

FE model - a shell-element based model comprising of upper and lower skins, structural ribs, spars and spar-cap (Figure 2.19)

DLM model - based on the planform of the empennage concentrated point masses for non-structural components provisions for splining using the load reference axis (LRA) method, necessary for aeroelastic analysis (Figure 2.20)

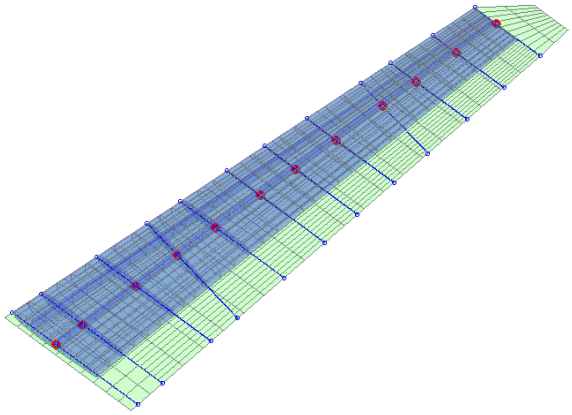

Figure 2.19: Overlay of FE, DLM model and LRA-based splining of empennage

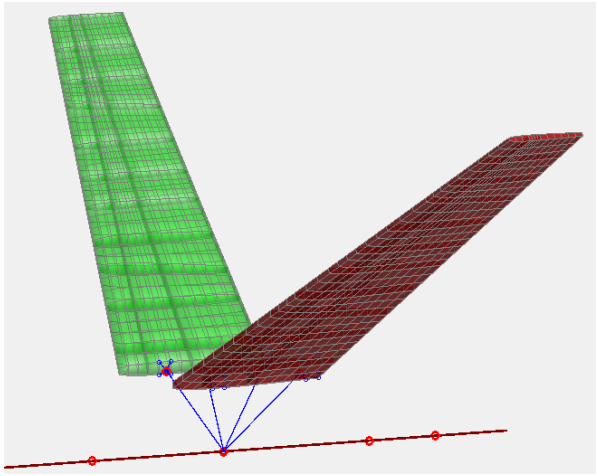

Figure 2.20: Empennage FE model generated using ModGen

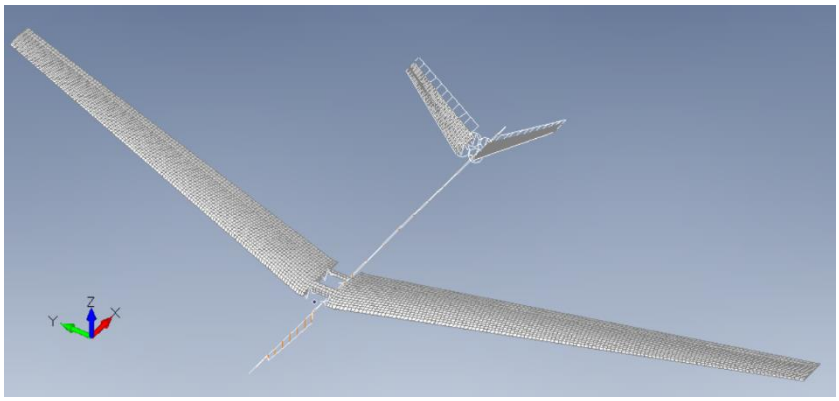

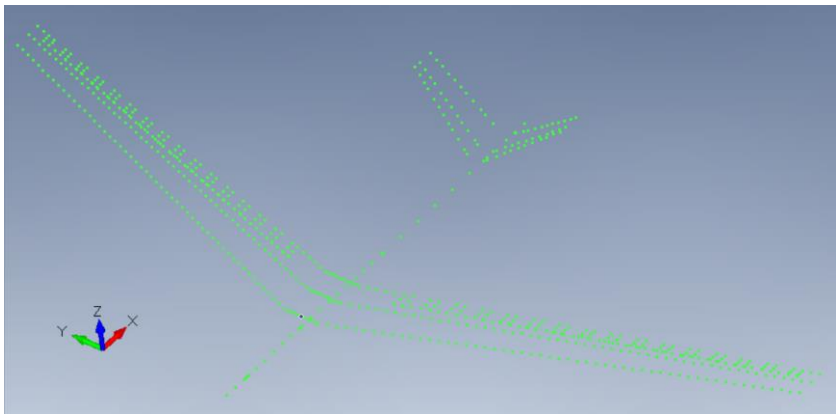

Figure 2.21: Full aircraft FE model (above), reduced model after Guyan reduction (below)

The structural and aerodynamic models of the fuselage and empennage are presumed to remain the same during the course of the MDO studies.

The wing models which will evolve during the course of an MDO run are referenced using suitable 'include' cards in MSC.NASTRAN in their respective solution decks.

Structural FE model condensation

Solution decks for MSC.NASTRAN are prepared beforehand for modal analysis using the full FE model and to export mass and stiffness matrices via the Guyan reduction.

The condensation points for the reduction include the following: fuselage nodes, nodes along the LRA of the empennage, nodes along the LRA of the wings and flaps.

A Python-script is prepared as a wrapper for the FE model integration block. Test runs for modal analysis, Guyan condensation, aeroelastic trim analysis and flutter analysis are performed once new wing models are generated and the FE model integration block is invoked. The output mass, stiffness matrices and additional bulk data required for aeroelastic analyses are then transferred to a suitable directory, for access to the MDO blocks downstream.

Drag estimation in NASTRAN

Given the necessity to account for drag in the MDO toolchain, a NASTRAN routine was setup to estimate far-field drag using a Trefftz plane implementation. The implementation makes use of the SOL200 sequence in MSC.NASTRAN that uses the lift forces using the aeroelastic solver to analytically estimate induced drag. The developed tool was tested on the FLEXOP -0 and -2 aircraft configurations to estimate which of the wings would show better potential for drag reduction using the control surfaces on the wing.

Implementation in RCE

The NASTRAN aeroelastic model integration block has been integrated in RCE. In a next step, the data transfer from the partner upstream and to the partner downstream using RCE needs to be tested.

Advance towards automated model reduction module (ONERA)

The high complexity of aero-servo-eslastic models generally induce a model reduction step prior to the control design itself. The challenge of this task lies in finding the right balance between complexity and

accuracy of the reduced-order model in an automatic manner, that is, suitable to be integrated in the MDO workflow.

Most standard model reduction frameworks assume that the target dimension is provided (e.g. by the user) and focus on finding the best model for this fixed dimension. This paradigm is not well suited for integration in an automated toolchain and the main objective here has been to modify this paradigm for that purpose.

A preliminary step towards this objective has been made by (automatically) choosing a reduction order based on the ratio of negligible Hankel Singular Values (HSV) associated with the system. This is a standard approach inspired by the Balanced Truncation. Exploiting the error bounds associated with the latter enables to trade the choice of a target reduced-order for a target relative approximation error, which is already a more relevant parameter to work with. Still, this approach suffers from two drawbacks: first, it can be computationally expensive as it requires the computation of two (large) Lyapunov equations and secondly, it cannot be applied to models with (internal) delays. The latter happen to present with the MLA and GLA models for instance.

In an attempt to alleviate those issues, the last few months have been dedicated to investigate a data-driven alternative of this approach. In particular, the objective is to estimate the HSV based solely on input-output frequency-domain data. This has been addressed with the Loewner interpolating framework, which enables to build a LTI model interpolating frequency-domain data. As shown in the figure below, it turns out that the HSV of the interpolating model can match very accurately the true HSV of the underlying system. However, this accuracy is largely dependent on the number of available data and it is difficult to make a guess a priori.

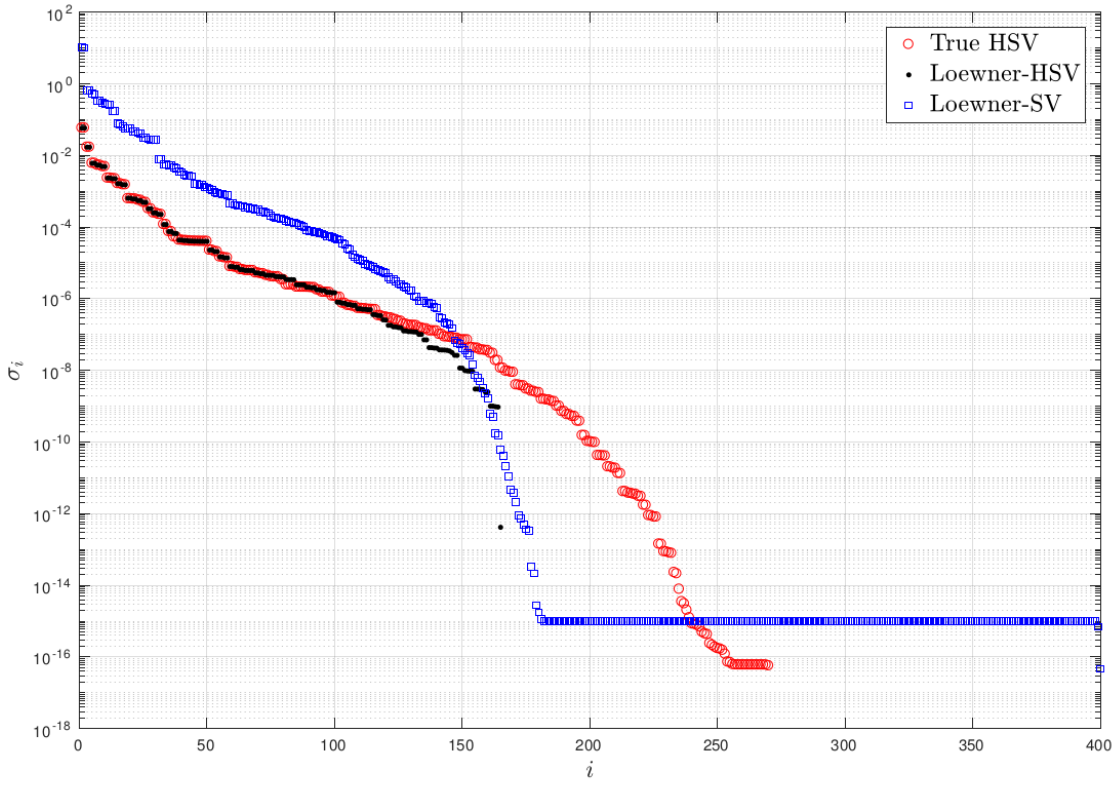

Illustration 1: Comparison of the true HSV with the HSV of the interpolating Loewner model on the

For this reason, a constructive approach is now under investigation. It iteratively increases the number of interpolation points by choosing frequencies where the previous interpolant model exhibits strong dynamics. The algorithm has been tested on several standard benchmark and it has shown better performances than the usual logarithmic choice of interpolation points. This algorithm is an interesting candidate for the automated reduction step but additional tests still need to be done to see the impact of delays on its accuracy.

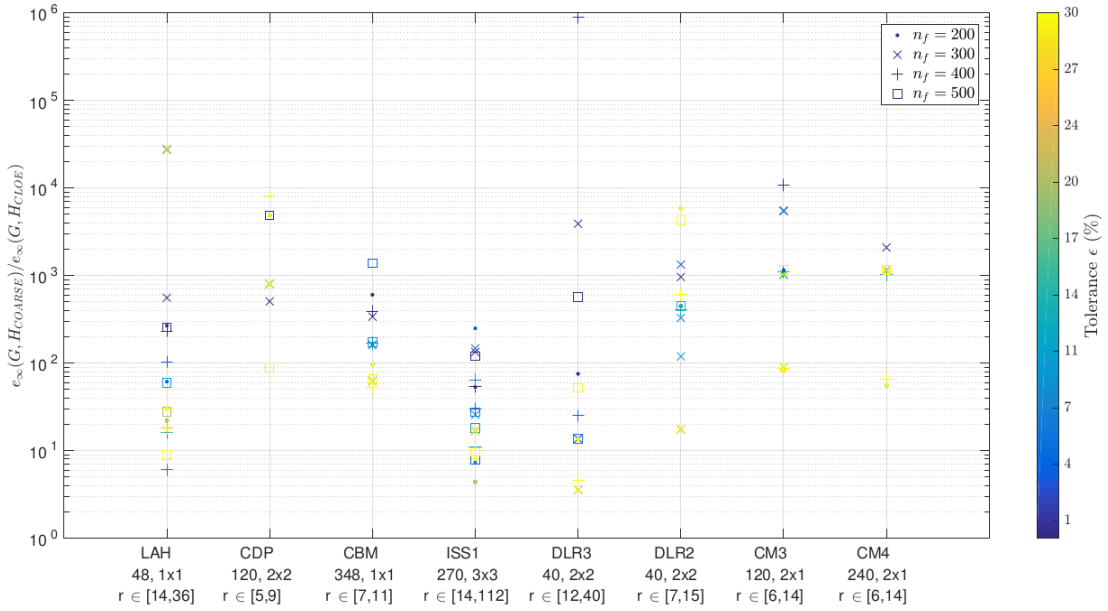

Illustration 2: Error ratio between the logarithmic choice of interpolation points and the incremental choice for several models and various parameters of the algorithm.

Aeroelastic uncertain (LPV) model frame for flutter (SZTAKI)

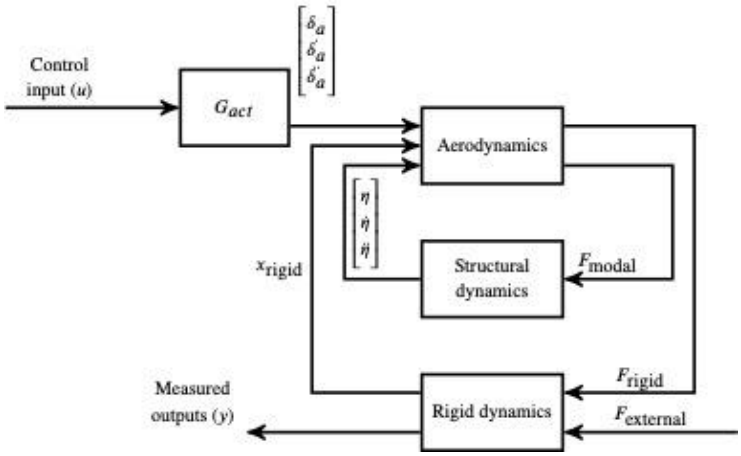

The key idea of the bottom-up modeling is the following. The subsystems of the ASE model in general have simpler structure than the nonlinear ASE model. Therefore, the subsystems containing the structural dynamics and aerodynamics model can be reduced by simpler, more tractable reduction techniques. Combining these reduced order subsystems results in a low order **nonlinear ASE model** upon which a nominal, low order, control oriented models can be obtained. The main milestones of the modeling block are the following. The ASE model is formed by combining the structural dynamics model, the aerodynamics model and the flight mechanics model. In order to obtain an ASE model suitable for control design, model order reduction needs to be carried out. The model order reduction is based on the bottom-up modeling approach.

Manoeuver Load Alleviation (MLA) functions (ONERA)

Manoeuver load alleviation are closely related to the GLA (detailed in what follows). However one specificity is to design a control law that tends to monitor the loads in case of specific manoeuvers (such as the +2.5g or -1g in longitudinal). Such a function is needed to prevent unwanted loads. Following the philosophy of constructing an automated scheme to be implemented within the MDO (via RCE software), the process allowing designing an MLA function has been constructed.

Such an automated process is embedded in a MATLAB function package, provided to all project participants, and called “+MLA”.

With the considered aircraft geometry / dynamical model, and following the model structure, the MLA function (based on the reduced models obtained as previously presented) connects the following measurements provided by sensors

- Theta (the angle at the CoG level)
- Q (the angle velocity at the CoG level)
- Az- AzRef (the vertical acceleration at the CoG level - the vertical acceleration reference provide by the “pilot” or supervisor)
- And its integral;

to the control surfaces

- Ailerons (control surface #4)
- Rudders.

The resulting controller is only function of the desired response time of the aircraft to the vertical acceleration reference, and of the desired complexity of the control law. As an illustration, the below figure shows the results on a single flight point, when a response time of 6 seconds is sought with a controller embedding a dynamical complexity of 6 internal states.

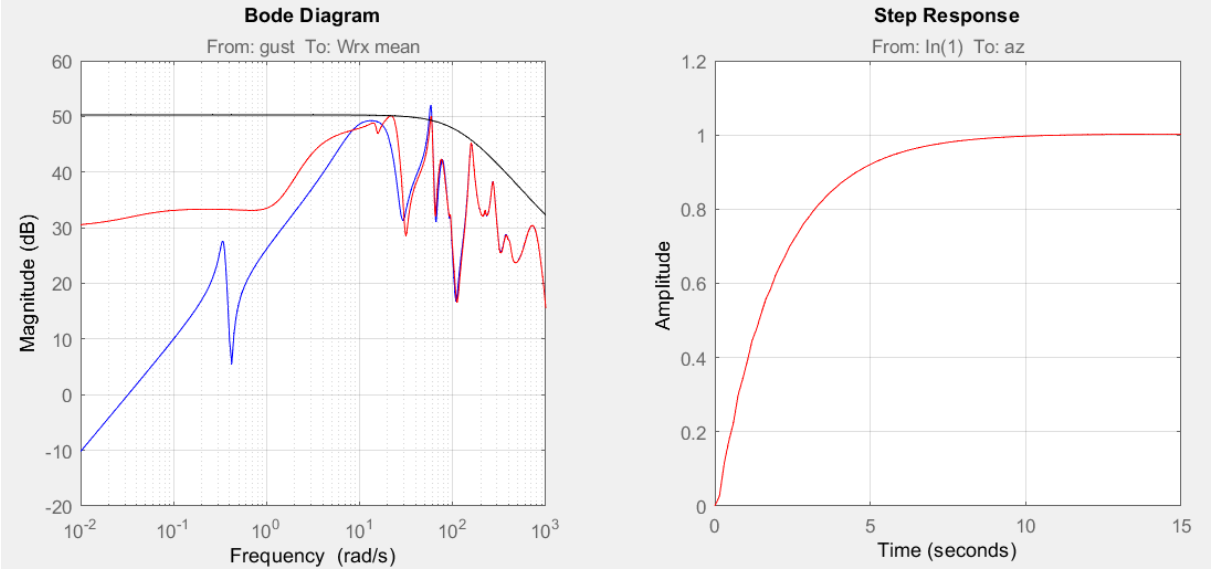

From this result, one observe:

- Left frame – transfer from gust to bending moment: the peak gain of the uncontrolled aircraft (in blue) is attenuated by the controlled one with MLA (in red).
- Right frame – step response to a pilot stick: the vertical acceleration rises up to the reference 1 in 6 seconds, being the objective.

Gust Load Alleviation (GLA) functions (DLR, ONERA)

As part of the secondary control functions a gust load alleviation (GLA) controller is designed based on a single point reduced linear model. The overall goal is to reduce the maximum loads due to gust encounter by means of a controller. The starting point was the non-linear model developed within the flexop project. Besides the nominal inputs the model is extended by ten gust inputs. The aircraft is divided in ten gust zones along the aircraft longitudinal axis. Within each zone the aerodynamic panels of the experience the same gust velocity. This kind of modelling is an approximation, which reduces the complexitiy of the gust model strongly, while the effect of the gust on the aircraft is almost unaffected. In order to analyse the performance of the gust load alleviation controller load outputs at the wing roots and at the V-tail roots are provided.

As a first step the GLA controller should be designed at a velocity of 38 m/s and an altitude of 800 m, for which the non-linear model is linearized. The gust is considered a vertical 1-cos gust, like shown in Figure 2.2.2.2, that hits the aircraft symmetrically starting at the nose.

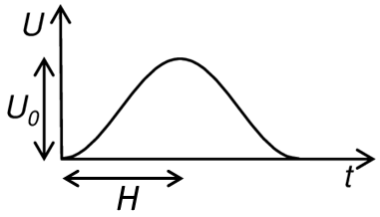

Figure 2.2.2.2 Gust illustration

The gust velocity is given by U_0 and the gust half length by H. With increasing time the gust zone moves to the aft of the aircraft. In each gust zone the corresponding aerodynamic panels are affected by the gust speed, that is observed at the front edge of the gust zone. Namely, within a gust zone the gust speed is constant. The difference of gust speeds in two neighboring gust zones is defined by a time delay. As a transfer function a delay can be defined by

$$G_{delay}(s) = e^{-t_{delay}*s},$$

where t_{delay} is the time delay in seconds and s is the Laplace variable. To simplify the handling of time delay, it is approximated by a second order Padé approximation

$$G_{delay}(s) \approx \frac{s^2 - \frac{6}{t_{delay}}s + \frac{12}{t_{delay}^2}}{s^2 + \frac{6}{t_{delay}}s + \frac{12}{t_{delay}^2}}.$$

The selected control synthesis method is the structured H-infinity one. It solves the optimisation problem

$$\min \left| |T_{w\to z}(K)| \right|_\infty,$$

$$K \in \mathrm{K}$$

for which the H_∞ norm of the closed transfer function T is minimized, while the structure of the controller is predefined. Here, the controller is considered to be a simple gain matrix. Like shown in Figure 2.2.2.3, the inputs to the controller are the pitch angle y_θ, the pitch rate y_q, the

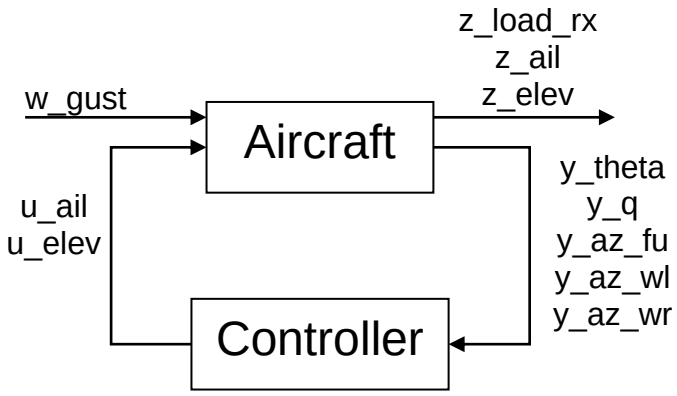

Figure 2.2.2.3 : closed-loop scheme

z-acceleration measured in the fuselage y_az_fu and the z-accelerations at the wing tips y_az_wl and y_az_wr.

Based on these measurements the controller provides the deflection of the outer ailerons u_ail and all elevators u_elev. As the aircraft is almost symmetric along the longitudinal axis and only vertical gust encounters are considered, the deflection of the two ailerons are identical as well as the deflection of the four elevators. Therefore, the commands of the controller can be combined to two signals. The inputs and outputs of the aircraft state-space system used for the GLA control synthesis are also normed for a better numerical handling. At this point the state-space system has more than 400 states. To reduce the order of the system in a numerical way the balanced reduction is used to decrease the system order to 60.

Before the structured H-infinity synthesis can take place, the requirements of the control problem have to be defined. Three different requirements are defined for the GLA controller synthesis. Firstly, the H_∞ norm of the wheighted transfer function from gust to the wing root bending moment should be minimised. The transfer function is multiplied with a weighting function to emphasize for which frequency domain the wing root bending should be reduced especially. Secondly, the action of the aileron and the elevator actuators is limited in deflection and deflection rate for GLA controller. Additionally no interaction of the GLA controller with the flight dynamics is wanted as well. This leads to requirements with respect to the transfer function from gust to the aileron and elevator deflections. As the maximum deflection rate of the ailerons and elevators differ, two requirements are defined in Figures 2.2.2.4-6 show the defined requirements (black), the open-loop (magenta) and closed-loop (blue-red) transfer functions.

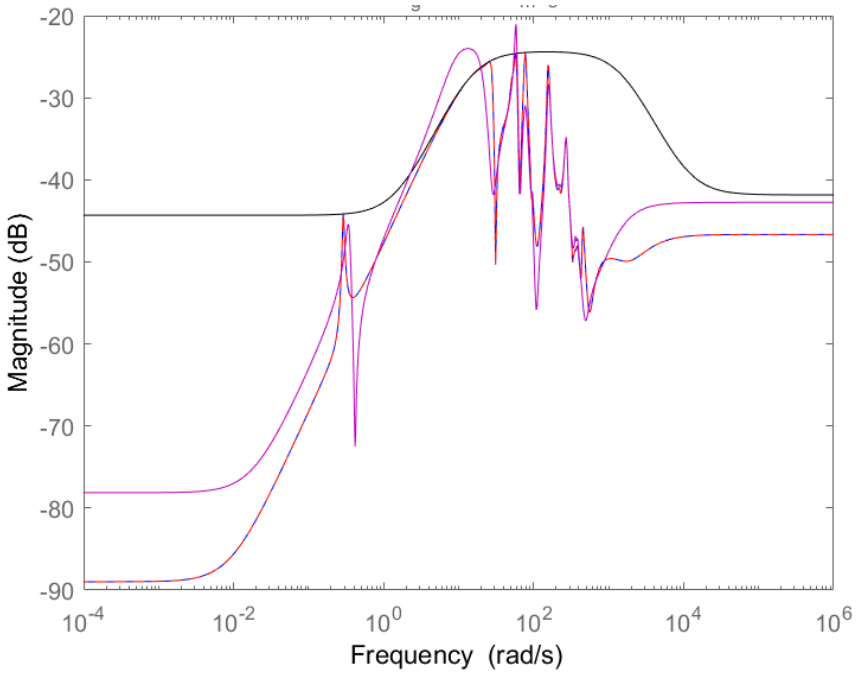

Figure 2.2.2.4 : Bodeplot of the transfer function from w_gust to z_load_rx

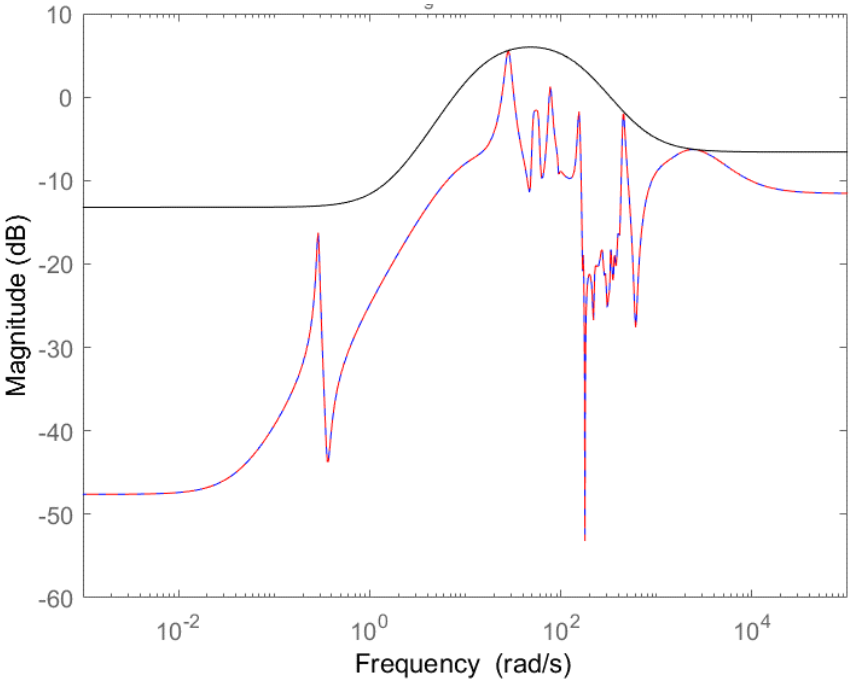

Figure 2.2.2.5 : Bodeplot of the transfer function from w_gust to z_ail

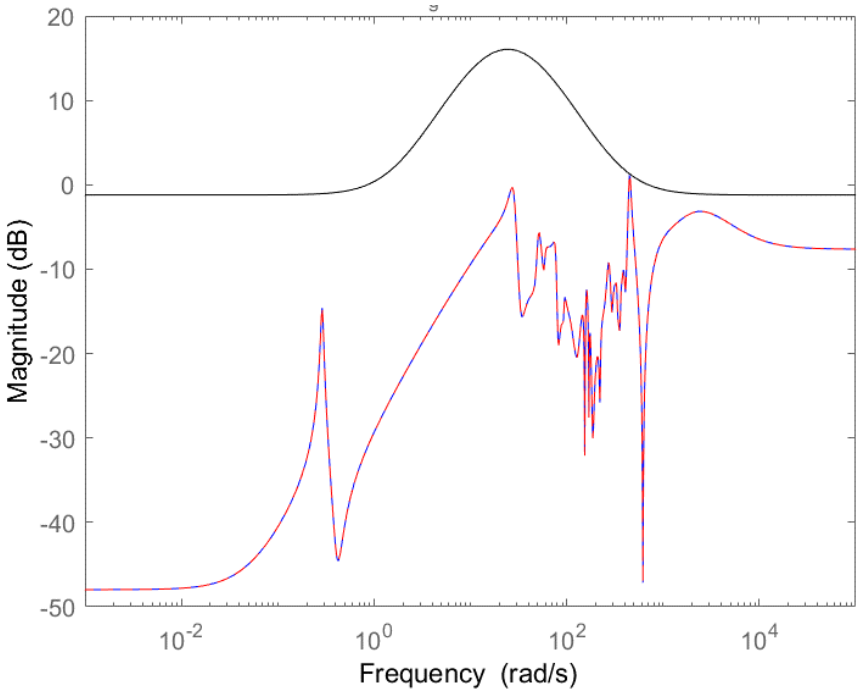

Figure 2.2.2.6 : Bodeplot of the transfer function from w_gust to z_elev

The deflection of the ailerons and the elevators stays within the predefined bounds, while the wing root bending can be reduced with a GLA controller in a frequency range of approximately 2 - 11 rad/s. Furthermore, the maximum peak of the open-loop system at 58.4 rad/s is reduced significantly. At various frequencies the closed-loop wing root bending moment might exceed the one of the open-loop case, but anyways the maximum value is reduced.

Time simulations of the different gust excitations show the reduction in the maximum peak load as well. Figure 2.2.2.7 shows the wing root bending to a step excitation at the gust input.

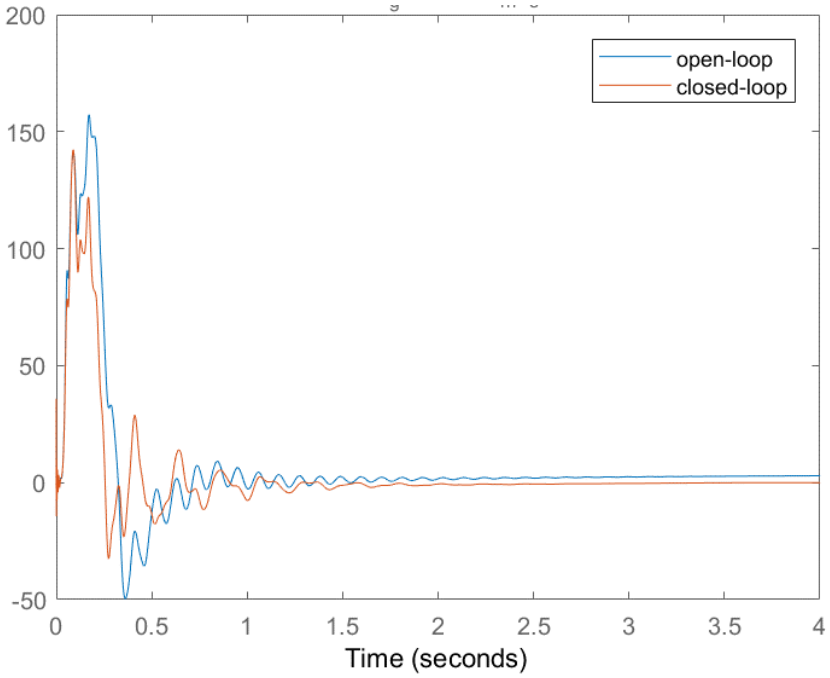

Figure 2.2.2.7 : Step response from w_gust to z_load_rx [Nm]

It is visible, that the maximum load is reduced by almost 10 %. In addition, two 1-cos gusts refering to a frequency of 58.4 and 25.6 rad/s are considered. For a frequency of 58.4 rad/s, at which the maximum wing root bending for the open-loop case is reached, the simulation shows only a 3 % reduction of the maximum load in Figure 2.2.2.8.

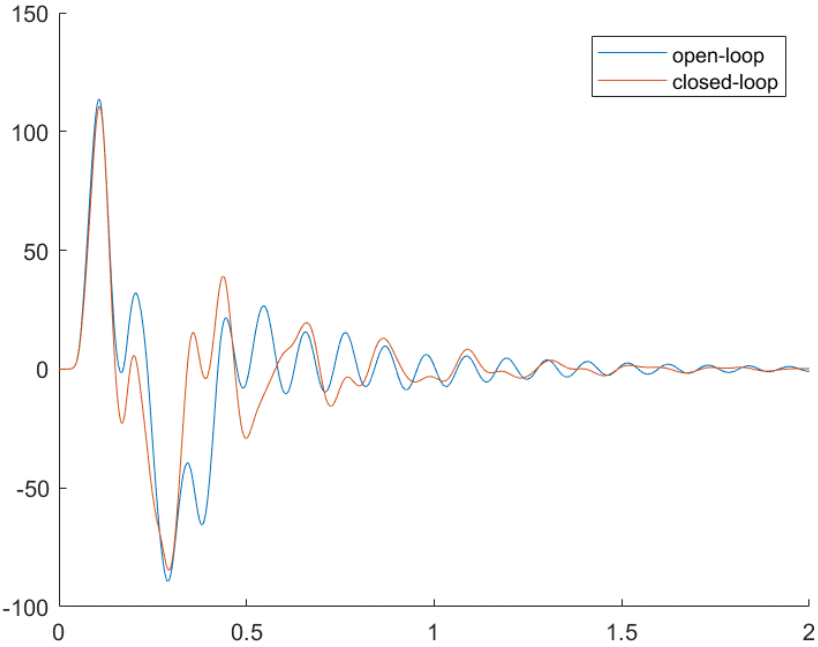

Figure 2.2.2.8 : z_load_rx [Nm] due to 1-cos gust (58.4 rad/s)

As the excitation by a 1-cos gust cannot be restricted to a single frequency, it is possible, that the load reduction is not as high as expected. For a critical gust half length defined by Pratt's method

$$H_{crit} = \frac{25}{2} c_{ref},$$

where c_{ref} is the reference chord length, a nominal 1-cos gust excitation of 25.6 rad/s is achieved. The time simulation for this excitation is shown in Figure 2.2.2.9.

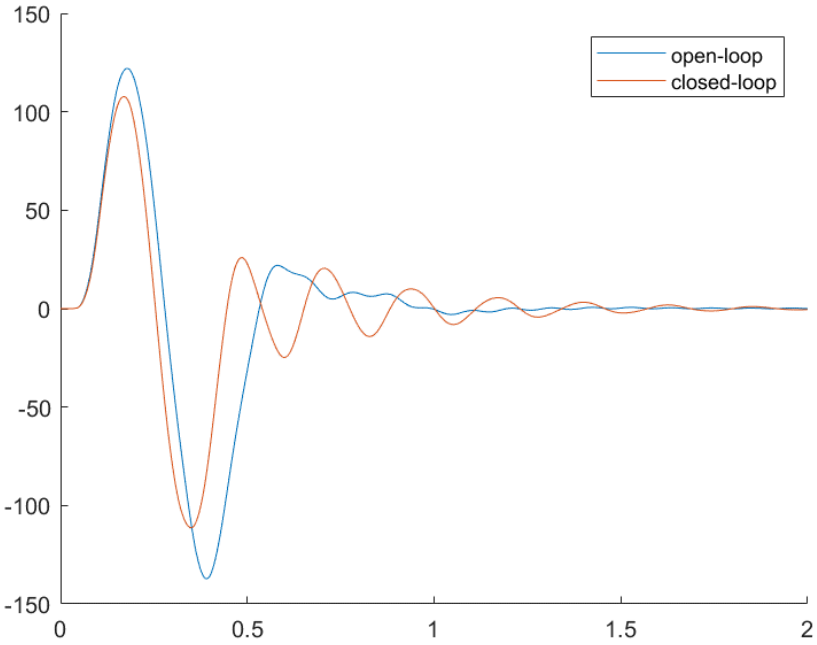

Figure 2.2.2.9 : z_load_rx [Nm] due to 1-cos gust (25.6 rad/s)

Here the maximum wing root bending is reduced by almost 12 %. However, the wing tends to vibrate longer. For now, the synthesized GLA controller is considered sufficient for an integration in the overall toolchain of the project. Therefore, the next step will be the implementation of the GLA control synthesis algorithm into RCE.

Simplified LPV model construction for flutter (SZTAKI)

The next step is to develop uncertain LPV models of the aircraft. Uncertain models can be developed by extending the structural dynamics model with the uncertain parameters. These uncertainties appear in the stiffnes matrix and in the damping matrix of the nonlinear ASE model. Based on this uncertain, nonlinear model a grid-based uncertain LPV model is constructed. The grid-based uncertain LPV model is obtained over a 3 dimensional grid. A similar work can be done with unstructure uncertainties.

Linear parameter-varying (LPV) and linear time-invariant (LTI) models are typically used to design controllers for flexible aircraft. LTI control design techniques are mature and allow straightforward application, while LPV approaches lead to controllers with better overall performance. Therefore, grid based LPV models of the flexible aircraft need to be derived for the control desing. These models need to have sufficiently low order for practical application and one of the main challenges of flexible aircraft modeling order reduction. High fidelity models may contain thousands of states. The low order, control oriented model of the aircraft is obtained via the bottom-up modeling aproach. The key idea is to reduce the structural dynamic and aerodynamics model before integrating these systems into the nonlinear model. The resulting low order aircraft models are then used in the successive blocks in the toolchain, namely the baseline and flutter control design blocks. In order to achieve the most realistic

results in the analysis block of the toolchain, high-fidelity, non reduced aircraft models are also obtained. The controllers are evaluated after interconnection with this high-fidelity model.

The initial model order reduction produced the following results. The structural dynamics model can be reduced in the following way. In order to keep the ν-gap between the high fidelity and the low order model low the first six structural modes and modes 19, 20, 21 are retained for the reference aircraft model. The removal of the latter results in a large increase in the ν-gap. This way, a 18 state structural dynamics model can be obtained from the 100th order model. In case of the aerodynamics model, retaining two lag states results in a low order model with acceptable accuracy. The resulting nonlinear ASE bottom-up model has 32 states that consists of 12 rigid body states, 18 structural dynamics states, 2 aerodynamic lag states. Note, that the actuator dynamics are not included in the control oriented model. The ν-gap between the nominal, high-fidelity and the reduced order model for different airspeed values is given in Figure 2.2.3.2.

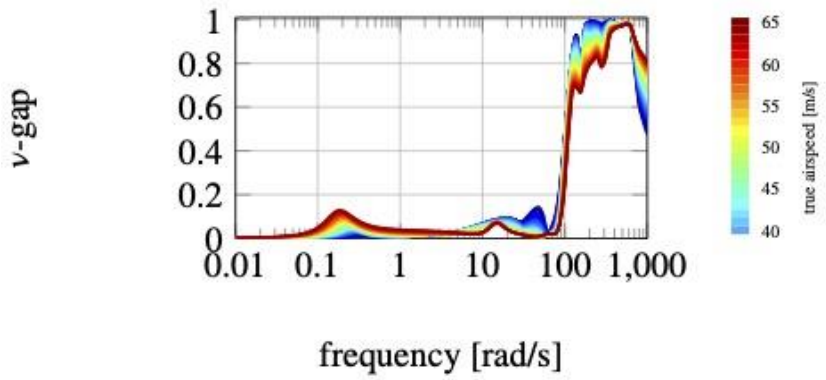

Figure 2.2.3.2. ν-gap values between the nominal low order and high-fidelity models.

Flutter control design main algorithm (SZTAKI)

The flutter controller design is done based on the uncertain LPV ASE model of the aircraft. The flutter control design takes the outer aileron (denoted by L4 and R4) actuator dynamics and the flutter control design model FlexACModel as inputs via CPACS.

The airspeed and the uncertainties in the structural dynamics model are treated at parametric uncertainties and dynamic uncertainty is added to account for the model reduction. There are two main sub blocks in the flutter control design blocks. First, the design model is split into longitudinal and lateral. These models are then used to synthesize a stabilizing controller for the symmetric and asymmetric flutter mode respectively. Second, the control design consists of the construction of two uncertain plants, performance definitions, and the synthesis of two low-order controllers. These controllers are blended together to obtain the flutter controller. The stability of the resulting flutter controller and a couple of implementation criteria are also tested.

In case of the flutter suppression control desing, the airspeed and the uncertainties in the structural dynamics model are treated at parametric uncertainties and dynamic uncertainty is added to account for the model reduction. In order to reduce the computational time of the control synthesis, structured H_∞ design is chosen that result in an LTI flutter suppression controller. Similarly to the baseline control

design algorithm, the flutter suppression control design block needs to be augmented with basic analysis algorithms to verify if the resulting controller satisfies the control performance specifications. As a main measure, the multi-input multi-output (MIMO) disc margins are selected.

Analysis of the designed (flutter) controllers, prior RCE integration (SZTAKI)

The analysis of the closed-loop is based on disk margin calculations. Complex scalar uncertainties are injected into the channels involved in the feedback loops and the phase and gain combination at which the closed-loop becomes unstable is computed in each channel, simultaneously. First, the robustness of the baseline controller is analyzed without the flutter controller. The speed at which the disk margins become zero is considered the open-loop flutter speed. In the next step, the flutter controller is also connected to the system and the margins are recaclulated. This step reveals how much the flutter controller is able to extend the safe flight envelope functioning simultaneously with the baseline controller.

This procedure shall be extended to GLA and MLA.

Integration of the baseline controller design in the MDO workflow (SZTAKI)

The design process of the baseline controller is carried out on the basis of the mathematical description for the aircraft. Structurally the controller consists of several loops targeting different dynamical modes. Accordingly, intuitive design specification for the loops can be formulated by the user in terms of settling times, reference tracking or robustness margins. The control design itself automatically optimizes the corresponding gains, in order to satisfy the specified design goals. Once the optimization found a feasible solution it provides the corresponding control gains and control structure which is then used for the numerical analysis. However, a simple metric is also returned for the user which indicates the performance of the control loops. This allows the interaction with the automated design process: the user can formulate tighter or loser specifications according to the individual needs. A clear graphical representation is also provided which can be included in the reporting. In addition, the controller generation process adjust the speed-dependence of the control gains in order to achieve the best possible performance and the simplest scheduling function. Frequency and time tomain results can be seen if Figure 2.2.1.10.

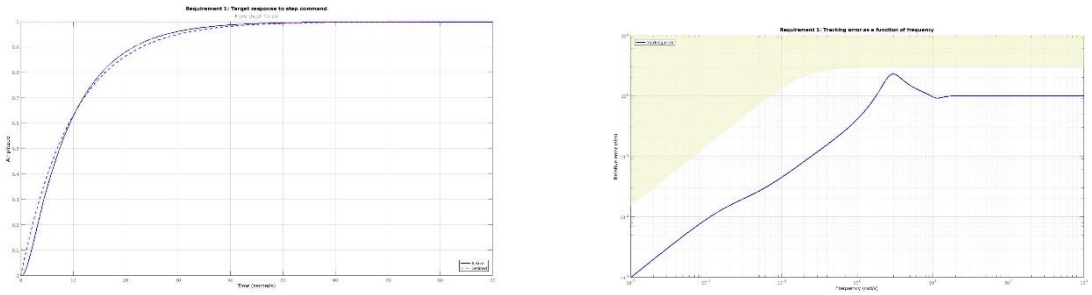

Figure 2.2.1.10 : Time domain results (left) Frequency domain results (right).

Fault detection filter design (SZTAKI)

For the flexible aircraft of the FLiPASED project, we want to detect two faults in the longitudinal motion of the aircraft: angle of attack sensor and elevator actuator faults. (Note that the tail of the aircraft is outfitted with ruddervators, therefore it would be more precise to say that we want to detect a fault in the ruddervators that affect the longitudinal motion of the aircraft. We will continue to refer to the control surface as elevator for simplicity.) The block diagram of the FDI filter design problem is

depicted in Figure 2.22. We design optimal FDI filters with different bandwidths using the rigid and the flexible model of the aircraft. Then, using a simple decision mechanism, we calculate the smallest detectable fault and the detection time for each fault and for each filter. Based on these results, we make recommendations on what sensor configuration and which model to use for certain performance requirements.

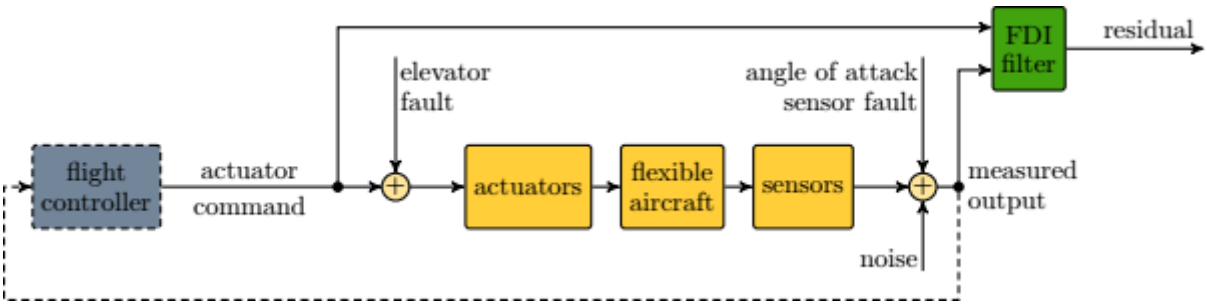

2.22. Figure: Block diagram of the joint actuator and sensor fault detection problem.

The sensors and actuators relevant for the fault detection are illustrated in Figure 2.23. Two models of this aircraft are used for filter design in this chapter: a low order rigid body and a higher order flexible model. Both are linear longitudinal models obtained in straight and level flight (at 38 m/s).

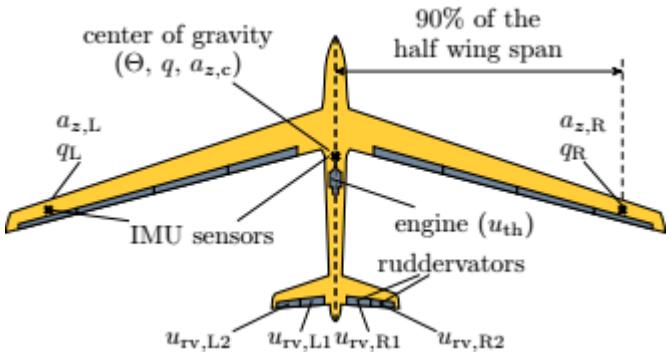

2.23. Figure: Control surface configuration and sensor positions of the flexible aircraft. Thecontrol inputs and sensor signals are marked at the corresponding control surfacesand sensors.

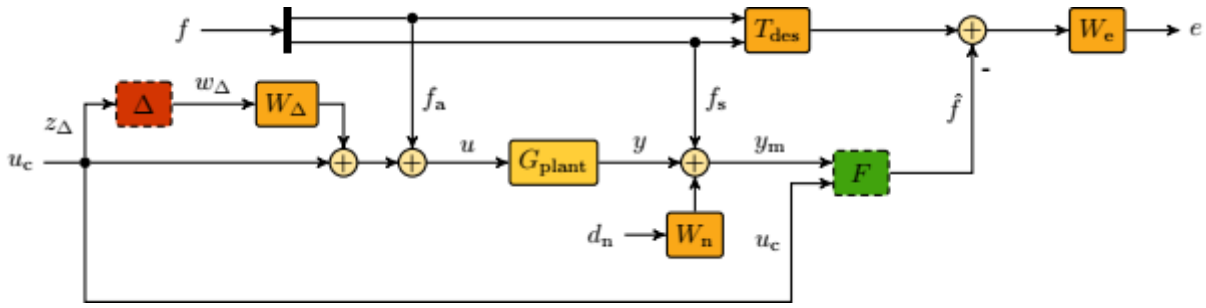

The FDI filter design is articulated as anH∞optimal synthesis problem similarly to thesolution of [8]. The generalised plant interconnection is depicted in Figure 2.24. The fault which is modelled as an additive disturbance on the elevator actuator command and the angle of attack measurement. The output of the FDI filter is called the residual. It is the estimate of the fault signal. The control command is normally the output of the flight controller but since no controller is considered in the design process, it is treated as a known external disturbance. The objective of the design is to find a filter such that the H∞ norm of the closed loop is minimal for all possible uncertainties. This optimization is solved using the standard H∞ synthesis tool implemented in the hinfsyn function of MATLAB.

Our calculations revealed that the accelerometers placed close to the wing tips do not improve FDI performance. Hence, we only compare configuration 'no acc.' and 'acc.' in the rest of this chapter. Figures 2.25 and 2.26 present the data that are the basis of the comparison. Each figure has graphs that correspond to the flexible and rigid model-based designs (flex. and rigid) and to sensor configuration 'no acc.' and 'acc'. Specifically, Figures 2.25 and 2.26 present the trade-off between the smallest detectable fault and the detection time for the actuator fault detection. If accelerometer measurements are used, the performance of the filters designed for the rigid and flexible models are very similar for high detection times. If we aim to achieve lower detection time than 0.8 s, then a flexible model is clearly required, since the performance curves diverge in this domain. Without accelerometer measurements, the achievable performance is strictly worst but it is not affected by the choice of design model so heavily.

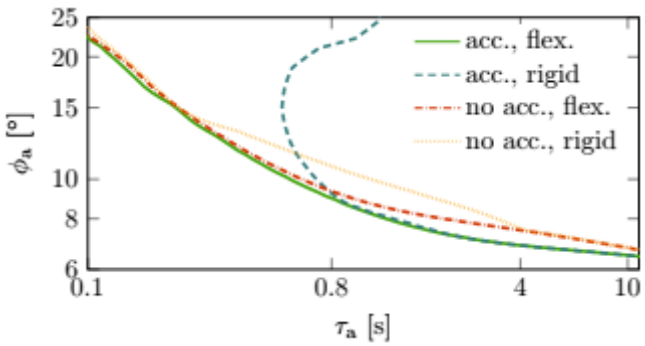

2.25. Figure: Trade-off between the smallest detectable fault and the detection time for the actuator fault detection.

The angle of attack sensor fault estimation is not affected as much by the model uncertainty and flexibility as the elevator actuator fault. Hence, faster and more precise fault detection is attainable overall. For low filter bandwidths (high detection times), the values are very close for all four options in Figure 2.25. Similarly to the elevator fault detection, the difference between flexible and rigid model-

based designs only show if we aim for low detection times. The difference however, is small (less than one degree) for the domain of our analysis. The worst performance clearly corresponds to the case when no acceleration measurement is used and the filter is designed for the rigid model. But since the performance measures track close to each other for all four cases, we conclude that the performance of the angle of attack sensor fault detection is not impacted greatly by the choice of design model or sensor configuration.In conclusion, guidelines are established on when a flexible model is required for FDI filter design for a flexible aircraft. It is concluded that only minor performance improvement is attainable for the angle of attack sensor FDI with the involvement of the flexible model. In contrast, the elevator FDI is greatly impacted by the choice of sensor configuration and design model. If good performance is expected at high frequencies (beyond the frequency of the first bending mode), then both acceleration measurement at the center of gravity and the flexible model are required. Still using the acceleration measurement, good performance is achieved using the rigid model up to half of the frequency of the short period mode. At the cost of some loss in accuracy, a design based on the rigid model is capable of providing acceptable performance up the frequency of the first bending mode if the acceleration measurement is not used.

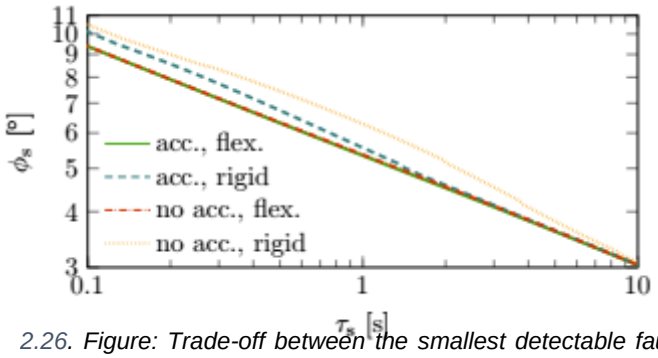

2.26. Figure: Trade-off between the smallest detectable fault and the detection time forthe sensor fault detection.

RCE with Modeling and Control Design Blocks (SZTAKI)

The performance evaluation is done in two steps. First, it is critical to evaluate the RCE implementation. This is presented for the modeling and control design blocks for the flutter suppression control design. The RCE implementation of these two blocks is shown in Figure 2.2.3.11.

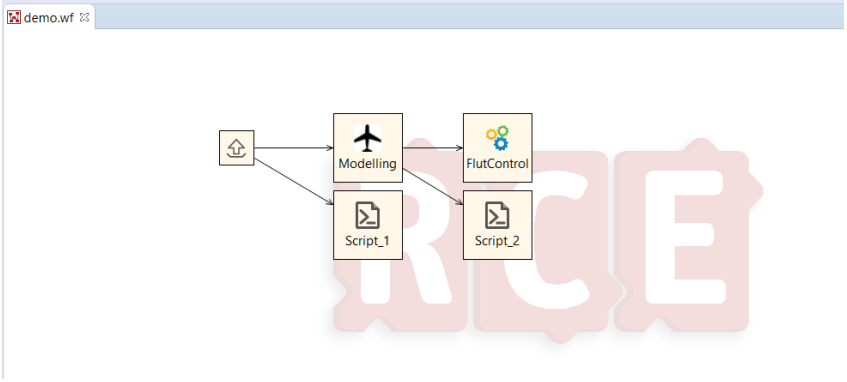

Figure 2.2.1.11 : RCE implementation of the modeling and flutter control design blocks.

First, an 'Input Provider' is used to send the initial CPACS file, then the Modeling component start processing and sets an output based on the actual modelling script, the output is forwarded to the Flutter Controller component. Both the modeling and the flutter controller design components function with a help from external scripts which act like wrappers between them and the actual Matlab files. The scheduling between the blocks is based on the data that is the output of the preceding block. The output is set using the post-execution commands of the modeling block. The output is written in the output directory in accordance with the wrapper, so when the current block finishes, the post execution commands are executed.

All RCE block communications and data sharing needs to be specified in addition to the scheduling of the RCE blocks. The control oriented modeling blocks output files are referenced in CPACS. These output files are given in the ToolSpecific field of the CPACS xml file. The control structure specifications of the four controllers needs to be defined in advance and these need to be set up in the ToolSpecific filed as advance. Besides the main control structure, the field needs to contain the sensors used by each controller as well as the control input signals.

The second step is to evaluate the results of the control design blocks. This step is carried out for each controller individually first. For the baseline controller the first step is to evaluate if the handling qualities are satisfied or not. If this can not be achieved by the resulting controllers then the handling qualities need to be relaxed. In addition to the handling qualities, robustness, gain and phase margins of the resulting controller is evaluated. The analysis results are also written in the corresponding ToolSpecific field of the CPACS xml file. The flutter controller is also analyzed if it satisfies the robustness analysis criteria.

A crucial aspect of the performance evaluation is to verify that the controllers do not degrade each others performance when all 4 controllers are connected with the aircraft model. Such behavior of the controllers needs to be considered already in the control design process blocks. The frequency grid separation, as presented in the previous section should prevent such behavior of the controllers. Namely, the bandwidths of each controllers should be clearly separated. If such frequency separation is not possible, then a remedy could be to design the controllers with overlapping frequency grids either as integrated controllers or by successive loop closures.

Finally, time domain simulations are also checked to see if the controllers work well with the nonlinear models.

2.3 Explanation of the work carried per WP- Work Package 3

The Work Package 3, Demonstration and Testing, has the following objectives:

- Model refinement using GVT data
- Model refinement using flight tests
- Performance verification of active control methods

In addition, the activities, related to all mechanical work such as manufacturing and integration are also covered by the work package.

Most of the tasks, as defined in the project proposal, are already active. Task 3.1, dealing with preparation of the demonstrator, has seen much activity starting in December, 2019, with planning of the needed upgrades for safe operation of the demonstrator. For the Task 3.2, Demonstrator Wing Design, sensor concept has been discussed for the new wing design, as well as an alternative plan in case manufacturing a completely new wing becomes impossible due to time constraints. Task 3.3, Manufacturing and Integration, had activities related to design and manufacturing of a new control module of the Flight Control Computer, the RXMUX. Most of the work has been performed under Task 3.4, Ground Testing of the Demonstrator. This included software updates and integration, multiple taxi tests of the upgraded landing gear and simulator training in preparation for the flight tests. In addition, ground vibration tests are in planning phase. During Task 3.5, Flight Test Specification and System Identification, plans for 1st Phase Flight Test Campaign have been made. One test flight took place in 2021, where important milestones have been achieved regarding the landing gear and also sensor updates. This was the first step towards Task 3.6, Flight Test Campaigns.

2.3.1 Starting point and approach

Initial state of the demonstrator

The project for TUM has started with a demonstrator, which has already been used in the previous project, FLEXOP. The demonstrator has performed six flight test up to then. However, building on previous experience, landing gear proved to be one of the biggest challenges during the operation of the demonstrator. The aircraft was very difficult to control while on the ground, leading to a few very dangerous situations and one accident, where the aircraft skidded of the runway and hit a runway light. Therefore, upgrades were necesary to ensure sustainable operation of the aircraft.

Figure 2.27. FLEXOP Demonstrator during the last flight previous year.

As a starting point, the following design flaws have been identified:

1. The maximum angle of attack, achieved on the ground, is limited by very low main landing gear and a high tail wheel. This design solution limits the maximum angle of attack that could be achieved for takeoff to 3.3deg. This is very small for a taildragger aircraft and usually would be around 10deg. In addition, fixing such a design on an already manufactured aircraft is not easy.
2. Very narrow main landing gear makes it easy for the aircraft to bank from wingtip to wingtip. If this happens during takeoff or landing, the wingtip touches the ground and instantly creates a destabilizing moment.
3. Main landing gear is longitudinally far from the center of gravity. This means that the disturbing bank angle, required to tip the aircraft, is further decreased.
4. The tires of the main landing gear are too soft for the airplane. This makes it possible to deform the tires very easily and also significantly increases the rolling resistance during take-off run.
5. Unsteerable tail wheel makes the aircraft very hard to control while on the ground. The tail has to be lifted up first and aircraft is then steered with the rudder.
6. Retractable main landing gear proved to be an unnecessary design add-on to the aircraft which adds complexity, but not value to the demonstrator overall.

These problems were hard to identify during the conceptual or preliminary design phase of the FLEXOP project and were only realized during operations. Therefore further discussion was held how to make the controlability of the aircraft better.

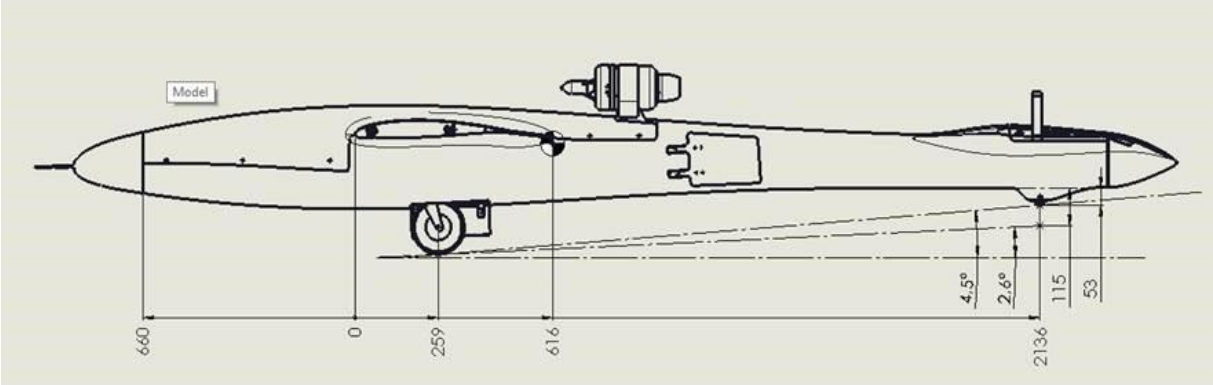

Figure 2.28. Comparison of the maximum angle of attack during take-off. 4.5 degrees is the initial tailstrike angle, 2.6 degrees is the tailstrike angle with steerable tailwheel assembly (wing incidence angle is -1.2 degrees).

Another objective during the first year of the project was to improve the operations of the demonstrator. This was done in three areas: streamline the operational procedures at the airport, change the electronic wiring to decrease number of actions required to set the aircraft up and improve role redundancy within the team. Therefore, further meetings were setup within the flight test team to discuss and streamline the preparation guidelines as well as think about how to make the crew planning easier. In addition, issues were identified in the electrical system of the aircraft that made the complexity of operations higher than it could be.

Since the data, gathered from flight test, had to be processed, some processing toolchains have already been implemented from before. Sensor errors were already being dealt with, as well as logging errors. The end product would be a single file with clear data structure inside that could be used with MATLAB for further analysis. However, the ultimate goal is to streamline the processing of the data as much as possible. This would include a completely automated data processing, where very minimal operator action is needed. In addition, the automated processing would compile a preliminary test report, allowing to analyse the outcome of the test on the fly.

2.3.2 Efforts and achieved results, name involved contractors

Improving the landing gear

Two different concepts for fixing the landing gear were discussed:

1. Fundamentally changing the landing gear layout.
2. Adjusting the current landing gear to make it acceptably safe for operation.

Because of the fact that the first option would require major fuselage changes and would take at least a few months, it was decided to start with the second option first. Ways to improve handling were discussed during the winter before the first flight test campaign. Due to the complex nature of the problem the solutions that were initially agreed upon did not completely resolve the issue. This resulted in an iterative process with different concepts being implemented as add-ons to the initial design along the way. The chronology of the process was:

1. Implement the steerable tailwheel with damping
    a. The initial solution to steering was to install an off-the-shelf tailwheel assembly. Unfortunately, the solution did not work because the load on the tailwheel appeared to be too big for the part. Therefore another, completely custom iteration was done. This included a custom milled aluminum fork for steering and a damping assembly. The

damping assembly was composed of glass-fiber-reinforced plastic plate acting as a leaf spring for longitudinal damping and two rubber dampers for lateral stiffness. The structure held well, but the steering made the aircraft hard to control and very sensitive to any pilot inputs.

2. Change the brakes of the main landing gear to more effective ones
    a. Tire brakes were changed to drum brakes. From previous testing it was noted that the tires wear out very quickly due to the brakes. Also, the braking power of the old system proved to be too little. Therefore, new type of brakes was implemented that would both conserve the tires and increase the braking force on the wheel hub.
3. Add a gyro to the tailwheel
    a. Introducing the steerable tailwheel did not solve the controlability problem as the team has hopped. The aircraft became very sensitive, especially at higher speeds. The solution was to introduce a gyroscope-based compensation for the gain on the steering. This proved to improve the steering somewhat.
4. Reverse the main landing gear frame to shift the ground contact point back
    a. One of the main findings, mentioned in the early research on taildragger aircraft is that the tendency to veer of the runway is decreased if the centre of gravity is kept as close as possible to the main landing gear. This was recorded in all the reports on the topic. Therefore, changing the location of the landing gear was considered. Luckily, the landing gear frame was easy to flip, moving the main landing gear backwards by 75mm. The outcome was lesser tendency to veer off the runway, an increase to the critical bank angle to tip on one wing, but also higher load on the main tires. Even though the weight increase was only 2.5% per wheel, the main tires were already overloaded before. The further steps would include looking for stiffer main tires, if possible.
5. Laterally stiffen the main landing gear assembly
    a. During the taxi tests cameras were mounted facing both the gears. This helped to observe the behavior of the landing gear and make further conclusions. One of them was that the main landing gear is too flexible laterally, which makes it easier to tip onto one wing and harder to get out of the tipped position. Therefore, further parts were introduced to stiffen the landing gear laterally.
6. Change the main wheels to stiffer ones
    a. Even though the gear was made stiffer, it was recognized that the tyres of the main gear are way too soft for the aircraft. This was discovered during one of the testing days, where the aircraft stood on the ground for a couple of hours. As a result the foam-filled tyres deformed plastically and were not usable anymore. Additionally, during high speed taxi tests a set of tyres burst into pieces after they got too hot (Due to braking and rolling). It was decided that a stiffer tyre is a must. And with no alternative tyres available for the same wheelset, a double sailplane tailwheel (TOST 150 MINI) instead of the original RC model grade wheels were bought. The TOST wheels would have a proper inflatable tyre moutned on, which would make the main gear stiffer laterally.
7. Add brakes with higher efficiency
    a. In addition to upgrading the wheels to stiffer ones, the TOST wheels also had a possibility to have disc brakes mounted on them. Since long braking path was also discovered to be a problem during our flight tests, this seemed like a good option.

The changes of both, main gear and tailwheel resulted in a considerably more steerable aircraft. Multiple taxi tests were done, including low speed and high speed tests, to make sure the aircraft has

enough controllability to safely resume flight testing. In the end, changing the main wheels from RC model grade to aviation grade seemed to make the biggest difference. The aircraft was declared as flight-worthy again.

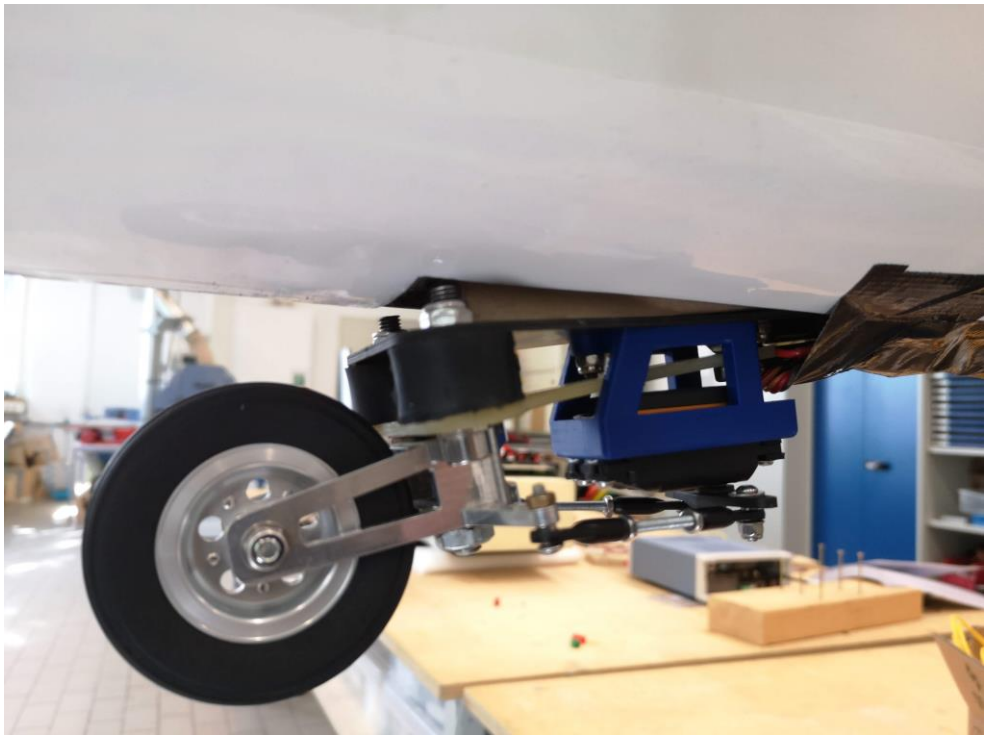

Figure 2.29. Steerable tailwheel assembly.

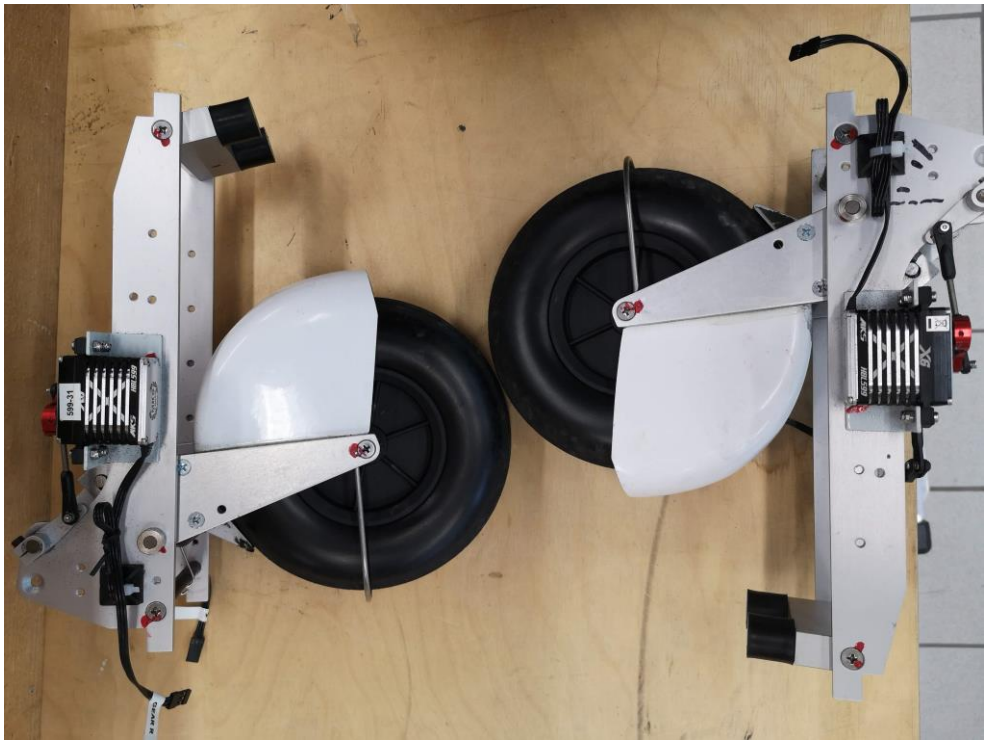

Figure 2.30. Comparison of two possible positions for the main landing gear. The difference is around 75mm.

Figure 2.31. Too soft tires deforming under normal load.

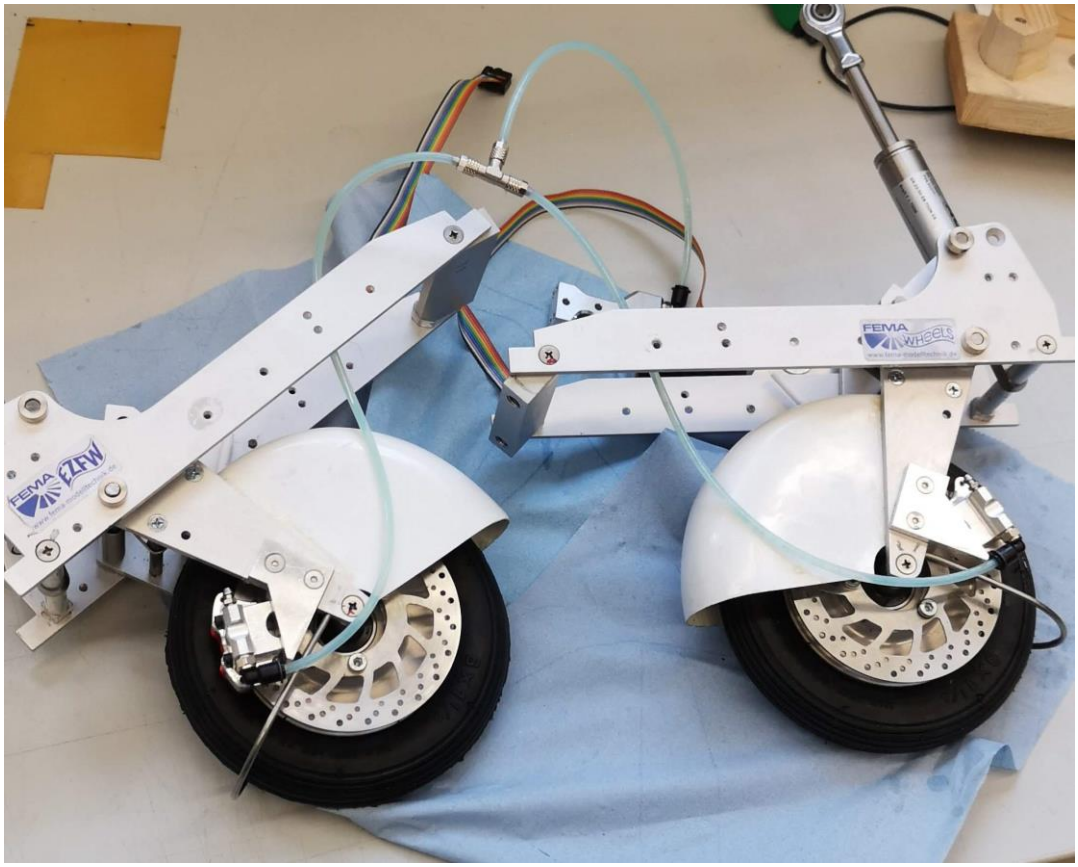

Figure 2.32. New main wheels being fitted with disc brakes before instalation.

Flutter damper mechanism

Another activity that relates to preparing the demonstrator for flight test campaign is the development of an emergency solution for the upcoming flutter tests. The idea was to be able to reduce risk of losing the demonstrator by creating a device that would completely change the resonant frequency of the flutter wing (-1), stopping it for flutter. The pilot would trigger this device in case of extreme wing flutter. Currently, the device is being designed and tests are being planned for the upcoming winter.

Improvements in electrical system

Past flight tests showed the need for the ability to put the FLEXOP demonstrator into a power-saving stand-by mode that allows extended waiting times with quick reaction times to use unexpectedly opening flight windows. The past efforts addressed these two issues.

In order to implement a stand-by mode for the aircraft, the power consumption of the demonstrator needed to be reduced to a practical amount by selectively shutting down components that feature a high power consumption, should not be operated idle for extended times and/or have a quick und uncomplicated boot-up process. The power supply system has to be capable to either run the remaining components over an extended period of time or capable of keeping the components running while batteries are being swapped. After an analysis of the existing system and iterative review of different possibilities the following measures were decided upon:

1. Adding a circuit breaker in the power line between one 2S-batterie and the power-distribution board.
2. Rerouting the cable supplying the RX-MUX-boards to the splitting point before the circuit breaker.

Thus, in order to put the demonstrator into a power-saving stand-by mode, the following main steps need to be performed:

1. Moving the power switches of the FBG-interrogators to “OFF”-position.
2. Disconnecting the 3S battery.
3. Removing the circuit-breaker of the first 2S-battery.
4. Disconnecting the second 2S-battery.

In this state, the 6S-battery is only powering the Raspberry Pie of the FCC flight stack, which can be supplied for several hours. In order to start up the demonstrator for flight tests, the above steps are undone in reverse order.

After the implementation of the changes to the power system, a new landing gear was rigged in. The new landing gear setup features linear actuators for retractiion and deployment, as well as drum brakes that were expected to have a higher holding force and less wear on the tyres than the stamp brakes used before. The b reakes work with three different voltage levels, i.e. 12 V, 7.2 V as well as 6 V. The different voltage levels are supplied by the 3S-battery and the 2S-batteries respectively. In order to provide a supply voltage of 6 V, a DC/DC-converter was introduced that supplied both gear system. During testing the brake servos did not operate reliably. Investigastions on the system yielded a signal-cross-talk from one servo signal line to another. The problem was solved by introduction of another DC/DC-converter.

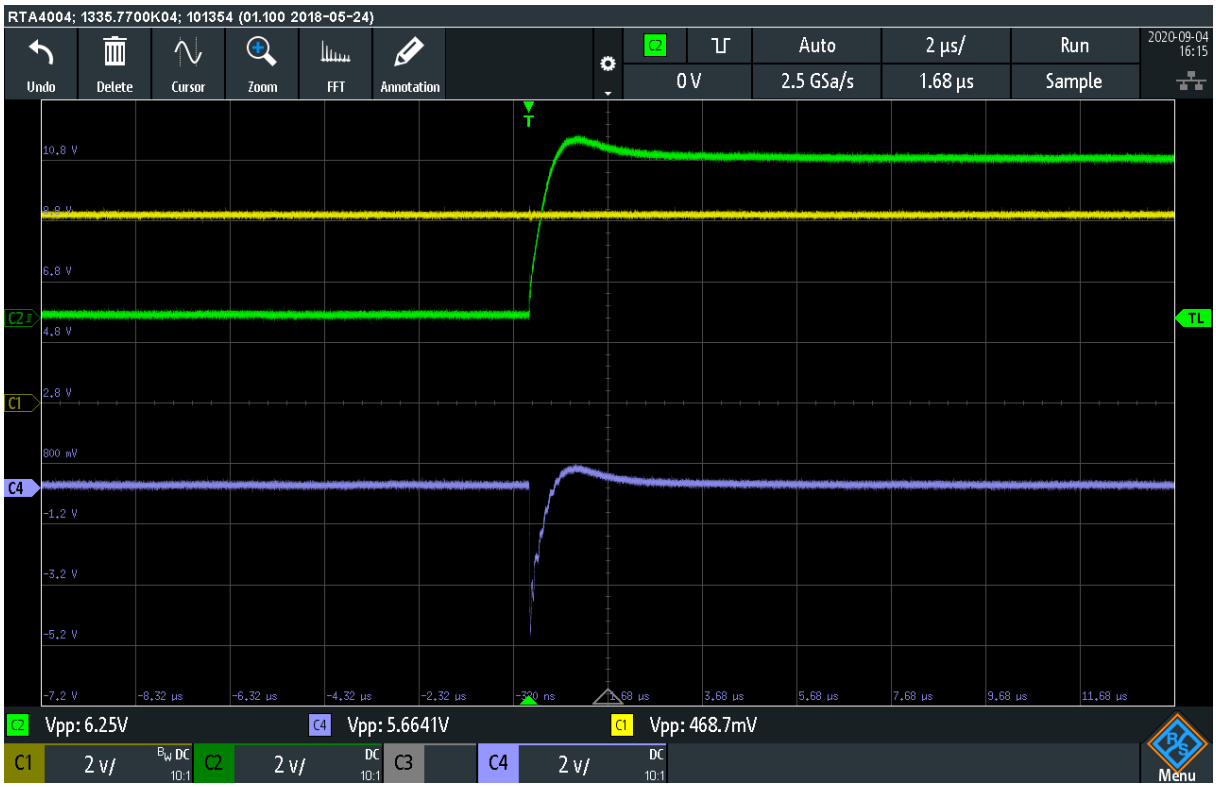

Figure 2.33 - Close look on the cross-talk, when only one step-down converter was used for both actuator. The peak value of the noise overshoots the standard TTL logical threasholds.

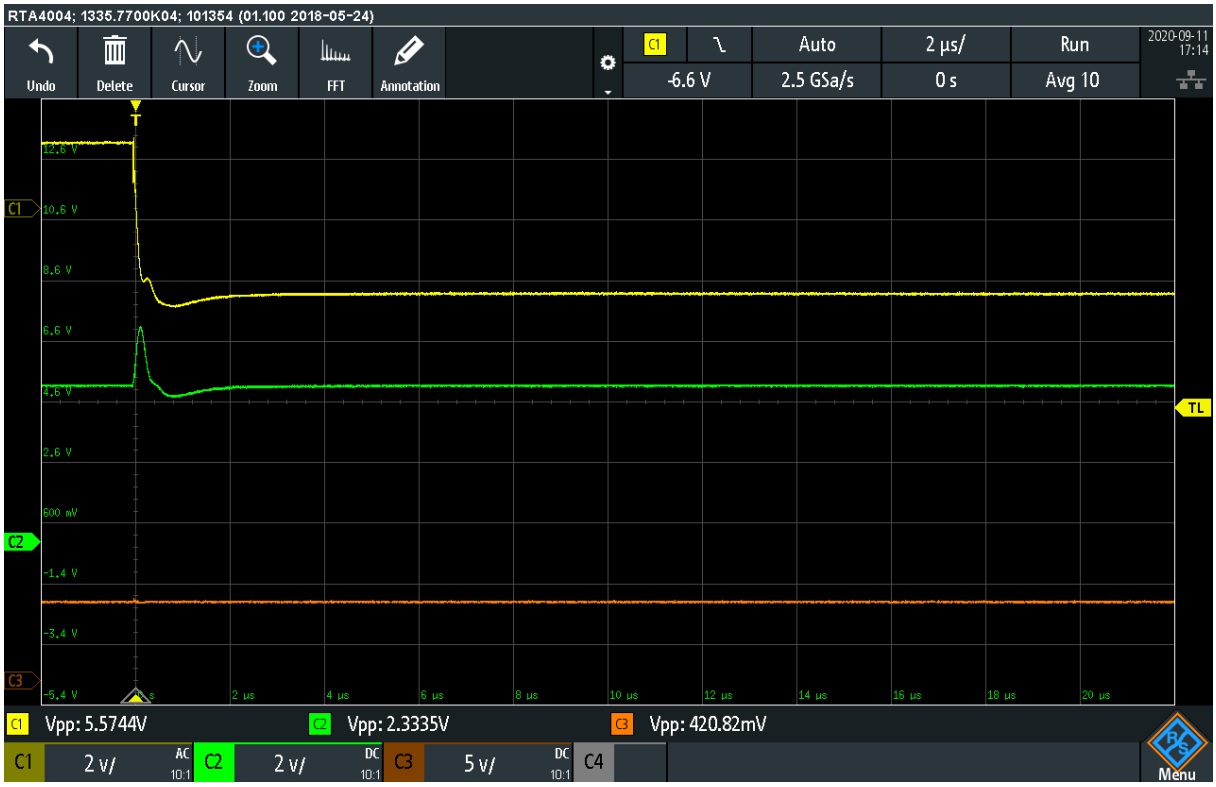

Figure 2.34 - Crosstalk still visible with dedicated step-down converters. The noise peak is still high, but it does not show visible error on the system itself.

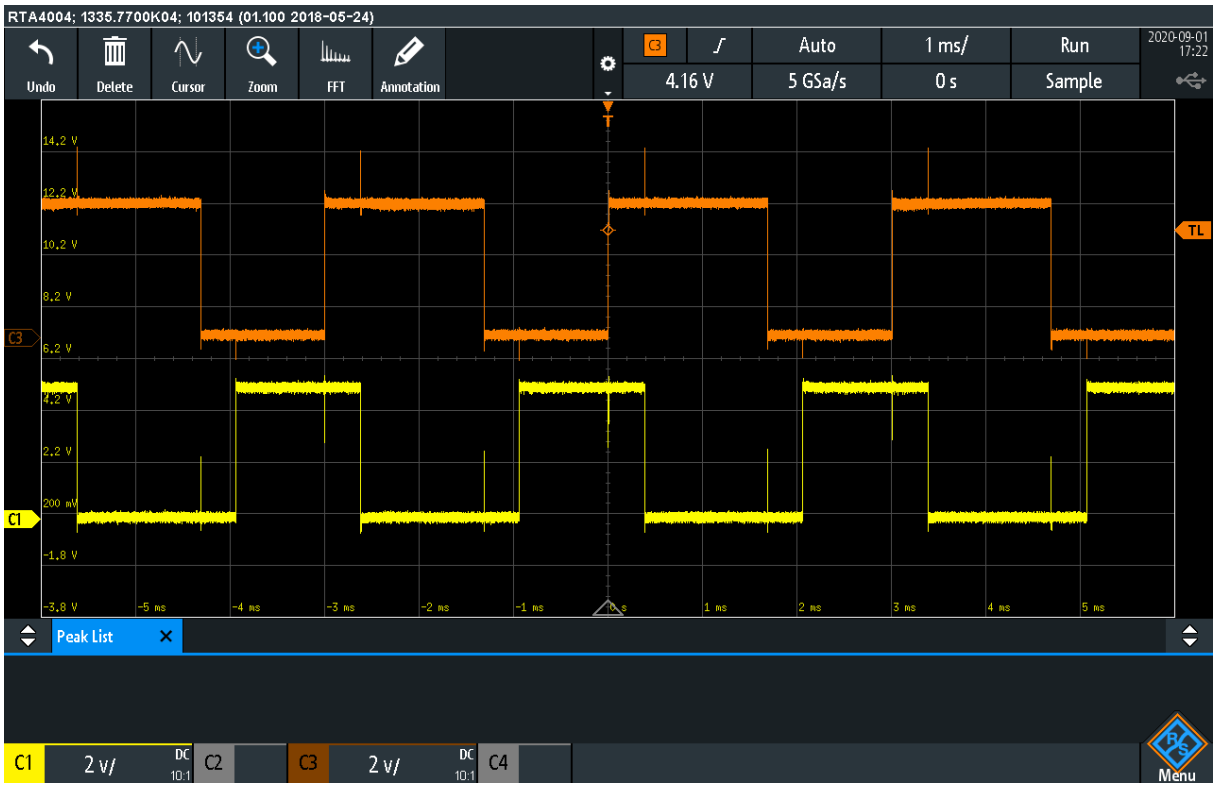

Figure 2.35 - Visible cross talk on the independently generated PWM lines, when actuators are attached.

A secondary on-board computer was added as well to the FCC stack. That system now runs a program developed by DLR. The secondary on-bard computer is a raspberry pi 4, and it has a direct telemetry connection to the GCS. Currently it runs dummy simulation, and provides live telemetry feed to the GCS for testing.

Later, this device will collect all additional measurements provided by newly introduced systems.

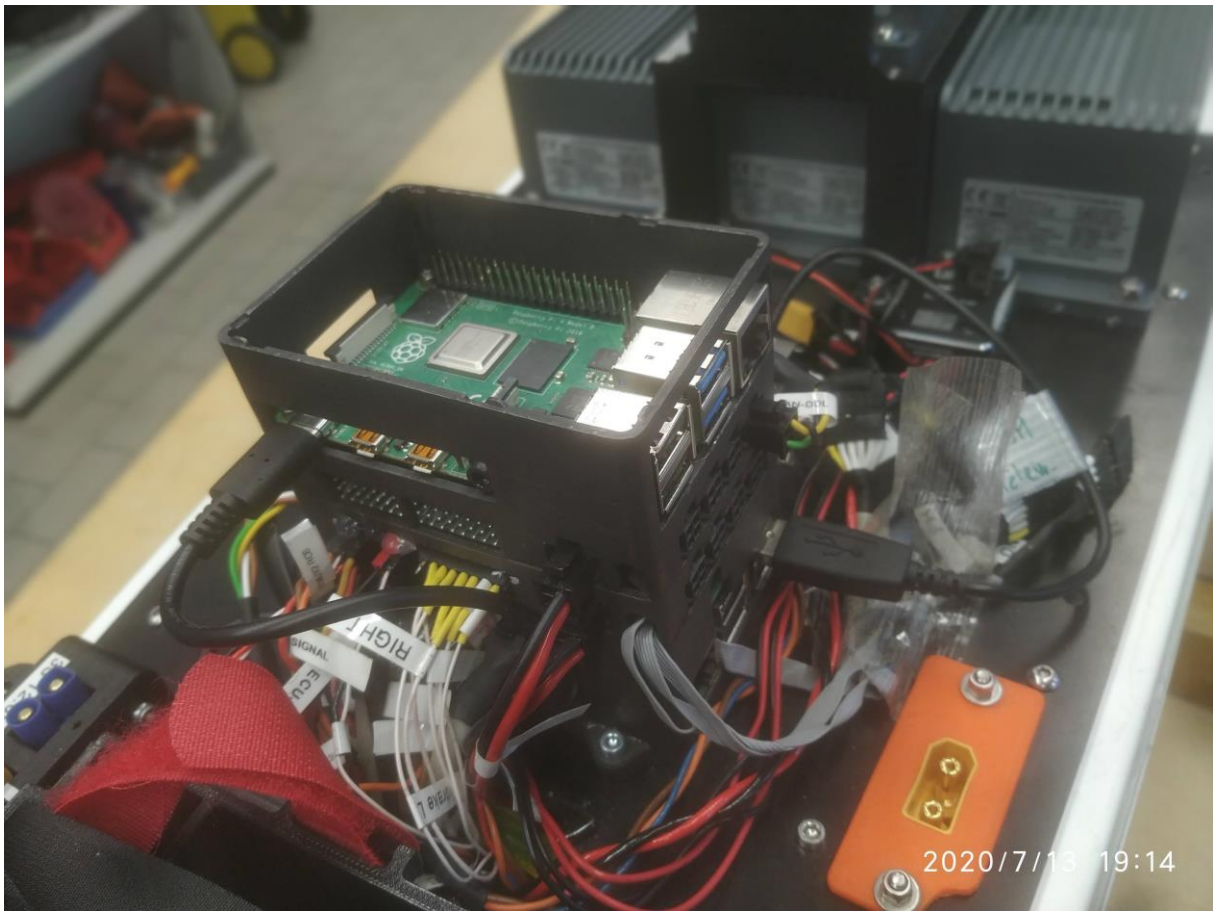

Figure 2.36 - Secondary on-board computer on top of the existing flight-stack.

Improvements in telemetry system

Former experience has shown, that the focus of interest in different data sources shifts between flight tests. While initial flight tests focus on system checks, data yielding information about the system performance such as temperatures, currents, voltages and fuel flows are of greatest interest to assure safe flying. With increasing routine and experience with the demonstrator, focus gradually shifts to different data such as airspeed or altitude to attain and keep the planned test conditions or the identification of different modes. This shift in focus also manifests itself by the adaption of the data displays and mode of visualization. The current display of the Engineering Data Link developed in Mathworks Matlab does neither offer the necessary flexibility to change display layouts fast nor does it offer a great variety of different modes of display. In order to improve the flight test efficiency by usage of more flexible displays, NASA's OpenMCT framework was implemented and adapted for flight testing of the FLEXOP flight demonstrator. Expected advantages of the new visualization framework are flexible adjustment of data displays, saving of different views that can be switched easily, a wide variety of widgets already available, data "playback" functionality that greatly improves and facilitates flight test debriefings as well as the increase of flight test participants by providing flight data live to remote participants, that can provide additional expertise.

Figure 2.37: Display of NASA's OpenMCT visualization framework during flight tests using the DG-800 S flying testbed.

A working state of August 20 is displayed in the Figure. The moving graphs are widgets that can be adjusted in size and colour as well as types of data displayed.

To date the functionality that has been tested with the FLEXOP flight demonstrator is the display of different modes and normalized eigenfrequencies identified by the secondary Raspberry Pi developed by DLR Göttingen using OpenMCT. Flight monitoring functionality – including safety critical - and flight test adjustment ability has been field-tested and validated using the DG-800 S flying testbed of LLS. This type has great resemblance with the FLEXOP configuration (sailplane with dorsal turbine) and has already been employed for pilot training. Combined with an antenna-tracker, which provides a high-bandwidth connection to the testbed using 5GHz-Wifi, data collected for sytem identification of rigid modes has been streamed down and displayed live in OpenMCT. During flight tests conducted, the reliability and flexibility of the framework was proven: E.g. the data visualization enabled the identification of a sensor failure, which allowed the adjustment of the fight test routine including a change of data displayed. Furthermore, the display proved to be so realiable, that a reduction of safety margins concerning fuel available was possible, which resulted in a near-optimal use of flight time. Initial tests showed the possibility to increase the number of flight test participants by streaming available data to a server, from which it is accessible remotely.

Upcoming efforts will target the implementation of a 5GHz Wifi, high-bandwidth downlink from the FLEXOP flight demonstrator and development of display templates required for future flight tests. Therefore, a Wifi-connection will be established to the secondary RaspberryPie, which will send down data necessary to duplicate the Engineering Data Link. The amount of data will gradually be increased in order to provide flight test relevant data to the operators. On the hardware-side, integration of servers and an LTE-router are ongoing and will enter consolidation and commissioning phase next.

In order to make full use of the capabilities of OpenMCT, an antenna-tracker was field-tested and commissioned for flight tests using the same DG-800 S flying testbed as employed for testing OpenMCT. The antenna tracker depicted in the figure below.

Figure 2.38: The antenna tracker being prepared for DG-800 S flight tests.

The tracker uses its own as well as the UAV's position to align the antenna to a position facing the UAV in air. During flight tests, 400 values per second were received and processed without experiencing drop-outs. The testcases included distances of 700 m and more, as well as close inverted flybys to test the systems robustness in case a bad GPS-reception. Given the experience of related projects, it can be assumed that the system's capabilities are not maxed out yet.

Therefore, next efforts will focus on further testing of the system as well as increasing the traffic on the data link to use the antenna tracker to its full potential.

Following up, efforts have been undertaken to integrate the telemetry links and assets (MAVLink, EDL, antenna tracker and Open MCT) into one system, allowing for greater flexibility and simpler usability. It is planned to unite all data streams on a single server, hosting Open MCT and forwarding the required information to clients on the flight field and remote using a LTE connection. Furthermore, the GCS van is outfitted with a roof mount for the tracker that allows a setup before the GCS van is moved towards the runway before a flight test, saving valuable time just before a start. To date, a dedicated Open MCT display is being setup for controlling the antenna tracker as well as the network of a sample application integrated piece by piece.

Thrust measurement system

As one of the goals of the project is to use active control for drag reduction, drag measurement in-flight would be necessary. This requires the thrust created by the engine to be measured. Conversely, the thrust is a difficult parameter to measure.

Several methods have been developed and tested, whereas the most reliable require multiple sensors throughout the engine. These provide values that can be used to calculate the corresponding thrust. Such are known as gas-generator methods and are suitable for large aircraft, which have been designed with extensive sensory network within the engine. In contrast, smaller propulsion units such as the B300F that powers the FLEXOP demonstrator aircraft do not have provisions for the installation

of pressure and temperature probes. Thus, the required modifications to the engine's structure hinder theviability of gas-generator methods. As an alternative, simplified and swinging probe methods were considered. These require no sensors inside the engine but are limited to gross thrust measurement, not sufficient for drag determination. Further, brochure and acoustic-based methods were studied but due to limited data provided by the engine's manufacturer, calibration would be complex and limited reliability would be achievable. Consequently, the trunnion thrust method was the option chosen as the most viable for a thrust measurement system to be installed on the FLEXOP aircraft. This technique is usually not considered feasible for larger aircraft due to the high complexity of the engine attachments, including multiple connection points as well as cables, pipes and hoses that make load path determination difficult. However, for a small aircraft, the attachment structure can be significantly simplified without affecting other systems and having higher design flexibility. As a result, the trunnion thrust method is suitable for this type of aircraft. Accordingly, a new attachment structure between the B300F engine and the aircraft's body was designed, whereas particular attention was given to obtaining a well-defined path for load transmission. More specifically, the structure was designed to form a statically determinate system when modeled in the aircraft's XZ-plane (symmetry plane). Thus, it is possible to determine the thrust force by measuring the load at a single support point with a load cell. Moreover, alternatives that kept the measuring system simple were preferred. For this reason, interference from varying vertical and lateral force components during flight maneuvers is not counteracted by implementing multi-axial load cells or devices that offer compensation for off-center and lateral loading. Instead, the support to which the load cell is installed was designed to only transmit forces in the measurement direction. This was achieved by implementing the support as two heim joints with the s-beam load cell installed between them. Thus, sensory complexity was kept low and bulky and heavy electronic components were avoided.

Additionally, the mentioned support was placed in the aircraft's symmetry plane to limit effects caused by thermal expansion, which have been a factor in previous attempts to implement the trunnion thrust method. In comparison, the other support points were implemented as rolling-element bearings placed on the sides of the structure. This allowed increased lateral stiffness for safer handling of the unit during maintenance operation but maintained the mechanical characteristics in the symmetry plane. Also, the configuration allows for low friction, which has been identified in previous projects as crucial for limiting the bending moments transmitted by the bearings and for allowing precise measurements. The final design is displayed by figure Figure 2.39. The structure was also designed with high measurement accuracy as a goal. For this reason, the positioning of the components was defined such that it minimizes errors. In fact, due to the ratio between the relative distances of the support points to the engine's center, all errors induced by the load cell and the analog-to-digital (ADC) conversion are nearly halved. This was shown by an error estimation performed using data provided by the load cell's manufacturer to predict the deviation between the actual applied thrust and the expected measured value, as shown in Figure 2.40. According to the diagram, the system would deliver an accuracy of about 0.4N and better at lower thrust levels. However, this estimate accounts only for load cell errors as well as ADC quantization and amplifier drift error. Therefore, additional influences such as higher temperature oscillations, manufacturing tolerances and further errors from the ADC (e.g. noise) may lead to lower performance and must be considered for a more accurate and extended prediction.

The system has already been compared to a measurement with a running engine on a static thrust measurement stand. The comparison graph can be found in Figure 2.41. The maximum deviation at full thrust was found to be around 5N, or 1.7% (the spike in the graph is due to misalignment of the systems). This, however, does not take any possible misalignment of the two systems or the deflection of the engine stand. These sources of errors are currently under investigation and the accuracy is expected to be improved further on:

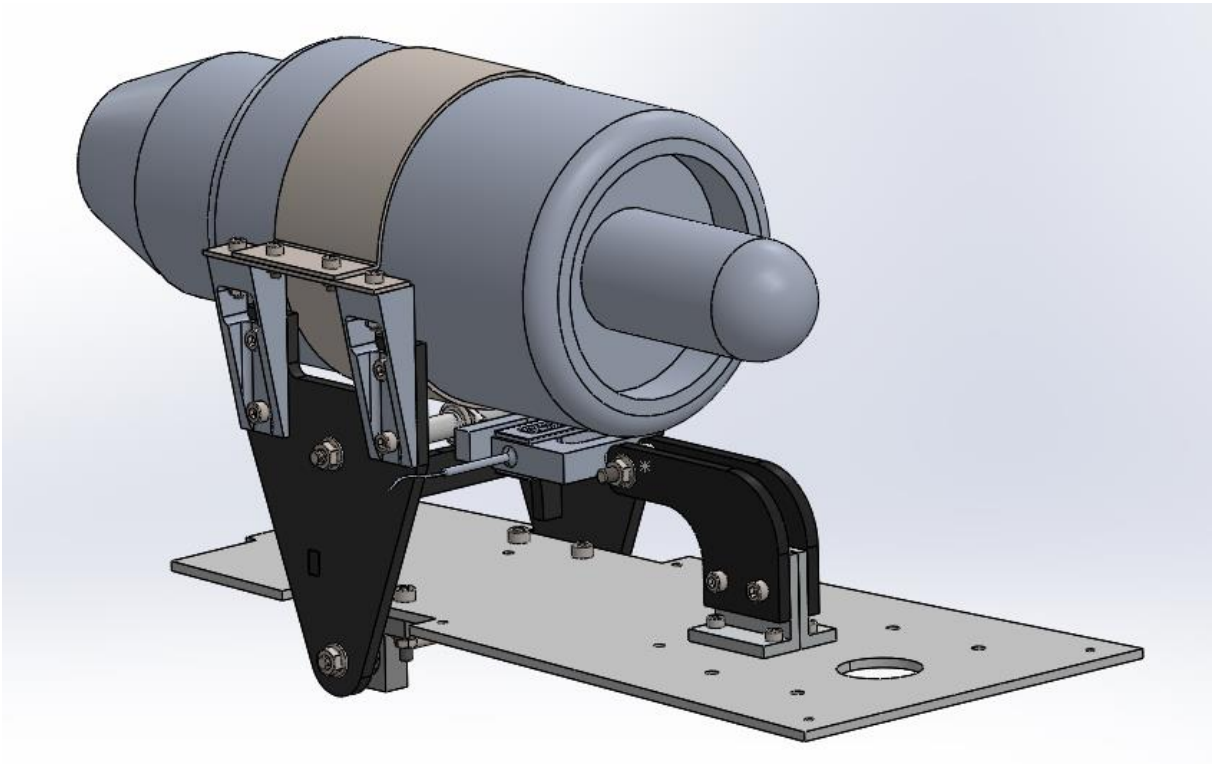

Figure 2.39. Thrust measurement unit with the mounted engine.

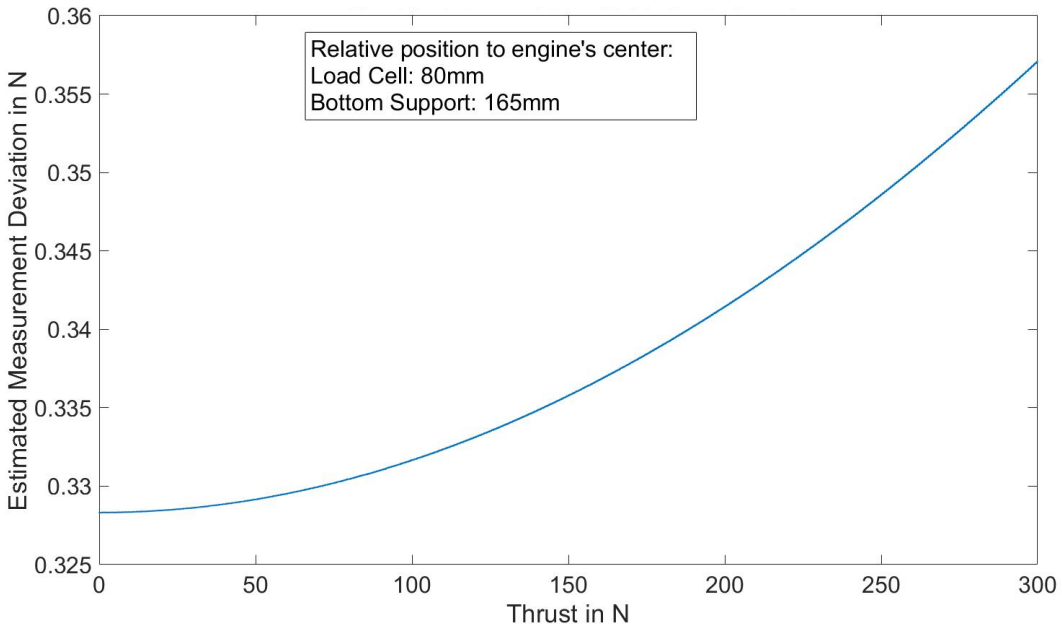

Figure 2.40. Estimated measurement error at chosen component positions for entire thrust range.

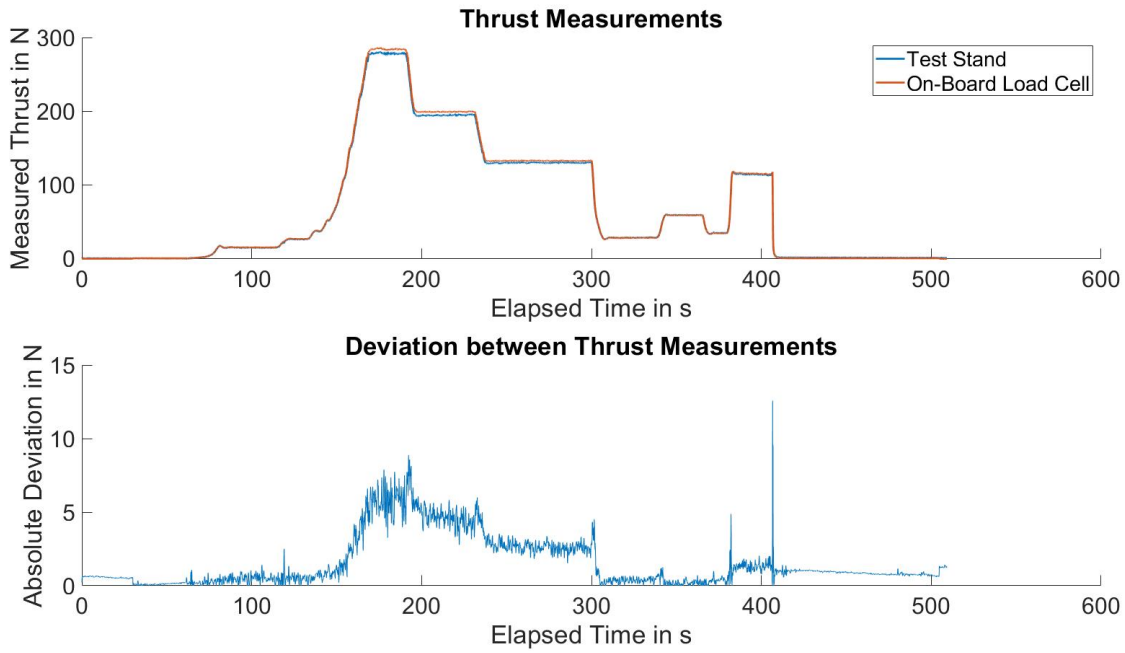

Figure 2.41. Comparison of on-board and static thrust measurements.

To decrease the errors within the system, deflection measurements were done. Initially it was suspected that the system deflects around 3deg during the maximum thrust phase. 3D scanner was used to check this (Figure 2.42). It was found that the system is stiffer than expected and only deflects 1deg at maximum thrust.

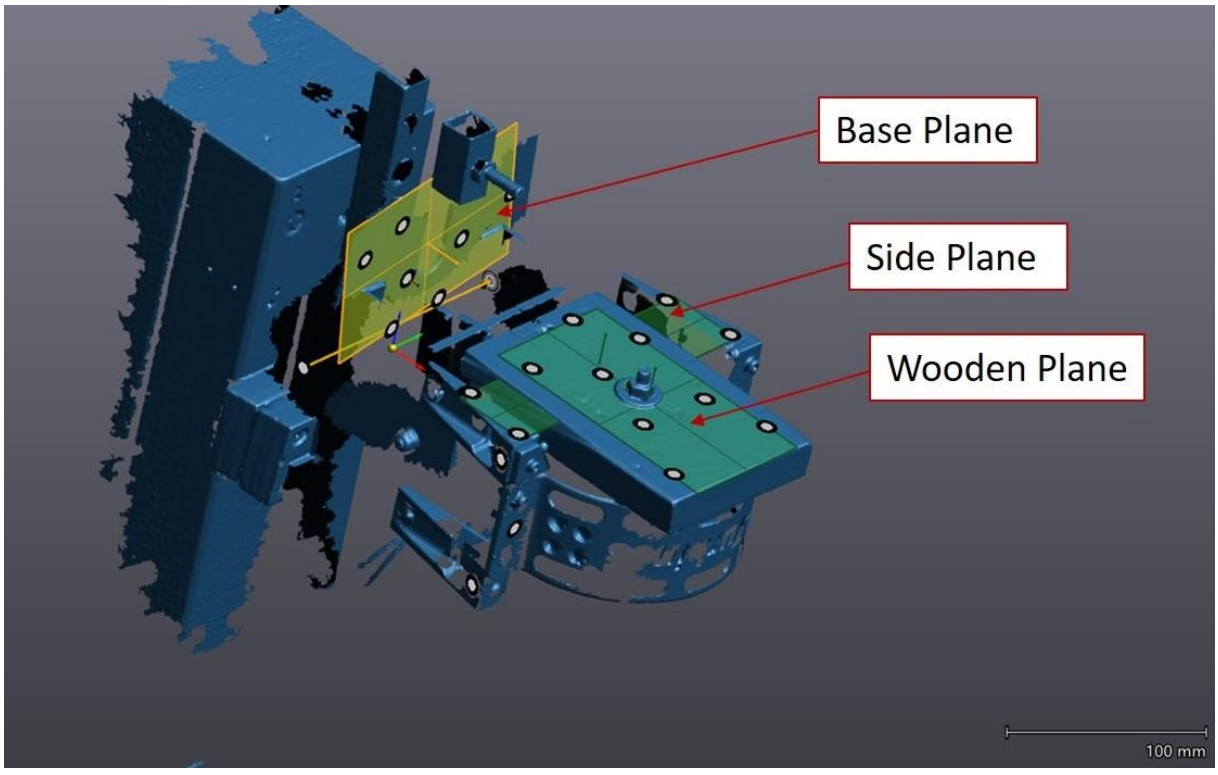

Figure 2.42 - Deflection measurements of the thrust measurement system using the 3D scanner.

Another calibration test with weights was performed. The resulting error plot can be found in Figure 2.43. Deviations within [-0.5:+2.0]N were measured.

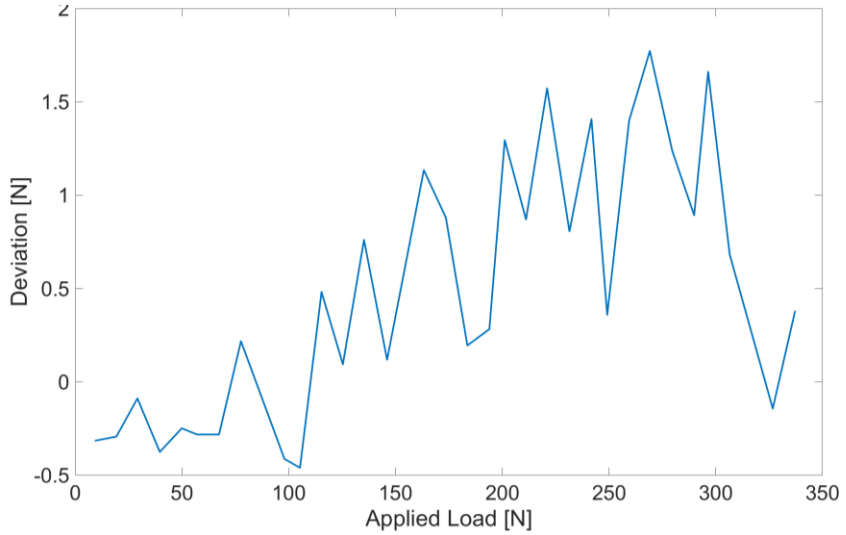

Figure 2.43 - Thrust measurement system deviations in between the measured and applied load.

After successfully verifying the system's functionality, it was installed in the demonstrator. To test the system on a regularly basis, a calibration procedure, which can be easily performed just before the flight, is required. Hence, instead of the weight blocks, the engine and its mounting structure should be used as a known weight. By tilting the aircraft, this weight induces a force on the load cell. This force can be calculated by using the pitch angle θ and

The data of this calibration should be evaluated by a Matlab code which calculates the Zero - Load Value and plots of the sensor value versus applied load. To verify the functionality of the Matlab code, the procedure of the calibration was as described beneath:

1. Tilt the aircraft forward (Nose down): This imposes a compression force on the load cell. It is the same calibration as with the weight blocks, and hence, simulates the running engine. The pitch angle θ is negative.
2. Tilt the aircraft backwards (Nose up): This imposes a tension force on the load cell. The pitch angle θ is positive.
3. Roll clockwise: The roll angle φ is negative.
4. Roll counter-clockwise: The roll angle φ is positive.

For this procedure the SFD, without the wings being mounted, was lifted by two persons. The rolling of the aircraft is only included to verify the correct mathematical implementation of the roll angle φ in the Matlab code. For the proceeding of this calibration just before the flight, it will not be possible to roll the aircraft in this scale, neither will it be useful because the rolling ideally does not induce any weight on the load cell. To provide sufficient data, the calibration procedure was repeated three times. A plot of the angles can be seen in Figure 2.44.

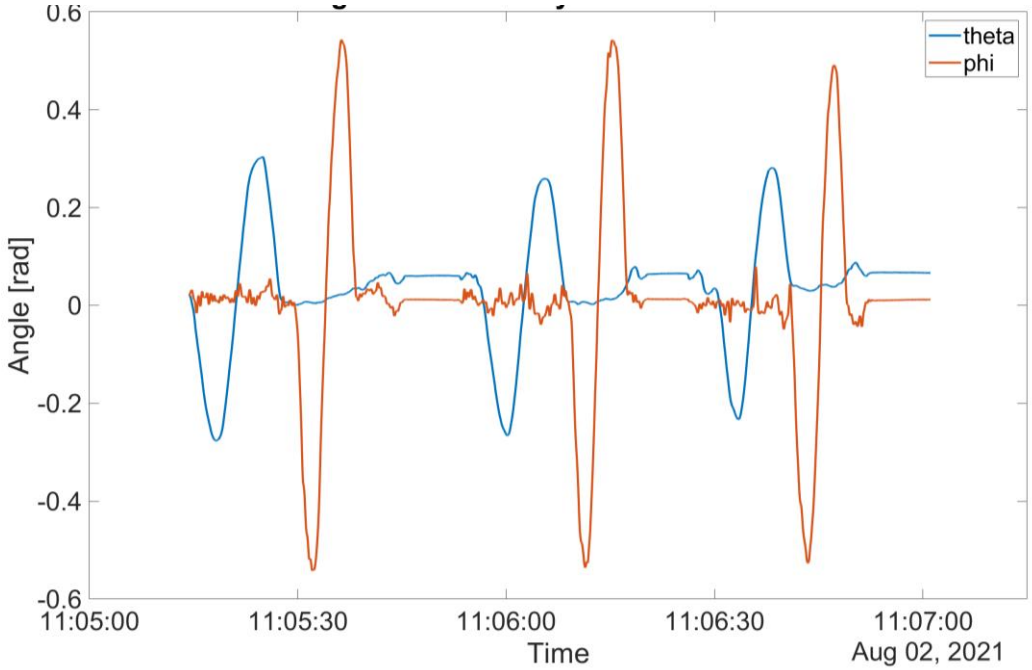

Figure 2.44 - The pitching and rolling procedure for in-situ thrust measurement system calibration.

As it can be seen the pitch angle θ is limited to roughly 17 degrees. This is due to the weight and the dimension of the aircraft. Unfortunately, this issue limits also the applied weight on the load cell to roughly 16N (Figure 2.45).

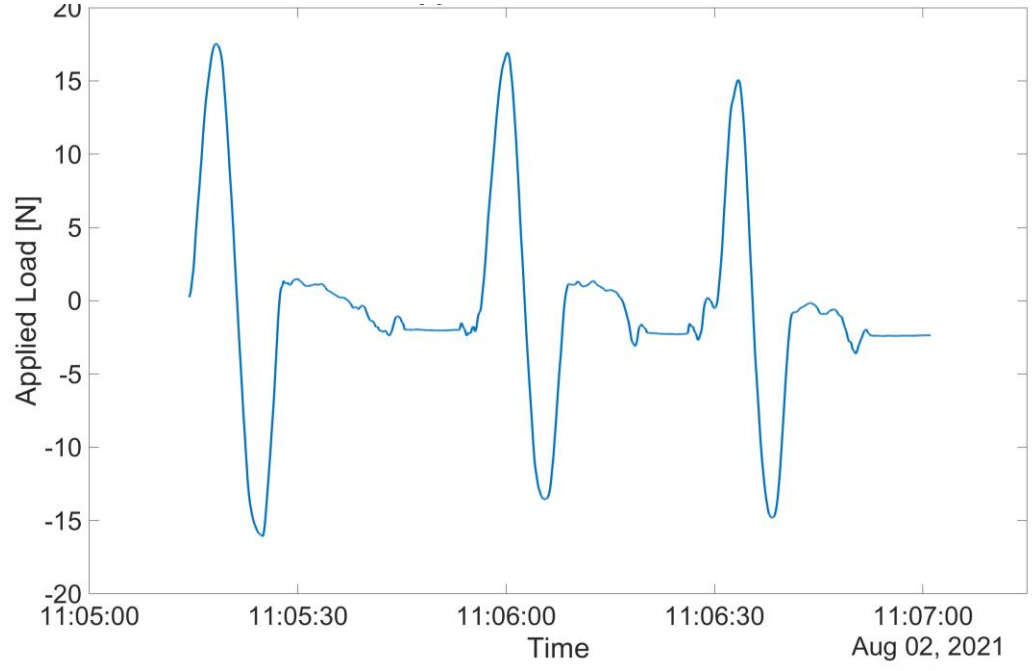

Figure 2.45 - Applied load during the in-situ calibration run.

The in-situ calibration results are further compared to the weight tests in Figure 2.46. The results are currently in further analysis to extract a methodology how to further decrease the measurement errors.

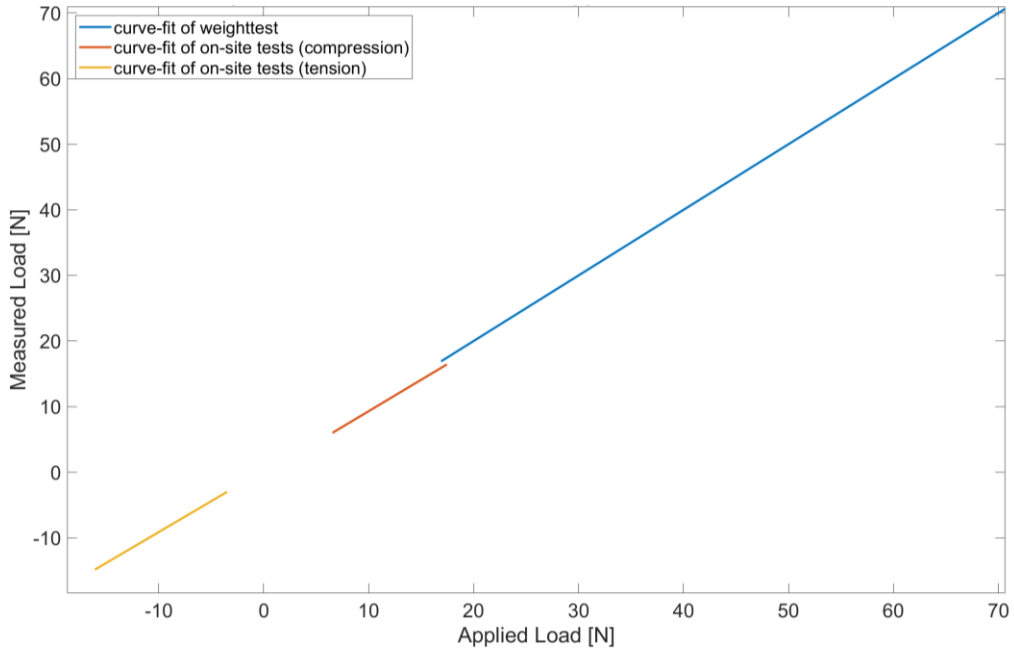

Figure 2.46 - Comparison of in-situ calibration and calibration with weights.

Air-data and IMU sensor mount updates

During the flight test data analysis phase (with the flight test data from 2019) it was noticed that the angle of attack signal is corrupted with noise which is not visible in angle of sideslip. Figure 2.47 shows this difference in signal noise during flight path reconstruction of a flight segment. Angle of attack sensor appears to have a visible adiditonal noise to it, which does not exist in the angle of sideslip. The sensor was checked in the wind tunnel and it was clear that the problem is not with the sensor itself as the spectral densities in both angles were the same (Figure 2.48, right). It was therefore postulated that maybe the mounting of the sensor is not rigid in the longitudinal plane.

The mounting of the pitot boom was therefore investigated. The mounting of sensor was done in a way that the air data boom would go through the nose section of the fuselage and then would be mounted on the payload rack board at the root (Figure 2.49 and Figure 2.50). It was then realised that the payload rack, which is a 3mm glass fibre board with many equipment mounted on it, would move vertically during manoeuvres and in this way would move the root mount of the boom as well. Considering that the middle point of the boom, which goes through the fuselage, acts as a rotation point, the actual sensor head therefore gets deflected (Figure 2.51). It was also recognised, that the main IMU sensor is also mounted on the flexible glass-fibre board. Therefore relocation of both main sensors (xSens and Aeroprobe) has to be done.

The air-data boom mount was upgraded by designing a new, rigid structure from carbon-fibre sandwich in the nose section of the fuselage (Figure 2.52). The purpose of the structure was to decouple the air-data boom mount from the rest of the payload rack and increase the stiffness of the point where the boom intersects the fuselage (the front wall). Solution was implemented.

In addition, the xSens was relocated onto a stiff mounting point next to the fuel tanks.

A single test flight has been done with the new sensor setup. The sensor error analysis of the new setup is not yet completed.

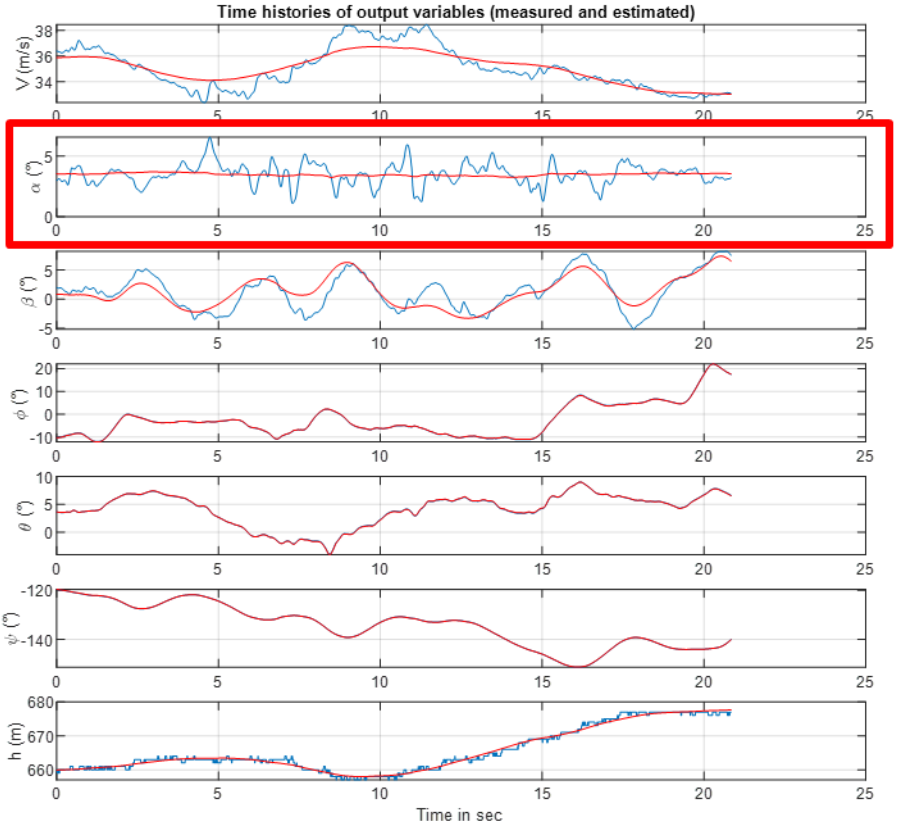

Figure 2.47. Data compatibility analysis (also known as flight path reconstruction). Ideally, the measured and estimated signals should match. Blue- measured signal, red- estimated signal. Clear difference in noise levels between angle of attack (alpha) and angle of sideslip (beta) can be seen.

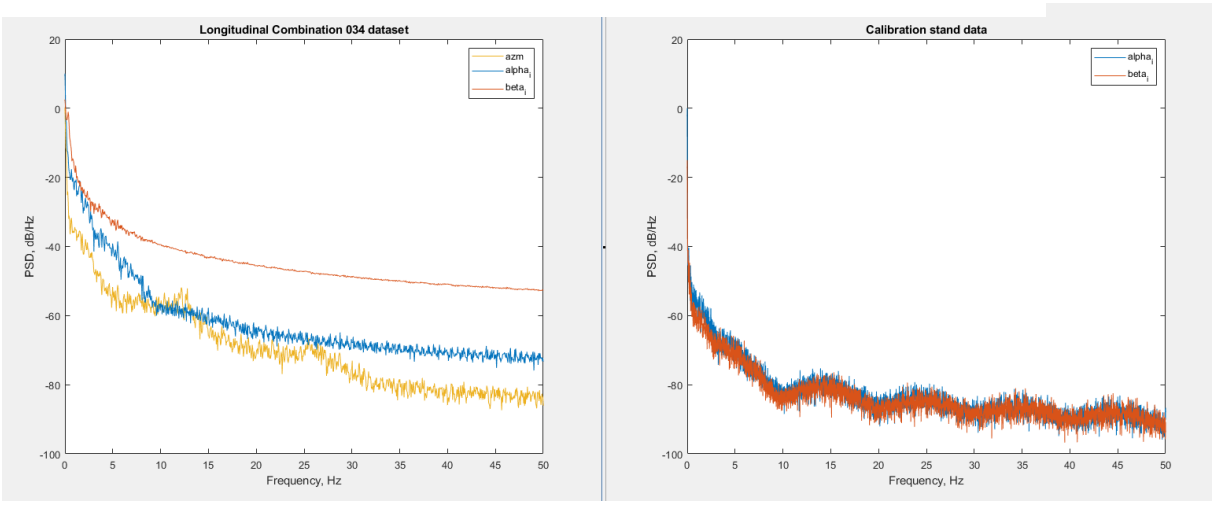

Figure 2.48. Angle of attack and angle of sideslip signal comparison from in-flight data (left) and wind-tunnel data (right).

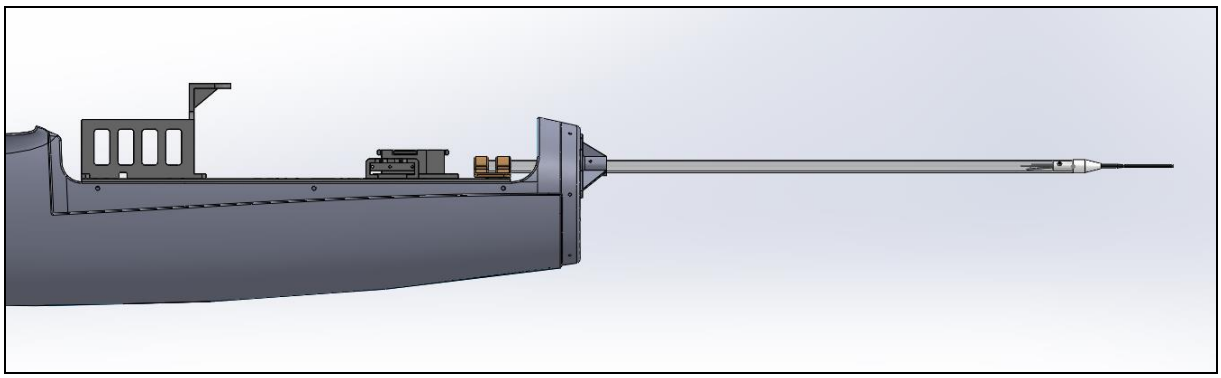

Figure 2.49. Air-data boom mount.

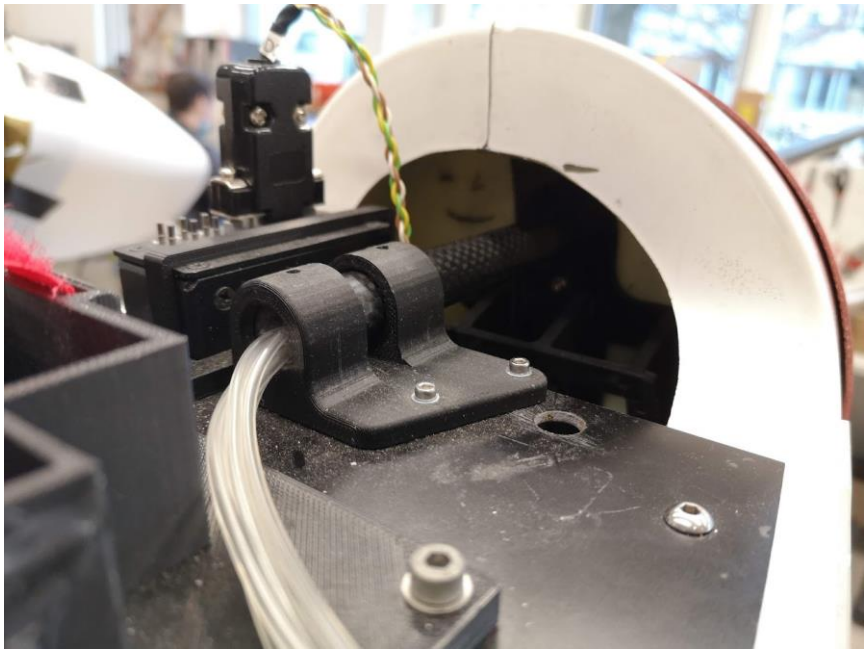

Figure 2.50. Air-data boom mount at the root.

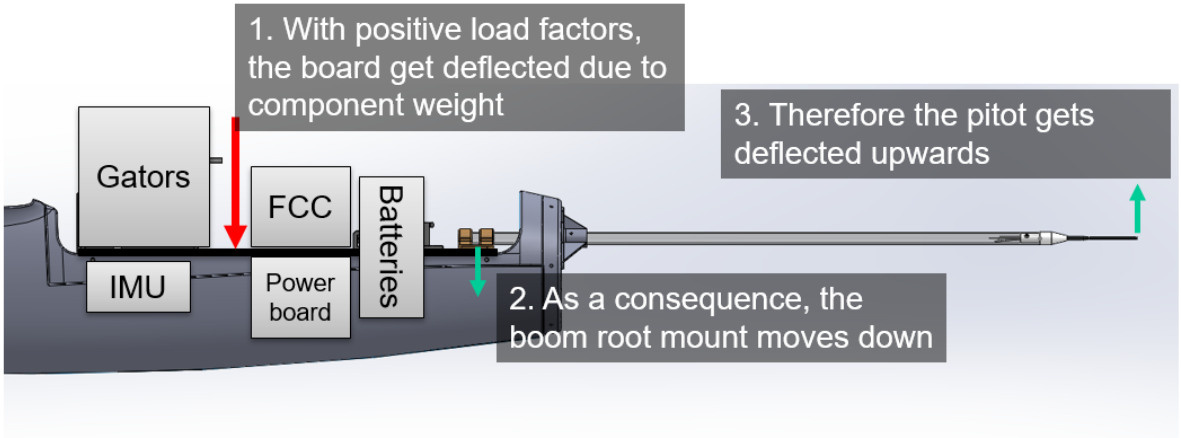

Figure 2.51. Air-data boom flexibility mechanism.

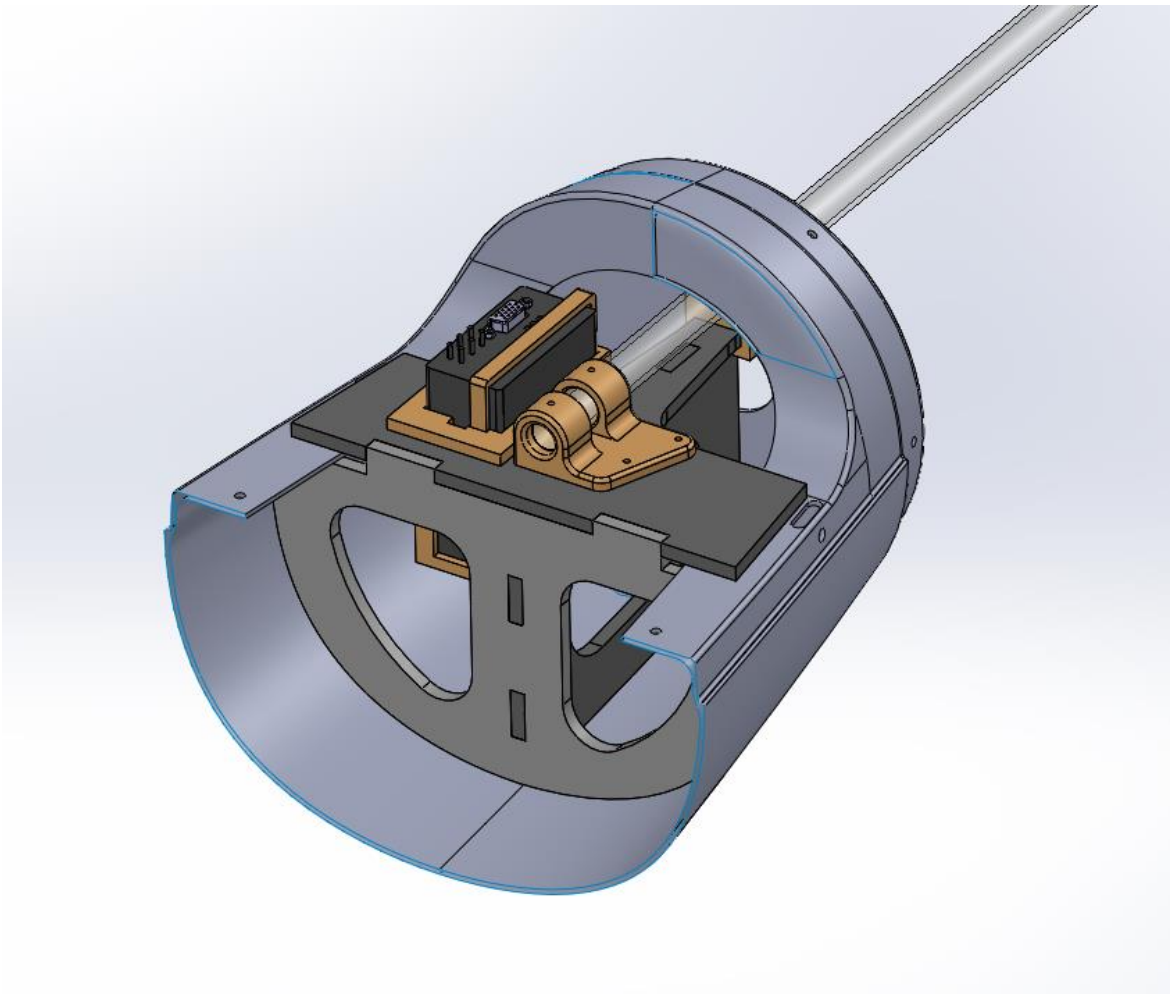

Figure 2.52. Upgraded air-data boom mount in the nsoe section of the fuselage.

Testing the Flight Control Computer

New IMU configuration

New IMU softwares are implemented based on the new concept. All the modification are backward compatible, so no need to worry if the FCC software's or the IMU software's version is different. In such cases, the reconfigured IMUs are working in the original operation mode.

The IMUs on the wing's leading edge (IMU No. 1, 2, 3, 7, 8, 9) give digital acceleration values in the x-, y- and z-direction and analog acceleration values in the z-direction only. All of these data are filtered with a high-pass filter. The IMUs on the wing's trailing edge (IMU No. 4, 5, 6, 10, 11, 12) provide gyro data around the axis x and axis y and both digital and analog accleleration values in the z-direction. All of these data are filtered with a high-pass filter. Data filtering is done with an IIR high-pass filter with a 0.1Hz corner frequency. It is used to filter out the offset error caused by the temperature. For better understanding, see the figures below.

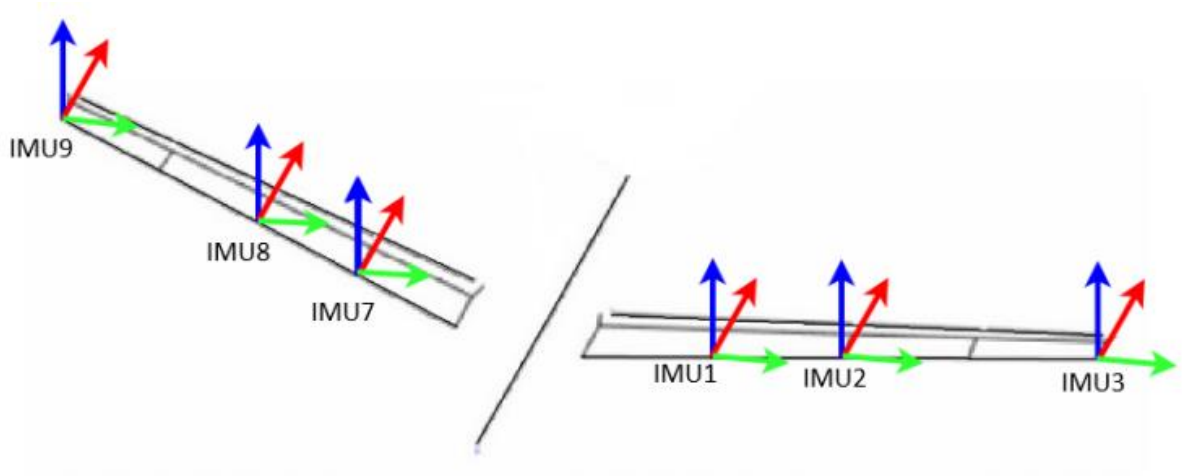

Figure 2.53 - IMUs on the leading edge

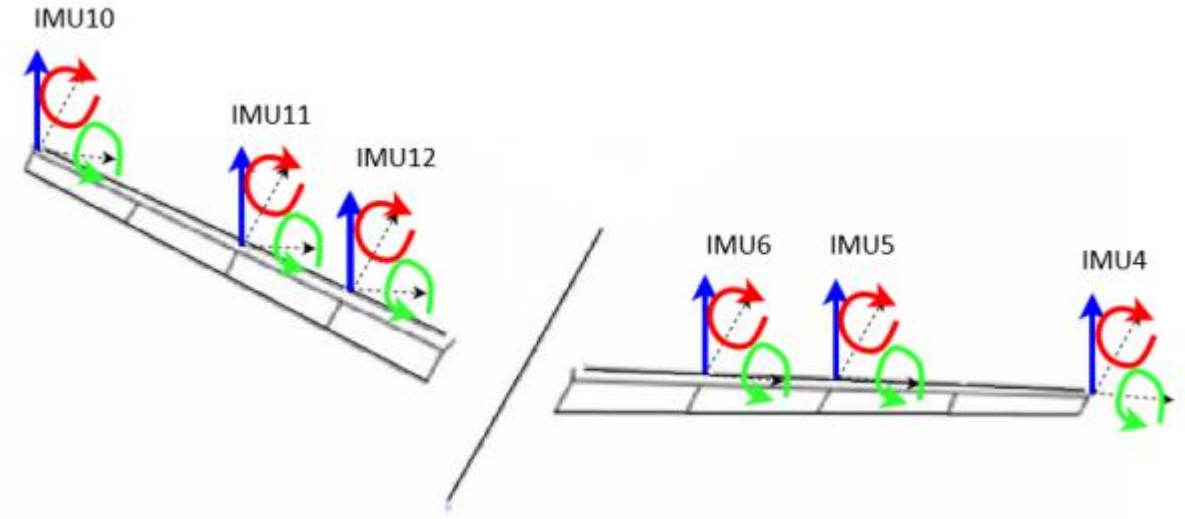

Figure 2.54 - IMUs on the trailing edge

Direct Drive

The actuator which responsible to move the 4th control surfaces during flutter control called Direct Drive. The actuator has an own controller, Flight Control Coputer just send position commands to it via CAN bus. Like all actuators, Direct Drive also connected to the RX-MUX. For compatibility with other wings which do not have Direct Drive just simple servos, the signal of 4th control surfaces will be sent throug the related PWM channels and in converted form through CAN bus as well. The following figure shows the route of the signal of the 4th actuator.

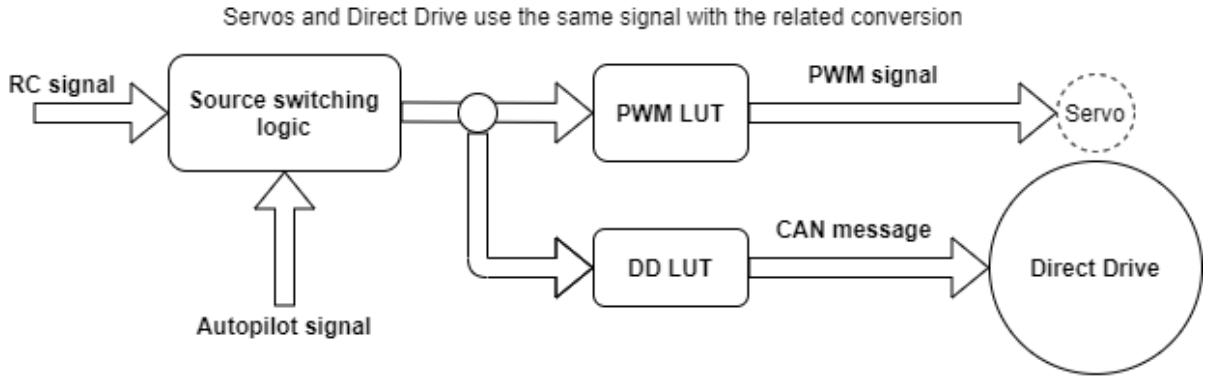

Figure 2.55 - Signal route of the 4th actuator

In the 1st period we implemented the CAN communication between RX-MUX and Direct Drive, created initialization code for the actuator which are sent when it turned on, and we solved the signal conversion. This moment Direct Drive can be managed by FCC from RC and from autopilot signal sources as well. Next steps are making the signal sending and geting diagnostic information from Direct Drive more robust.

RX-MUX v2.0

The RX-MUX has two main task to do. One of them is choosing the source of reference signals between the human pilot radio signals and the autopilot signals. The other main task is creating PWM signals from the incoming data and controlling the actuators. Recently, our team has completely redesigned the RX-MUX unit, both hardware and software. We are working on integrating the new version of RX-MUX in the Flight Control Computer system. The integration involves receiving the radio signals through its RC transmitters. Furthermore, we have to implement SPI communication between the FlightHAT interface panel and the RX-MUXs, which also cause the software redesign of the FlightHAT unit in order to optimalization. It is necesarry because the autopilot signals arrive from Raspberry PI through FLightHAT. The 3rd main part of our job is to create intervention signals according to the RC transmitter datas and autopilot datas. Finally, we have to establish communication channels between the RX-MUX and the actuators.

2.56. Figure - RX-MUXv2 software development progressshows the status of each software module of the RX-MUX v2. We distinguish software modules which are crucial for flight tests, and which are not. The crucial parts are any kind of RC input reading autopilot input reading, the channel selection module, the output mapping with Lookup Tables and the actuator handling modules. The most simple and universal RC input method is the PPM reading, which is already implemented and tested. Other digital input reading methods will be useful, but not crucial for first flight tests. To solve the communication between flightHAT and new RX-MUX modules, we had to change the flightHAT code as well. These blocks got the ‘almost done’ title, because during tests we foundminor issues which will solved soon. Output mapping ant Lookup Tables part of the software are crucial, but also almost fully implemented, we marked it almost done, because it will be modifiable from the client software of the module from a PC and these configuration data will be saved into the program memory of the microcontroller, while the embedded software runs in configuration mode. The configuration software component is crucial for the fligh tests, but its runtime modification is not. The new RX-MUX unit will be able to handle the currently used PWM servos and the CAN bus-controlled servos as well which likely will used for the advanced wing. The most critical part of the software is the channel selection logic, which currently under development and there is the Direct Drive handler module, which not

implemented yet, but due to the avaible CANOpen library for ST microcontrollers, that implementation will be easy.

The hardware manufacturing considerably delayed, because due to the chip shortage, we were not able to purchase microcontrollers at all, so we decided that with minor modification we will use the 144-pin microcontroller instead of 100 pin MCU, fortunately we could purchase some 144 pin MCUs, so after the redesign of the PCB we can start the manufacturing.

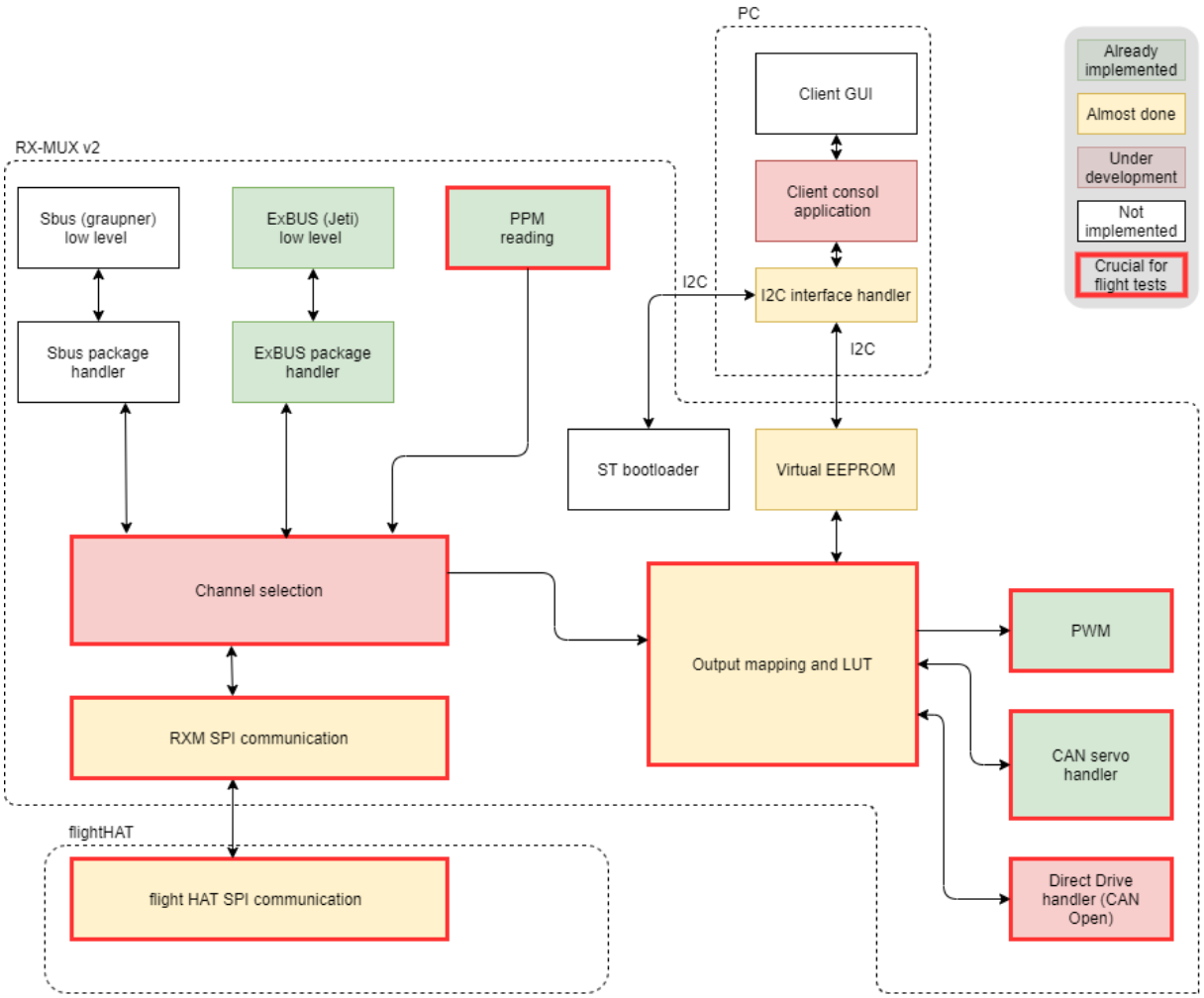

2.56. Figure - RX-MUXv2 software development progress

Ground tests

To test the functionalities of the Flight Control Computer and its software with the autopilot before flight tests, we performed tests in Hardware-in-the-Loop test environment and on the real aircraft as well. To select the required autopilot functionality, we created a graphical interface which managed by the test engineer in the groun control station.

The main autopilot functionalities we tested:

- Baseline functions
  - Autothrottle
  - Altitude holding
  - Course angle
  - Waypoint tracking
- Identification functions
  - Signal injection to the engine
  - Signal injection to control surfaces

Hardware-in-the-Loop tests

Baseline tests

For example, you can see how autothrottle test was performed in HIL. Figure 2.36 shows how throttle signal and airspeed changes if we give the following commands:

1. Use RC AP2 (augmented mode + autothrottle, nominal speed 38 m/s)
2. Reference velocity change from 38 m/s to 42 m/s
3. Reference velocity change from 42 m/s to 34 m/s
4. Reference velocity change from 34 m/s to 38 m/s

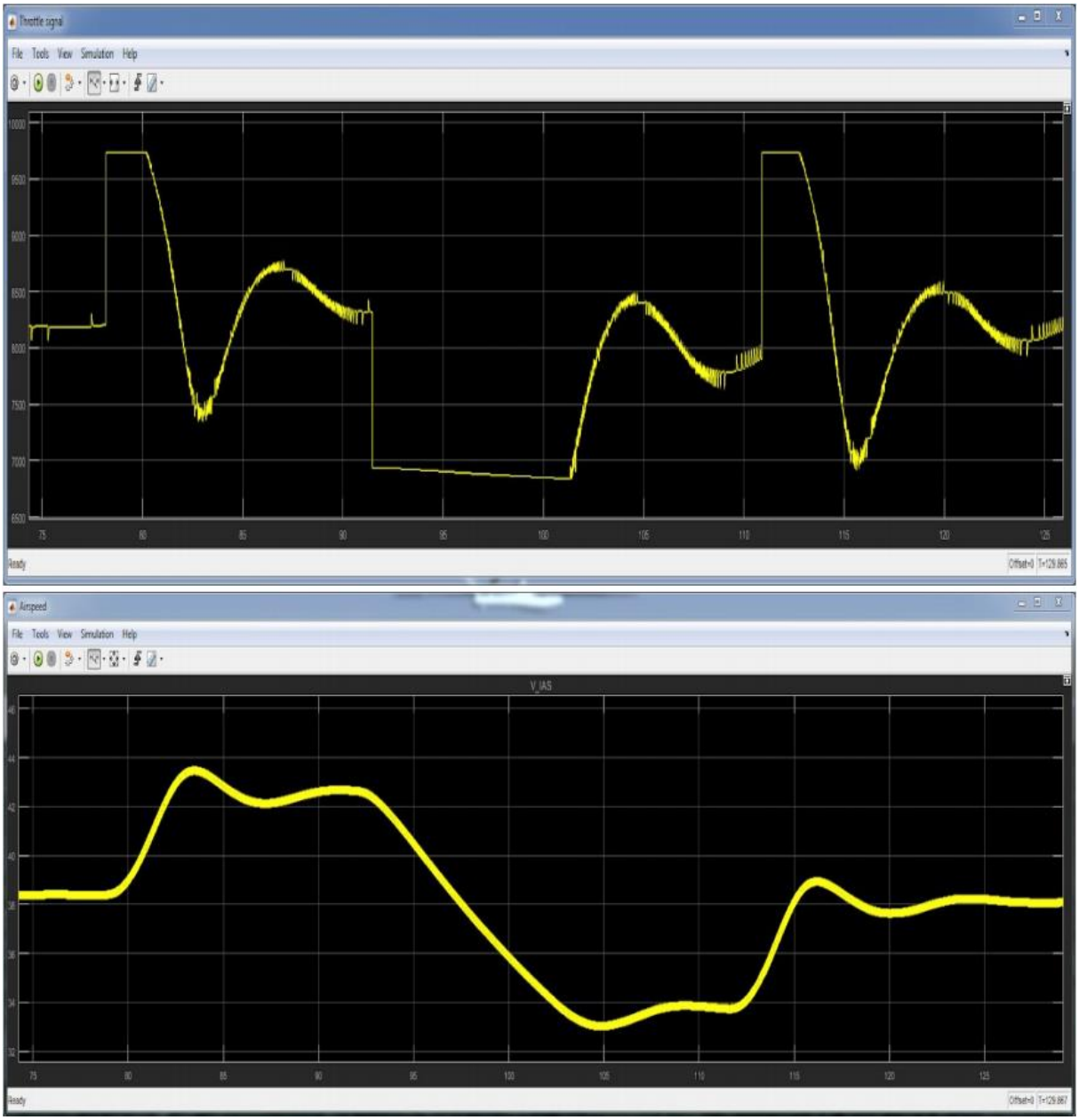

Figure 2.57 – Autothrottle HIL test

Identification tests

In engine identification mode, we inject step signals to the engine. Figure 2.57. shows how airspeed changes with an injected signal.

Throttle injection mode HIL test:

1. Mavlink in Baseline mode, augmented + throttle inject (open loop throttle in this SW_PI version) (velocity panel active)
2. 1st leg: start from RC AP1 trimmed 34 m/s straight and level (inner loop engaged), push 38 m/s button in Mavlink, switch to RC AP2, observe velocity increase with minimum pilot interference (RC throttle stick inactive) then switch back to RC AP1

3. 3rd leg: start from RC AP1 trimmed 34 m/s straight and level (inner loop engaged), push 42 m/s button in Mavlink, switch to RC AP2, observe velocity increase with minimum pilot interference (RC throttle stick inactive) then switch back to RC AP1

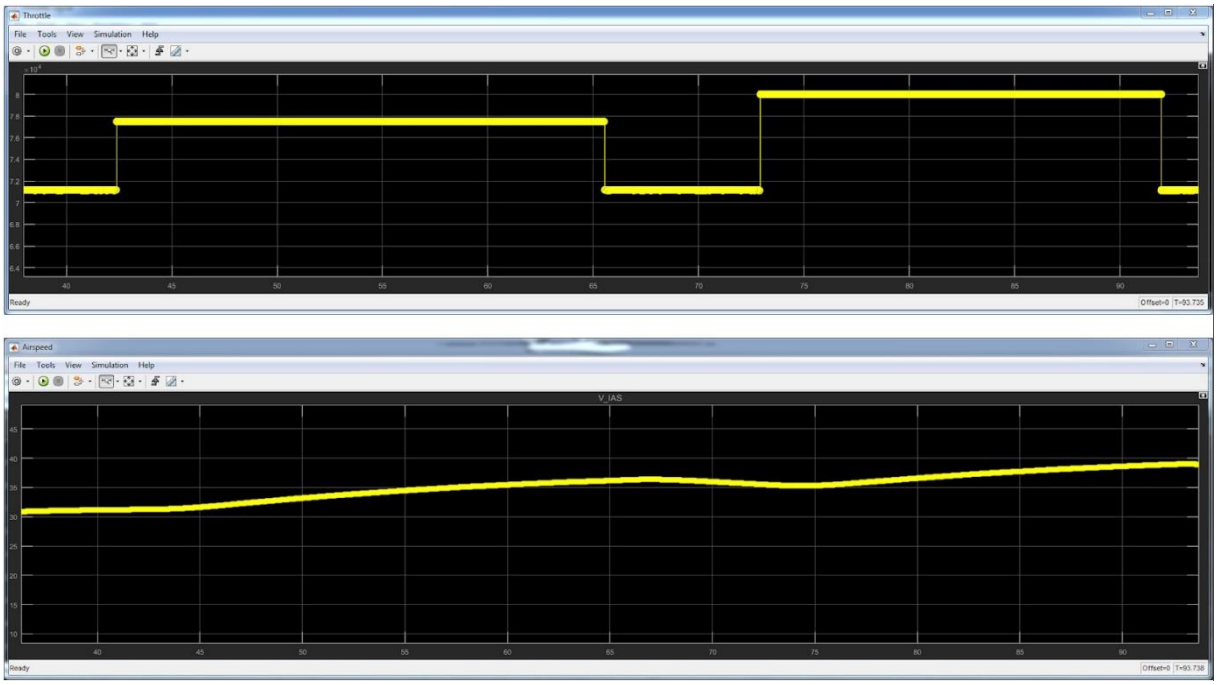

Figure 2.58 - Throttle signal injection HIL test

Signal injection mode HIL test:

1. Select Signal injection mode in Mavlink before flight and select between Flexible and Flight Mechanics tabs
2. Set initial velocity, amplitude multiplier and signal in RC AP1 during flight
3. Switch to RC AP2 to inject the selected signal

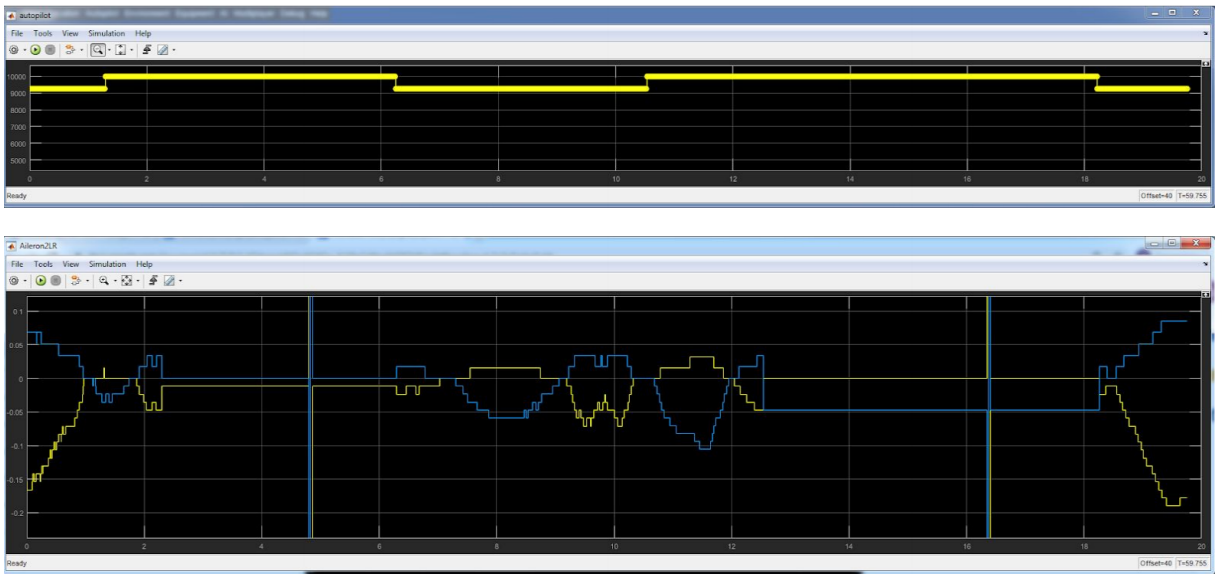

Figure 2.59 - Signal injection test in HIL

Ground tests on the demonstrator aircraft

For ground tests we prepared a test version of autopilot with only one difference compared to flight version: we gave a constant value for the controller instead of measured speed.

Augmented mode test:

1. Moved the aircraft to change pitch and roll
2. Control surfaces tried to stabilize the aircraft

Signal injection test:

1. Select initial velocity, amplitude multiplier and signal on mission planner (In RC AP1)
2. Inject the signal: switch to RC AP2
3. Related control surfaces moved according to the selected signal

Altitude and course angle test:

1. We gave altitude and course angle values via mavlink
2. Control surfaces tried to follow the given values

Autothrottle test:

1. We gave 38 m/s constant airspeed to the controller instead of measured value
2. Gave a velocity value via mavlink (in RC AP2)
3. The engine tried to increase or decrease the velocity depending on the given value

Table 1.**Hiba! A hivatkozási forrás nem található.** shows the given commands and Figure 2.60 shows the response of the engine.

Switching times [sample]:	**Commanded velocity [m/s]:**
373000	38
378100	42
379900	38
385700	34
390700	42
393600	34
405000	38
406700	42
409100	34
415300	42
417700	38
420600	34
423800	38

Table 1 - The given velocity commands

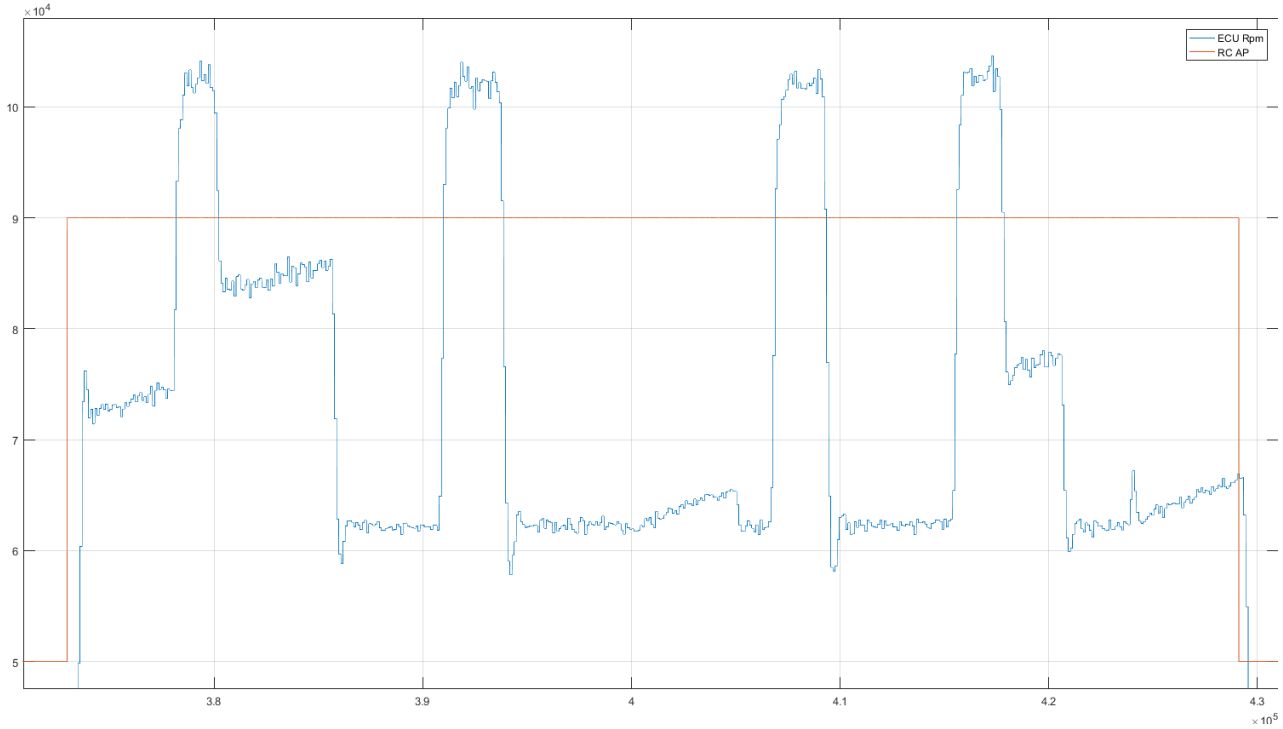

Figure 2.60 - Engine response for the given commands

New test environment using Speedgoat target machine

During Harware In the Loop tests we faced with many problems, eg. model running was not rel time, caused by host os, there was no enough interfaces to test all functionalities of the Flight Control Computer, that is why we started to build a new HIL test environment basen on a Speedgoat target machine. The target machine got many useful interfaces and it is capable to run our model real time.

The following table describes all interfaces and those purpose.

Interface	Amount	Purpose
RS-232	3	flightHAT (ADS, Mavlink, Sindy/Fibre)
CAN HS	6	flightHAT (IMU, SHM) RX-MUX (DD, new servos)
PWM	24	RX-MUX (actuators)
PPM capture	2	RC for SIL
UART (TTL)	3	ECU, RC for SIL

Figure 2.61 -Speedgoat interfaces

Implementation of the MATLAB HIL model of the aircraft on the new Speedgoat machine has begun. Currently it is in a state where the incoming CAN messages from the FCC are arriving via the IO612 card of the Speedgoat. Part of the Simulink block diagram which handles the CAN communication can be seen in the following figure.

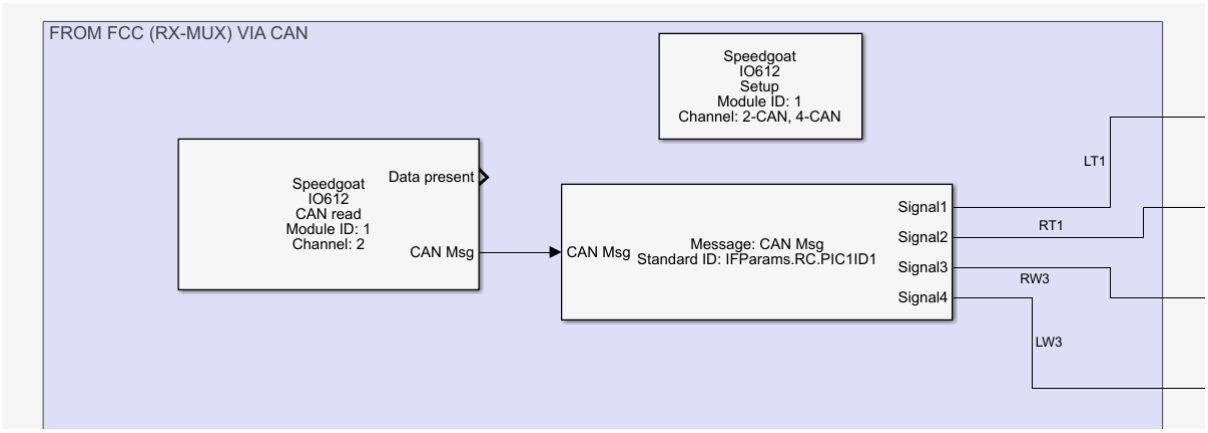

Figure 2.62 - Speedgoat interface blocks

The upcoming task is to make the aircraft model (Simulink S-function) compatible with the OS of the Speedgoat. After that the necessary I/O for the model outputs must be implemented as well. These are serial ports that emulate the xSens and air data sensors.

Direct Drive integration with RX-MUX v1.0

During last period we implemented the Direct Drive control and diagnostic handler in the RX-MUX v1 software, but after tests we found that it requires more improvements. The position feedback is not continuous and control signal is delayed, so investigation of these issues is in progress at this moment. 2.64. Figure - Direct Drive postition testshows that the sent position command delayed at several times and the value od the DD encoder position are 0 in more cases.

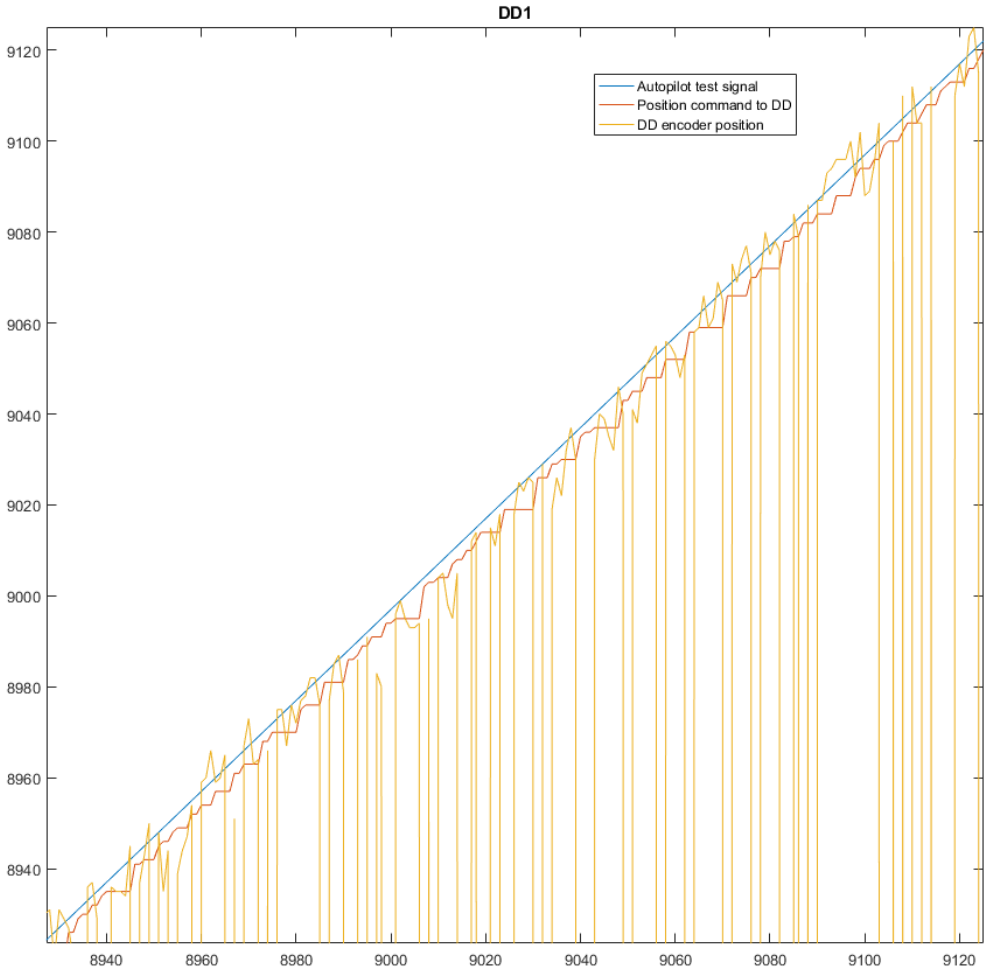

2.63. Figure - Direct Drive postition test

Actuator position feedback comparison tests

Comparison of Hitec MDTW950TW-CAN servos with built in diagnostics versus the current solution which is the MKS HBL599 actuator with SHM. The goal was to determine how the CAN servos internal position measurement compared to our current solution, and how accurate is it in absolute terms.

Test setup:

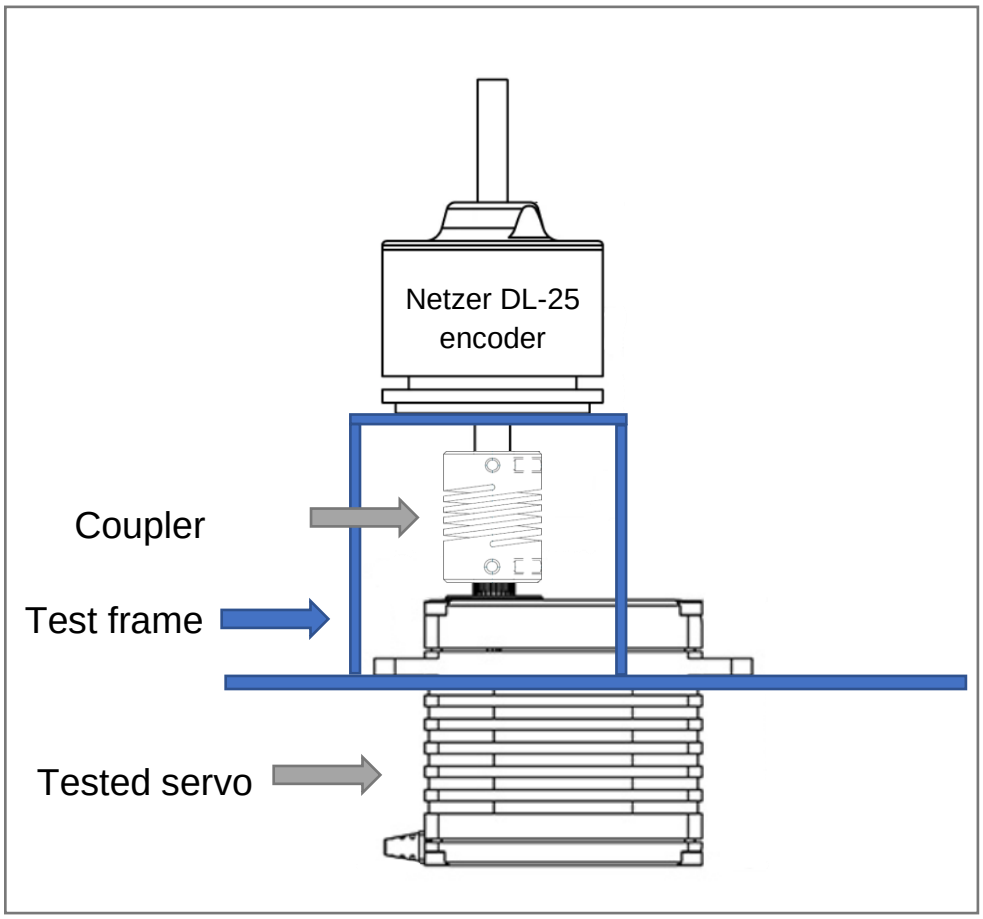

- Netzer DL-25 encoder, 17^2 counts/revolution
- CAN servo: MDTW950TW-CAN
- PWM servo: HBL599 + SHM
- PWM signal generated by new RX-MUX (Pulses precisely between 1ms and 2ms @333Hz)

Test signal:

- Stationer states because synchronization was not possible with the hardware at hand
- 11 different positions
- Each position twice, from both directions (except first and last)
- Full travel ~360° for CAN, and ~110° for PWM

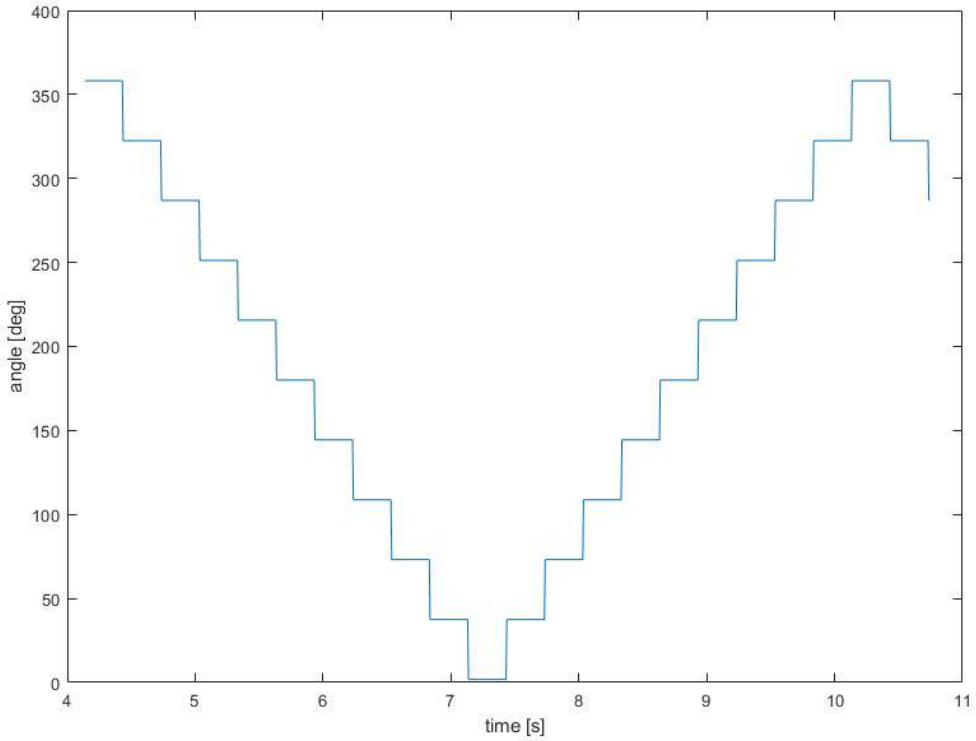

You can see the CAN servo results. At this zoom level the errors are hard to spot but are definitely there.

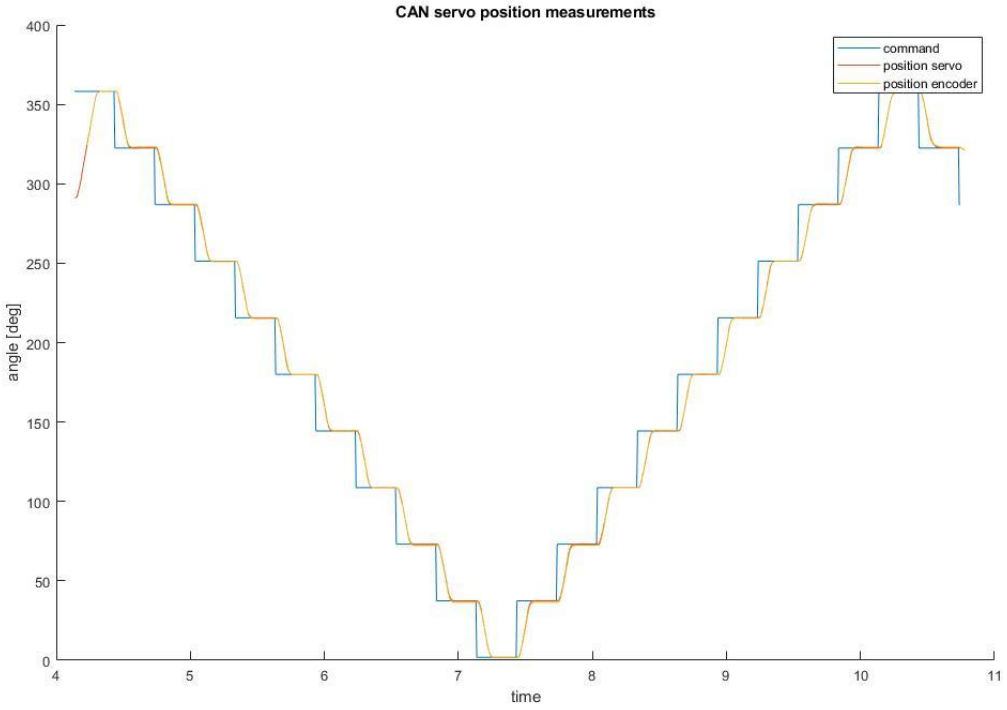

See the zoomed-in version:

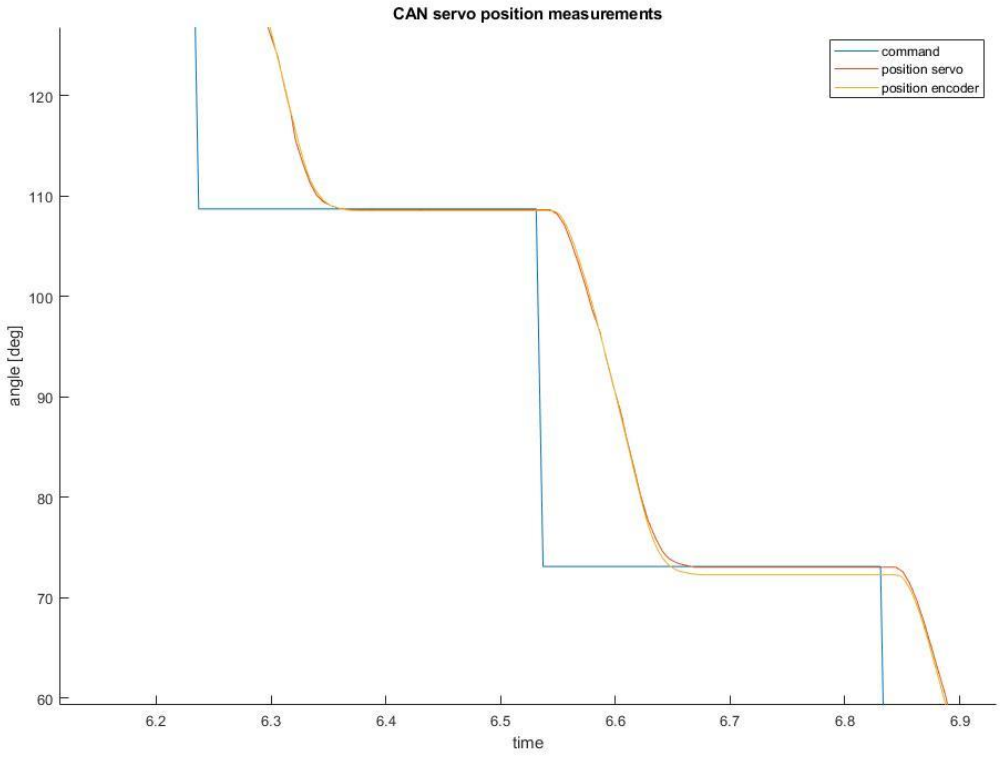

The PWM servo's results look the same at first glance, the most important difference is the noise on the SHM's position measurement. This is easier to see on the zoomed-in version.

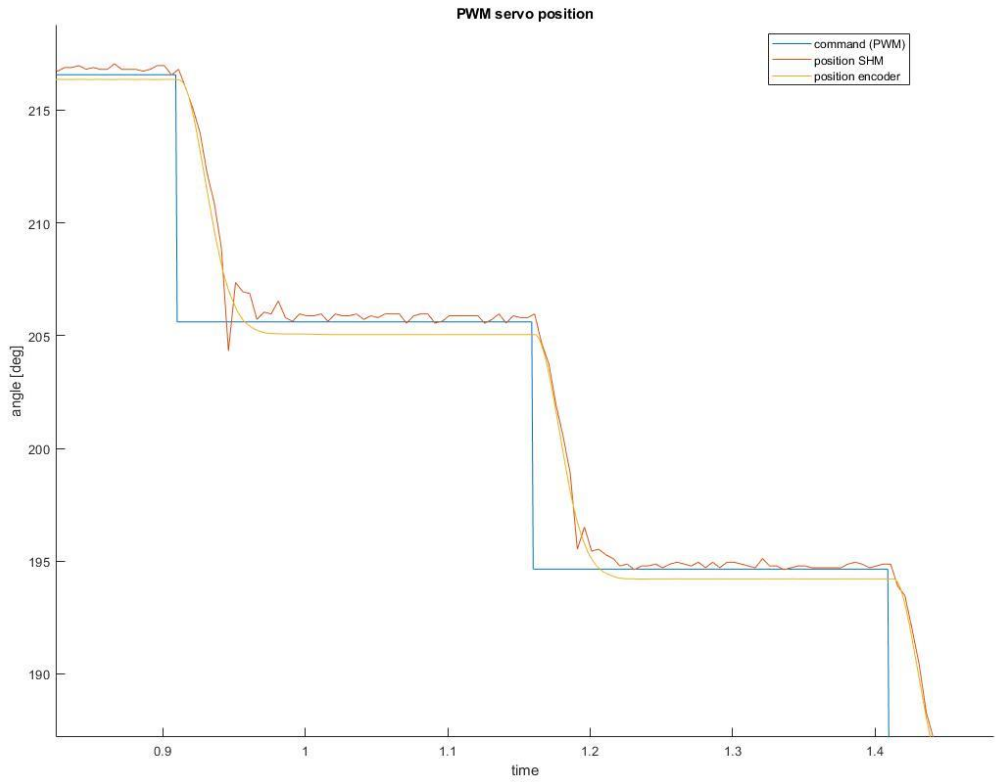

The interesting data for us now is the difference between the signals. Both between the command and the actual position (measured by the external encoder) as well as the command and the position measured by the servo (or SHM). You can see the graphed version of this for both servos. Note that the huge spikes (some of them were deleted in post) are there because external and internal measurements were not synchronized in time. Therefore, we only focused on stationer states, and you should only pay attention to these parts on the graphs.

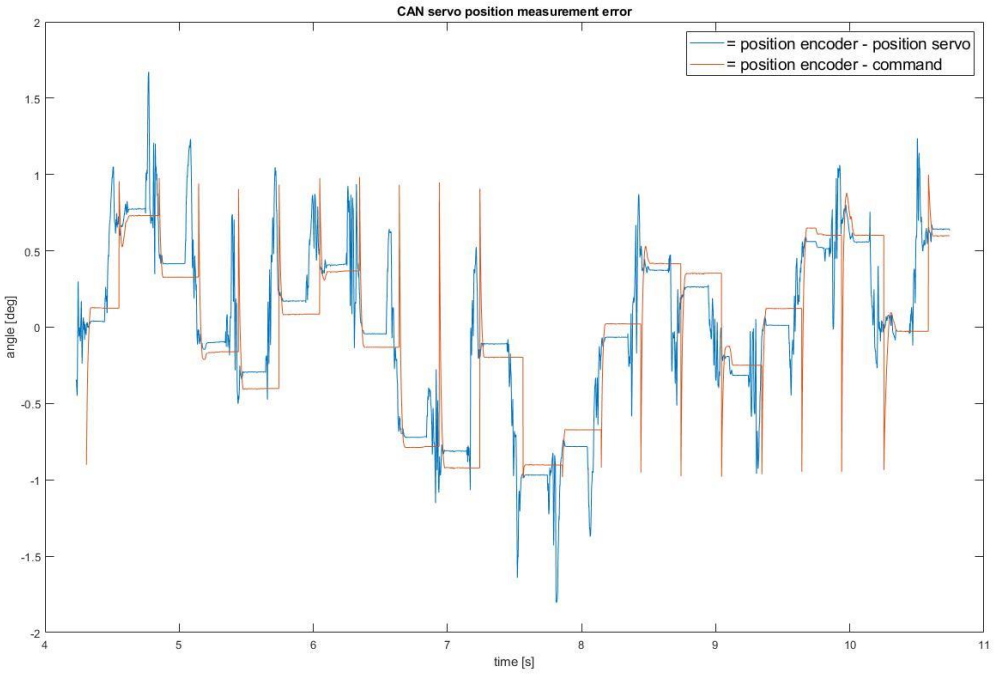

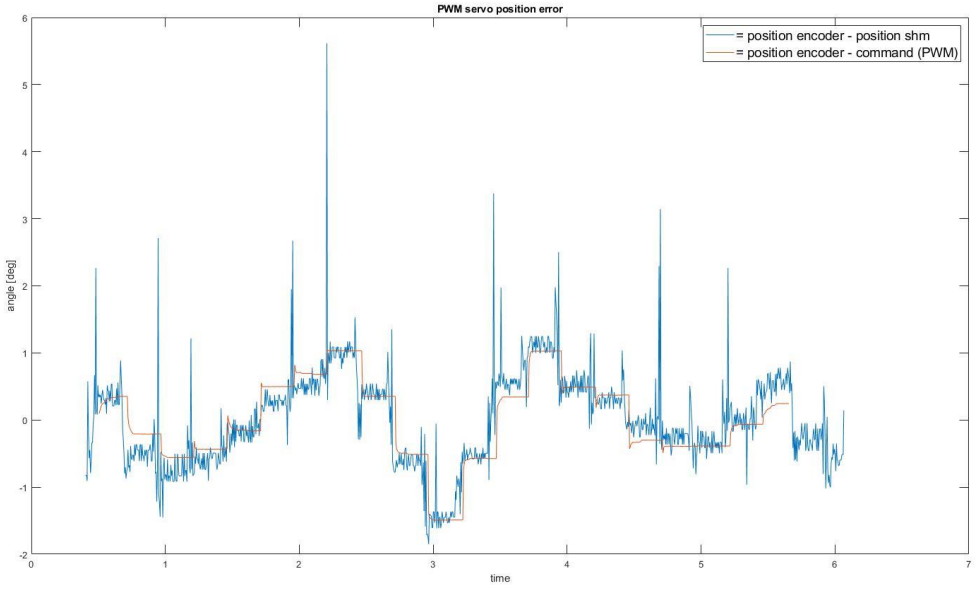

To help the comparison, we have also prepared statistical values. These were calulated after we cleaned the data from the aformentioned synchroniztaion errors, and removed any dynamic components. Avarage values were calculated for each step of the test signal. These values were used to create the following statistical results :

Servo	**CAN**		**PWM**	
Type of error	**encoder - servo measurement**	**encoder - command**	**encoder – SHM measurement**	**encoder- command**

Mean (abs) [deg]	0.38468	0.39818	0.51681	0.47856
Deviation [deg]	0.49351	0.50162	0.63124	0.59202
Min [deg]	-1.0089	-0.96196	-1.4503	-1.4866
Max [deg]	0.70397	0.66002	1.1686	1.0322

As you can see the CAN servo has an overall better accuracy. Both in terms of what it reports about itself, and the actual position error. Do not forget that the position measurement has much lower noise on the CAN servo, and the SHM has a problem, where the accuracy has a not insignificant temperature dependency. The results combined with the fact that the SHM requires much effort to install, makes the use of CAN actuators significantly more compelling.

Diagnostics capabilities of the Hitec MDTW950TW-CAN

The servo can provide diagnostics data about itself. The different parameters can be read form the servos different registers, with read requests. There are multiple types of these read requests, and there is an option to have them sent back automatically.

When we began the development on the CAN servo handling software module, on the new RX-MUX, it became apparent that the servo is not capable of reporting the amount of data that we have hoped for. The aim was to have position, temperature, and voltage data sent back in every loop. That means 200Hz for all 3 parameters.

So, we set out to find the maximum rate at which we can collect data reliably. The top priority was the position information. We discovered that the frequency of the new position commands also affects the amount of data that the servo can send back. We did not want to compromise on this, so we fixed the rate of the new position commands throughout the tests at 200 Hz.

Here is a list of all the combinations we have tried. All of them had new position commands going out at 200Hz (with normal write), I will not indicate that with every entry. Polling refers to sending some kind of read request. These are normal (1 register), double (2 registers) and short (1 register, but shorter CAN message). Stream refers to the servo's built in stream mode, where it sends back data automatically, without the need for a request. "Command with short message" means that the new position command was sent out at 200 Hz, but with the short write format instead of the normal write format. As mentioned before, position information has the highest priority, so we tried to stick to that, and lower the frequency of the voltage and temperature readings.

- Poll @ 200 Hz with 3 normal reads | not usable
- Poll position @ 200 Hz with normal read, stream 1 double @ 100 Hz | not usable
- Poll position @ 200 Hz with normal read, and stream 1 double @ 16.6 Hz | might be usable
- Poll position @ 200 Hz with normal read, and poll @ 100 Hz with 2 normal reads | not usable
- Poll position @ 200 Hz with normal read, and poll @ 100 Hz with 2 normal reads, offset within the 5 ms | not usable
- Poll position @ 200 Hz with normal read, and poll @ 100 Hz with 1 double read | not usable
- Poll position @ 200 Hz with normal read, and poll @ 50 Hz with 1 double read | not usable

- Poll @ 200 Hz with normal read, switch what data is requested every other message | usable
- Poll @ 200 Hz with double message, position is fix, other data is changed every other message | usable, this is the final solution
- Poll @ 200 Hz with 1 normal and 1 double read | not usable
- Poll @ 200 Hz with 2 double reads | not usable
- Poll @ 200 Hz with 1 short and 1 double read | not usable
- Command with short message, Poll @ 200 Hz with 1 normal and 1 double read | not usable
- Command with short message, Poll @ 200 Hz with 1 short and 1 double read | not usable

Not usable means that the answers didn't arrive during the cycle when the request was sent. This would occur every 2-5 cycles depending on the configuration. These would add up to a significant delay in the measurements, and cause problems.

We choose the double read solution, because it is robust, does not compromise on position data frequency, and can be expanded in the future to have even more parameters reported, at the cost of their frequency.

On-board Computer 2 (OBC2) improvements

As it was mentioned in the previous periodic report, there is a new Raspberry Pi 4 based on-board computer on the aircraft. We are after an intensive integration session where the people involved from TUM, DLR and SZTAKI successfully attached a prototype OBC2 to the T-Flex aircraft. The main improvement achieved is that an online running modal analysis software which calculates the frequencies and dampings of the T-Flex's wing bending. The results are then sent to a laptop running openMCT via a telemetry link directly connected to the OBC2.

Other improvements include autostart capability which means, that the necessary software start automatically when the operational system boots on the Raspberry Pi. This means, that the Pi does not have to be accessed and the tasks do not have to be launched manually.

On the other hand, the OBC2 is designed to be a host of multiple sensors, like the thrust measurement system developed by TUM.

Speedgoat based HIL

The new HIL system based on the Speedgoat machine has undergone some improvements. For instance, the xSens and uADS sensor emulators are now fully functional. Moreover, the PWM input capture module which reads the PWM signals coming from the RX-MUX units is also working. The system is tested with the bottom-up aircraft model from SZTAKI and verifies that it can be flown manually with a RC controller. Future improvements include that the IMU and SHM sensors are correctly emulated and the engine model has the correct version.

Direct Drive integration with RX-MUX v1.0

During last period we implemented the Direct Drive control and diagnostic handler in the RX-MUX v1 software, but after tests we found that it requires more improvements. The position feedback is not continuous and control signal is delayed, so investigation of these issues is in progress at this

moment. 2.64. Figure - Direct Drive postition testshows that the sent position command delayed at several times and the value od the DD encoder position are 0 in more cases.

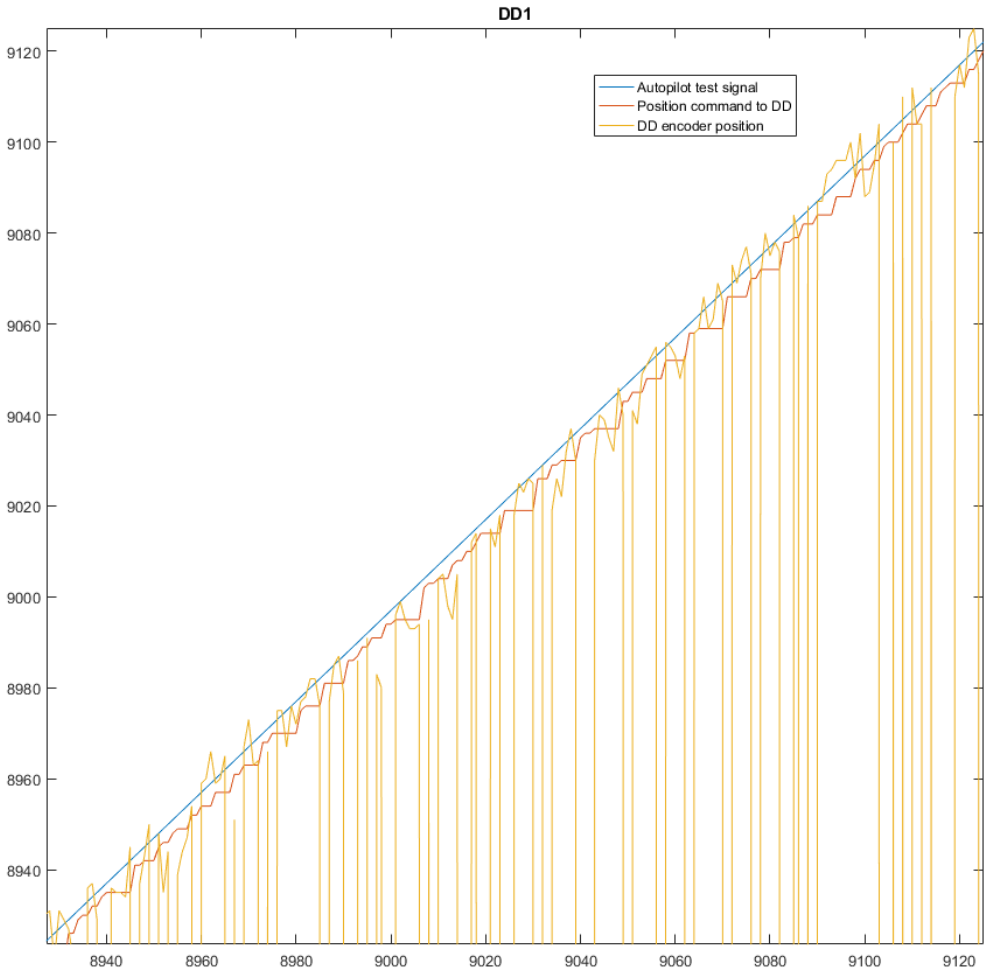

2.64. Figure - Direct Drive postition test

Actuator position feedback comparison tests

Comparison of Hitec MDTW950TW-CAN servos with built in diagnostics versus the current solution which is the MKS HBL599 actuator with SHM. The goal was to determine how the CAN servos internal position measurement compared to our current solution, and how accurate is it in absolute terms.

Test setup:

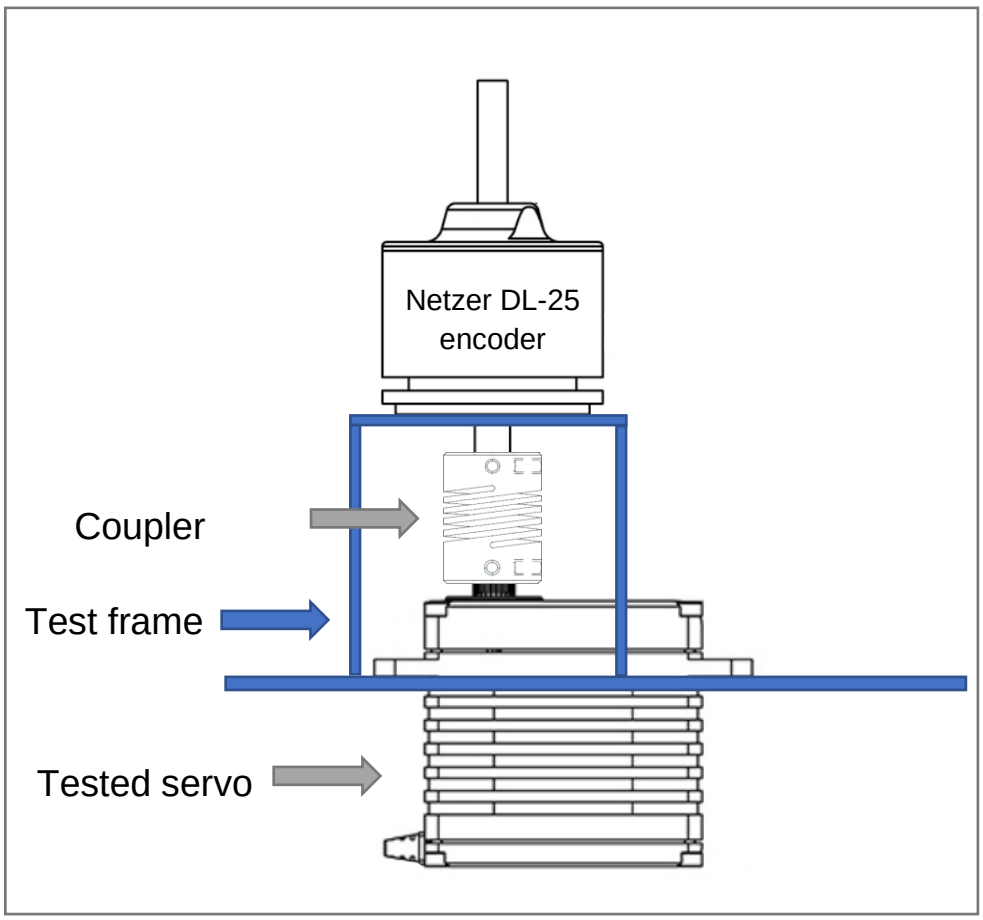

- Netzer DL-25 encoder, 17^2 counts/revolution
- CAN servo: MDTW950TW-CAN
- PWM servo: HBL599 + SHM
- PWM signal generated by new RX-MUX (Pulses precisely between 1ms and 2ms @333Hz)

Test signal:

- Stationer states because synchronization was not possible with the hardware at hand
- 11 different positions
- Each position twice, from both directions (except first and last)
- Full travel ~360° for CAN, and ~110° for PWM

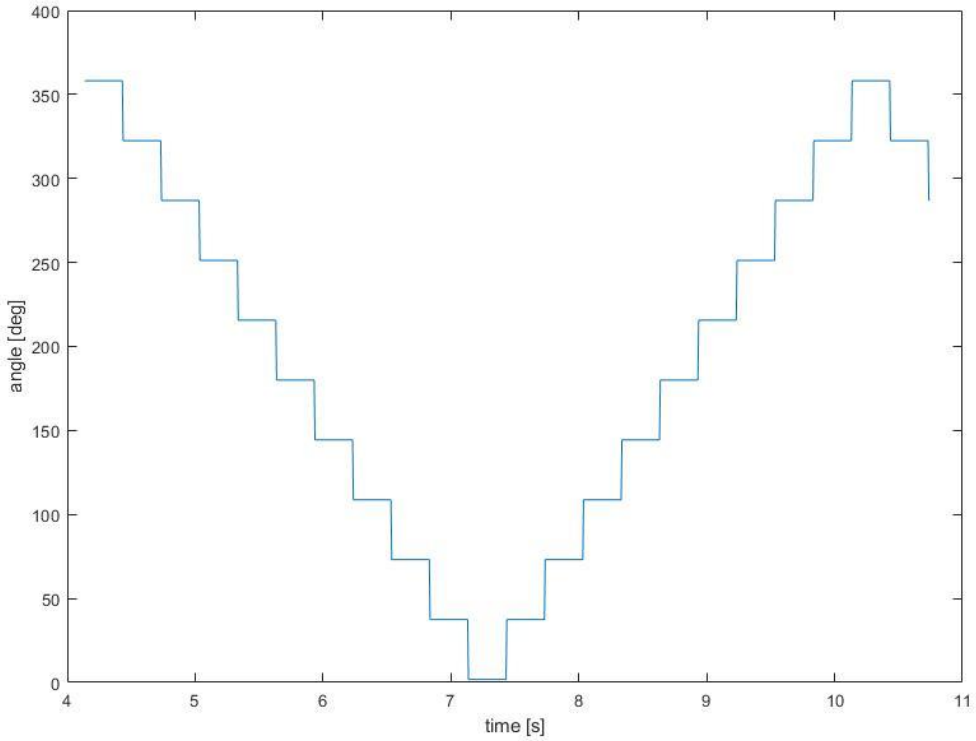

You can see the CAN servo results. At this zoom level the errors are hard to spot but are definitely there.

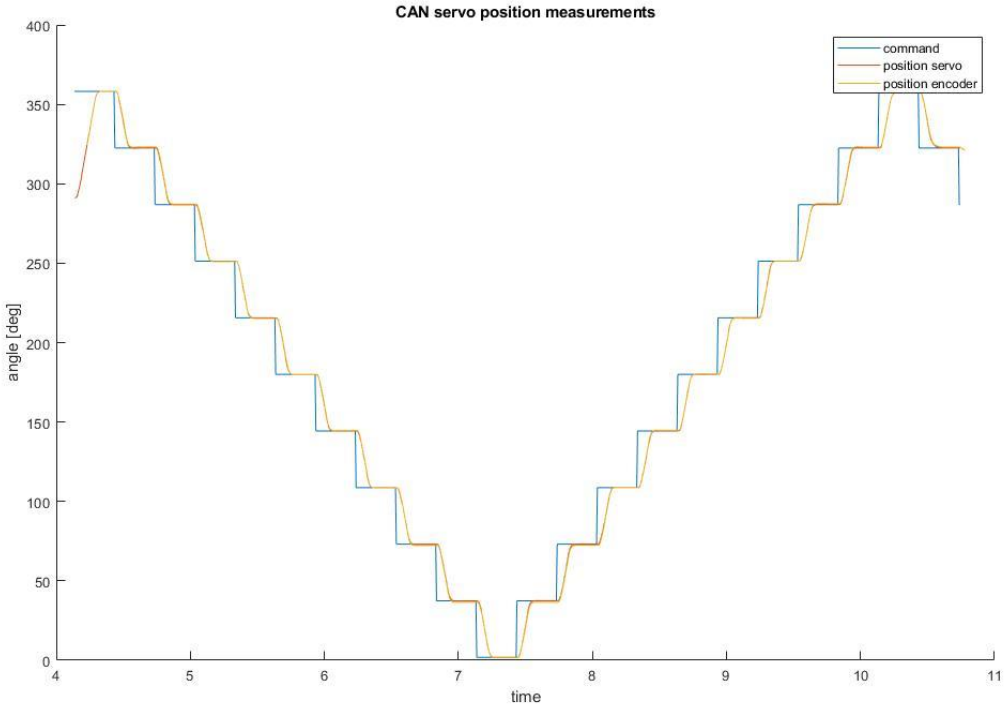

See the zoomed-in version:

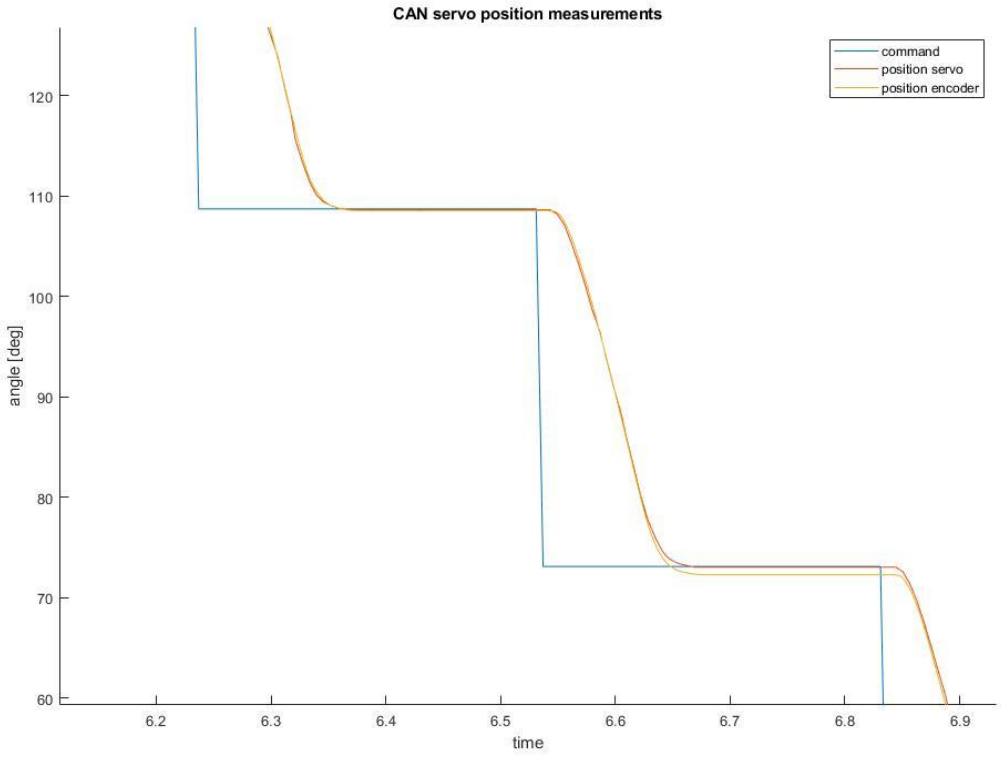

The PWM servo's results look the same at first glance, the most important difference is the noise on the SHM's position measurement. This is easier to see on the zoomed-in version.

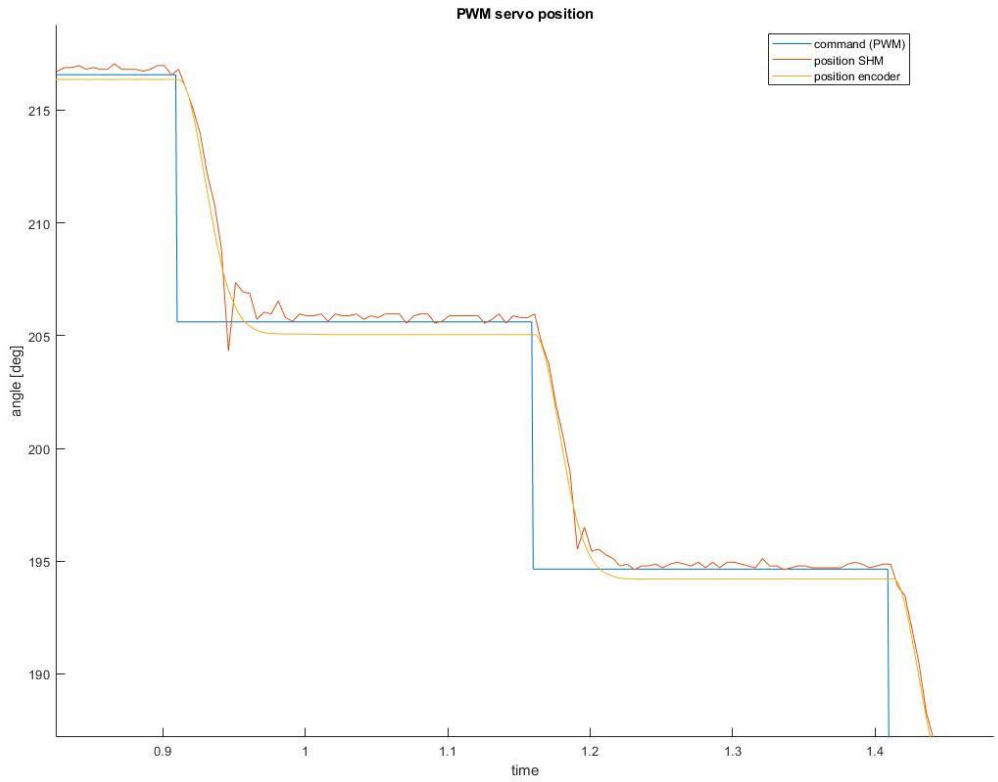

The interesting data for us now is the difference between the signals. Both between the command and the actual position (measured by the external encoder) as well as the command and the position measured by the servo (or SHM). You can see the graphed version of this for both servos. Note that the huge spikes (some of them were deleted in post) are there because external and internal measurements were not synchronized in time. Therefore, we only focused on stationer states, and you should only pay attention to these parts on the graphs.

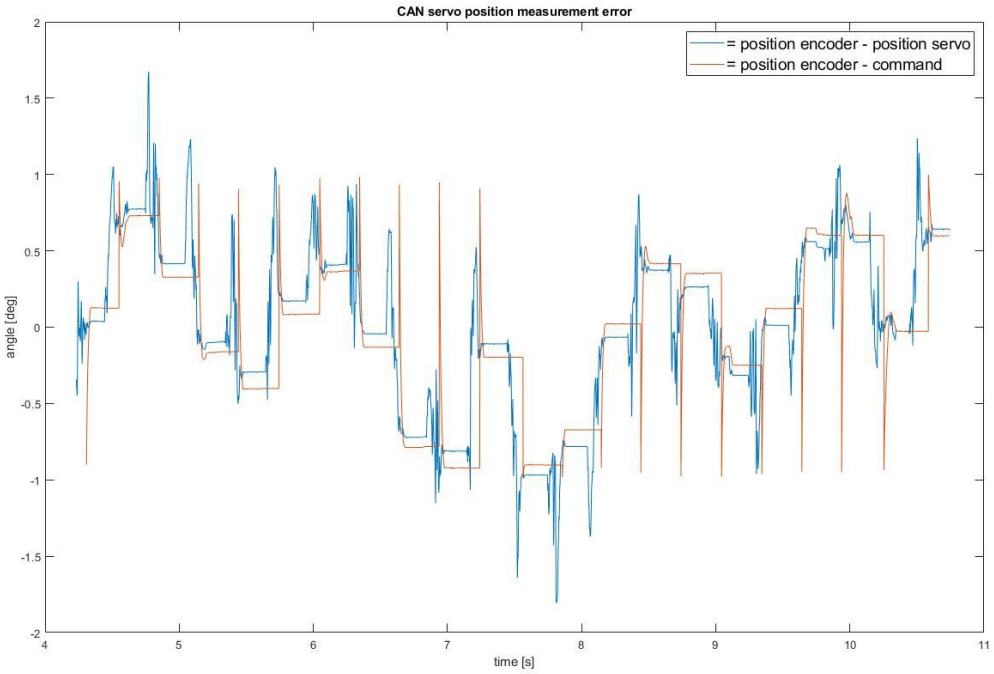

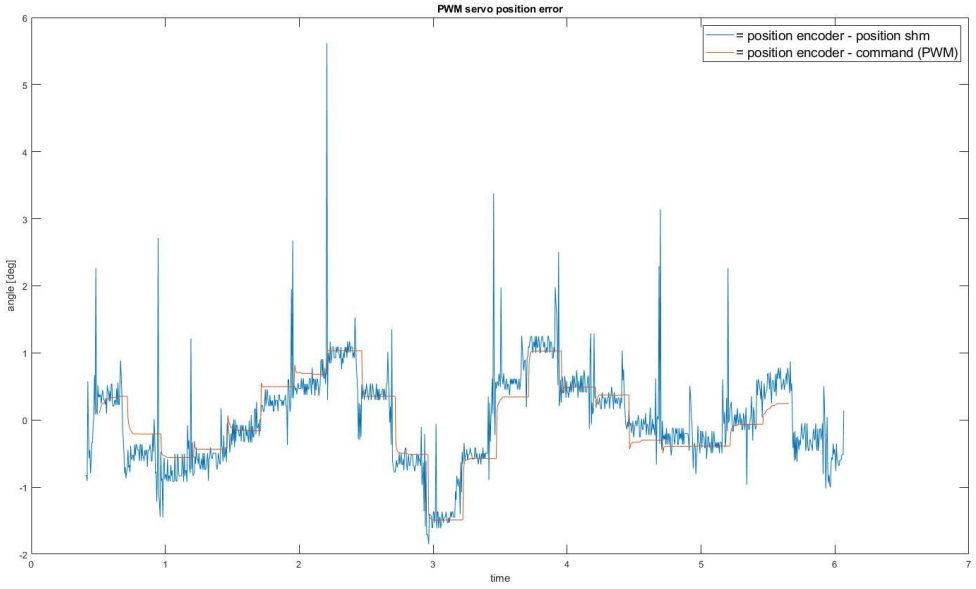

To help the comparison, we have also prepared statistical values. These were calulated after we cleaned the data from the aformentioned synchroniztaion errors, and removed any dynamic components. Avarage values were calculated for each step of the test signal. These values were used to create the following statistical results :

Servo	**CAN**		**PWM**	
Type of error	**encoder - servo measurement**	**encoder - command**	**encoder – SHM measurement**	**encoder- command**

Mean (abs) [deg]	0.38468	0.39818	0.51681	0.47856
Deviation [deg]	0.49351	0.50162	0.63124	0.59202
Min [deg]	-1.0089	-0.96196	-1.4503	-1.4866
Max [deg]	0.70397	0.66002	1.1686	1.0322

As you can see the CAN servo has an overall better accuracy. Both in terms of what it reports about itself, and the actual position error. Do not forget that the position measurement has much lower noise on the CAN servo, and the SHM has a problem, where the accuracy has a not insignificant temperature dependency. The results combined with the fact that the SHM requires much effort to install, makes the use of CAN actuators significantly more compelling.

Diagnostics capabilities of the Hitec MDTW950TW-CAN

The servo can provide diagnostics data about itself. The different parameters can be read form the servos different registers, with read requests. There are multiple types of these read requests, and there is an option to have them sent back automatically.

When we began the development on the CAN servo handling software module, on the new RX-MUX, it became apparent that the servo is not capable of reporting the amount of data that we have hoped for. The aim was to have position, temperature, and voltage data sent back in every loop. That means 200Hz for all 3 parameters.

So, we set out to find the maximum rate at which we can collect data reliably. The top priority was the position information. We discovered that the frequency of the new position commands also affects the amount of data that the servo can send back. We did not want to compromise on this, so we fixed the rate of the new position commands throughout the tests at 200 Hz.

Here is a list of all the combinations we have tried. All of them had new position commands going out at 200Hz (with normal write), I will not indicate that with every entry. Polling refers to sending some kind of read request. These are normal (1 register), double (2 registers) and short (1 register, but shorter CAN message). Stream refers to the servo's built in stream mode, where it sends back data automatically, without the need for a request. "Command with short message" means that the new position command was sent out at 200 Hz, but with the short write format instead of the normal write format. As mentioned before, position information has the highest priority, so we tried to stick to that, and lower the frequency of the voltage and temperature readings.

- Poll @ 200 Hz with 3 normal reads | not usable
- Poll position @ 200 Hz with normal read, stream 1 double @ 100 Hz | not usable
- Poll position @ 200 Hz with normal read, and stream 1 double @ 16.6 Hz | might be usable
- Poll position @ 200 Hz with normal read, and poll @ 100 Hz with 2 normal reads | not usable
- Poll position @ 200 Hz with normal read, and poll @ 100 Hz with 2 normal reads, offset within the 5 ms | not usable
- Poll position @ 200 Hz with normal read, and poll @ 100 Hz with 1 double read | not usable
- Poll position @ 200 Hz with normal read, and poll @ 50 Hz with 1 double read | not usable

- Poll @ 200 Hz with normal read, switch what data is requested every other message | usable
- Poll @ 200 Hz with double message, position is fix, other data is changed every other message | usable, this is the final solution
- Poll @ 200 Hz with 1 normal and 1 double read | not usable
- Poll @ 200 Hz with 2 double reads | not usable
- Poll @ 200 Hz with 1 short and 1 double read | not usable
- Command with short message, Poll @ 200 Hz with 1 normal and 1 double read | not usable
- Command with short message, Poll @ 200 Hz with 1 short and 1 double read | not usable

Not usable means that the answers didn't arrive during the cycle when the request was sent. This would occur every 2-5 cycles depending on the configuration. These would add up to a significant delay in the measurements, and cause problems.

We choose the double read solution, because it is robust, does not compromise on position data frequency, and can be expanded in the future to have even more parameters reported, at the cost of their frequency.

On-board Computer 2 (OBC2) improvements

As it was mentioned in the previous periodic report, there is a new Raspberry Pi 4 based on-board computer on the aircraft. We are after an intensive integration session where the people involved from TUM, DLR and SZTAKI successfully attached a prototype OBC2 to the T-Flex aircraft. The main improvement achieved is that an online running modal analysis software which calculates the frequencies and dampings of the T-Flex's wing bending. The results are then sent to a laptop running openMCT via a telemetry link directly connected to the OBC2.

Other improvements include autostart capability which means, that the necessary software start automatically when the operational system boots on the Raspberry Pi. This means, that the Pi does not have to be accessed and the tasks do not have to be launched manually.

On the other hand, the OBC2 is designed to be a host of multiple sensors, like the thrust measurement system developed by TUM.

Speedgoat based HIL

The new HIL system based on the Speedgoat machine has undergone some improvements. For instance, the xSens and uADS sensor emulators are now fully functional. Moreover, the PWM input capture module which reads the PWM signals coming from the RX-MUX units is also working. The system is tested with the bottom-up aircraft model from SZTAKI and verifies that it can be flown manually with a RC controller. Future improvements include that the IMU and SHM sensors are correctly emulated and the engine model has the correct version.

JETI Power supply update

During flight-testing, the flight-team encountered a low-voltage warning on the JETI remote control system. Ground testing showed, that a possible reason for the warning was a broke or partially

disconnected cable between the RX-MUX units and the Satellite receiver in the V-tail. Some facts of the original design and its limitation:

- Both remote control systems - JETI and Graupner – are powered from the internal 5Vdc over supply of the RX-MUX units.
- The JETI system needs 3 units to work as desired. One main receiver, one Power unit with enough PWM outputs – Central Box - and a satellite receiver for redundancy.
    - Two cable connected parallel to the Central box from the RX-MUX units, to supply enough current for normal operations.

We decided to drop the original design, and power the modules directly from the two 2S batteries. With that the Central Box 200 itself has unregulated power from the batteries, thus the system should be available all the time, if at least one 2S battery is connected.

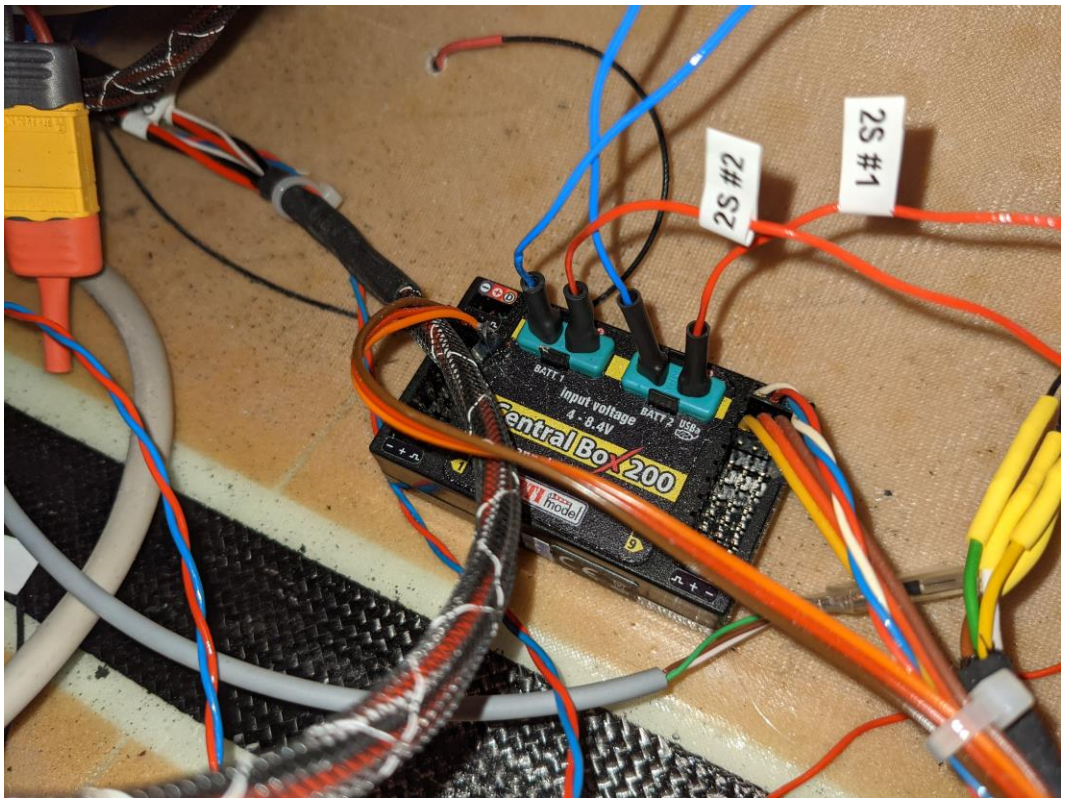

V-tailv2.0 update

A second set of V-tail was build, to house new IMU's for structural mode analysis. The same set of hardware were used as was in the first version. The IMU's are located in the outer section of the structure, in the farthest possible position from the root the V-tail.

The system had a successful ground and integration test, and ready for actual flight test.

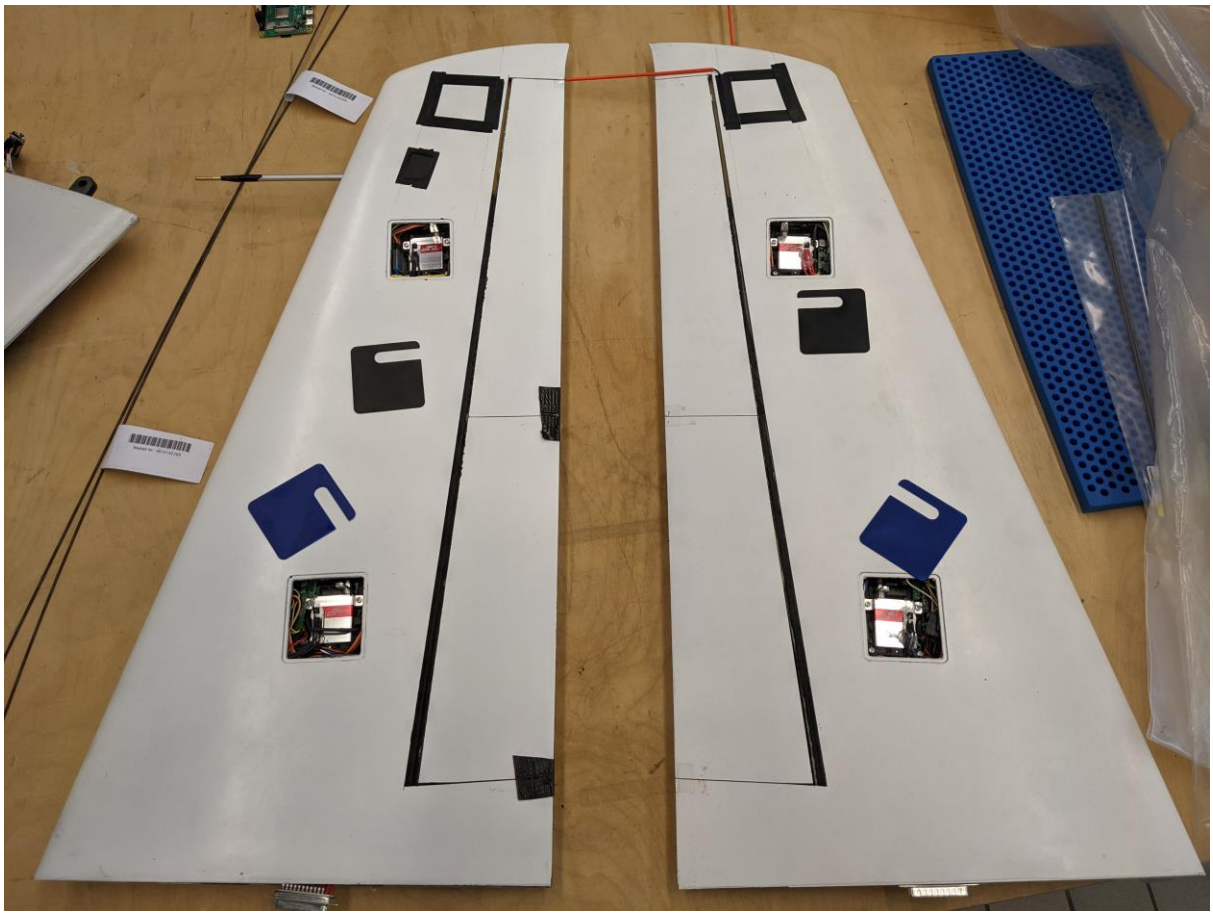

Preparations for flight test campaign

As discussed during the winter months, operations of flight testing had to be streamlined. This resulted in going through all of the checklists and trying to find out, which checklist points could be reduced without reducing safety. Checklists for packing and system start-up were improved. Additional equipment like a radio for airport communication, printer and additional tool kit all helped to decrease the time required to set off for flight testing.

In addition to acquiring new equipment, another pilot has been trained to operate the FLEXOP demonstrator. This required multiple flights with a smaller jet turbine powered glider to be conducted. As a result, three pilots are now available for flight testing, increasing the overall redundancy and flexibility of the flight test crew. Two additional flight test crew members are being trained for Ground Control duties at the moment.

In May 2020 it was decided to start planning the first flight test campaign. There were many uknowns still, due to landing gear not being fully fixed as well as uncertainty due to operational limitations imposed by Covid-19. In June, the first iterations of the landing gear were being tested, but the proper taxi test was only planned for the first day of the flight test campaign. Only the proper high-speed taxi test revealed that the solution applied did not give complete confidence to the pilots. Therefore for the

next few days other solutions were being tested on the field, resulting in a need to postpone the actual flight test further to next year. However, the flight planning was already finished for the first campaign and the test cards were fully prepared.

Figure 2.65. Third pilot preparing for training with a jet turbine sailplane.

	Flight Test Card	Page II	Flight Test Programme: FLEXOP-FTP-01-00	
	1.9 Baseline Controller Check	Time	CN	Remarks

1.	Engine **ON**	FLEXOP ONE, FLEXOP TWO	*		
2.	REPORT READY FOR TAKE-OFF	MANAGER			
3.	CHECK CONTROLS, FULL DEFLECTIONS	FLEXOP ONE			
4.	JETI WARNINGS **ON**	FLEXOP ONE			
5.	BRAKES **ON**	FLEXOP 1, FLEXOP 2, OPERATOR, ENGINEER			
6.	STANDBY TO ANNOUNCE TAKE-OFF AT 18m/s	OPERATOR			
7.	THROTTLE 100%, BRAKES **OFF** WHEN AIRCRAFT MOVES	FLEXOP 1			T-0
8.	ANNOUNCE **V1**	MANAGER			T+7
9.	FLIGHT STATE CRUISE, THROTTLE 70%, CLIMB 200	FLEXOP 1			At 30 AGL
10.	TRIM 38m/s	FLEXOP 1			
11.	SWITCH AUTOPILOT 1	FLEXOP 1			

Figure 2.66. First page of the test cards, prepared for the upcoming flights.

Flight Testing

After numerous iterations of the landing gear the pilots agreed that the aircraft is controllable. This allowed to continue the flight tests.

The first flight test under the name of the project was therefore conducted on 21st of April, 2021. Flight lasted for around 10 minutes and the autothrottle functionality was tested in the air. The graphs of the flight test can be seen below:

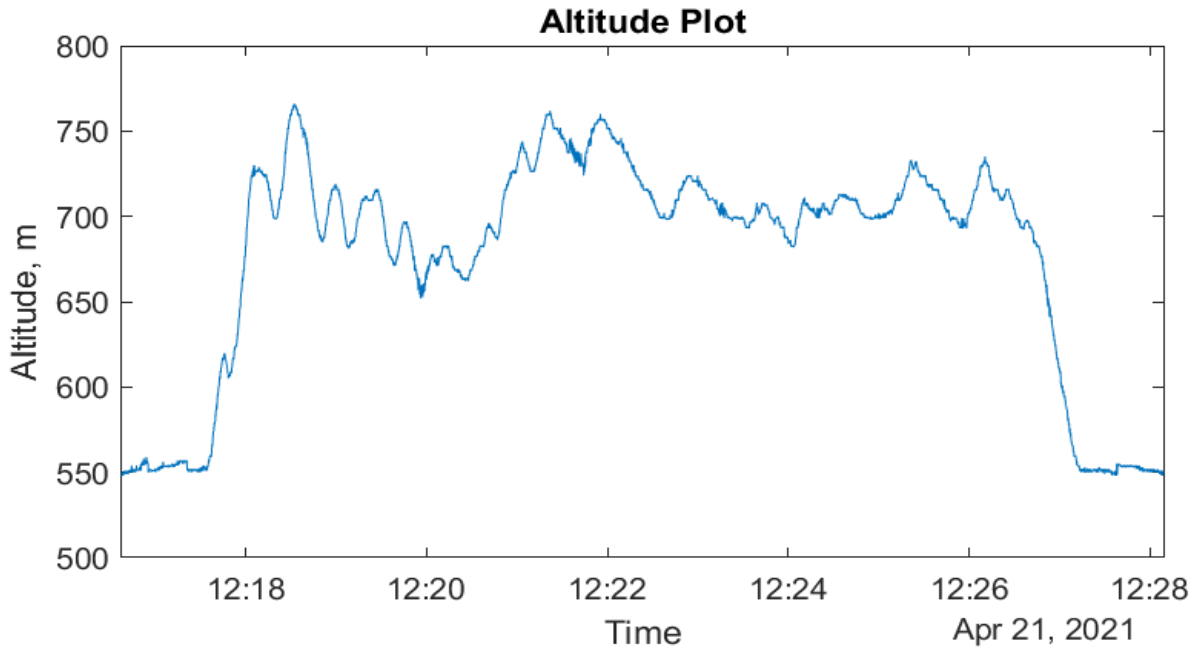

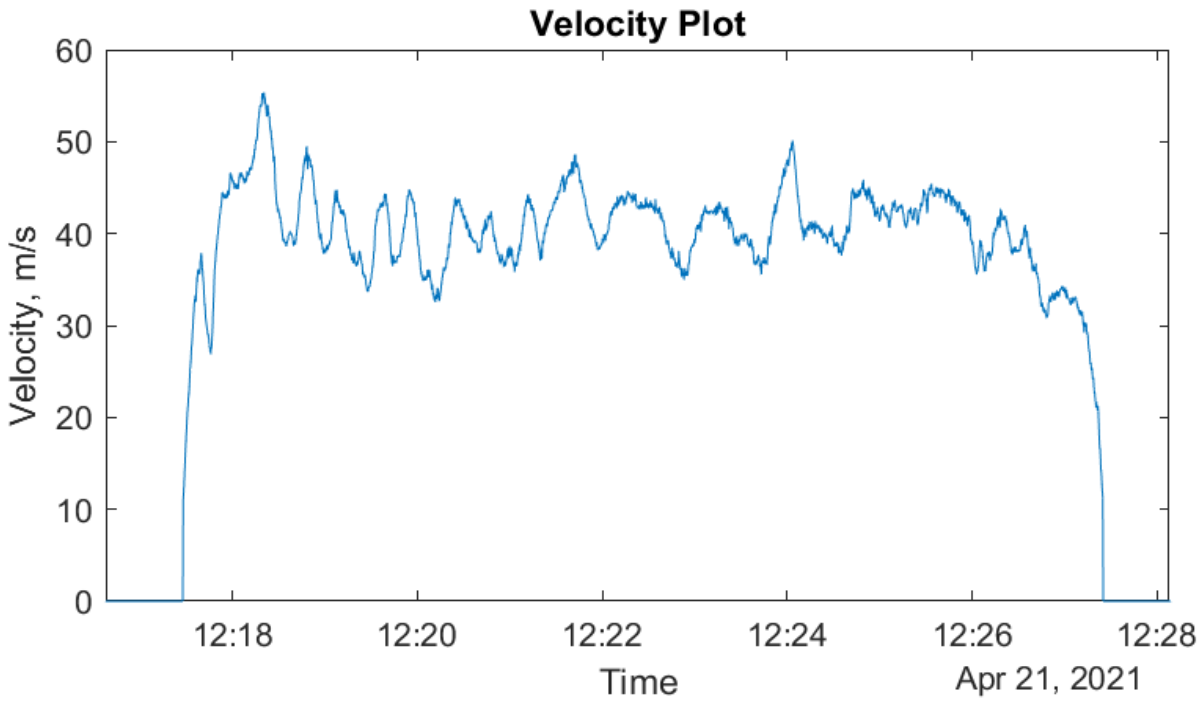

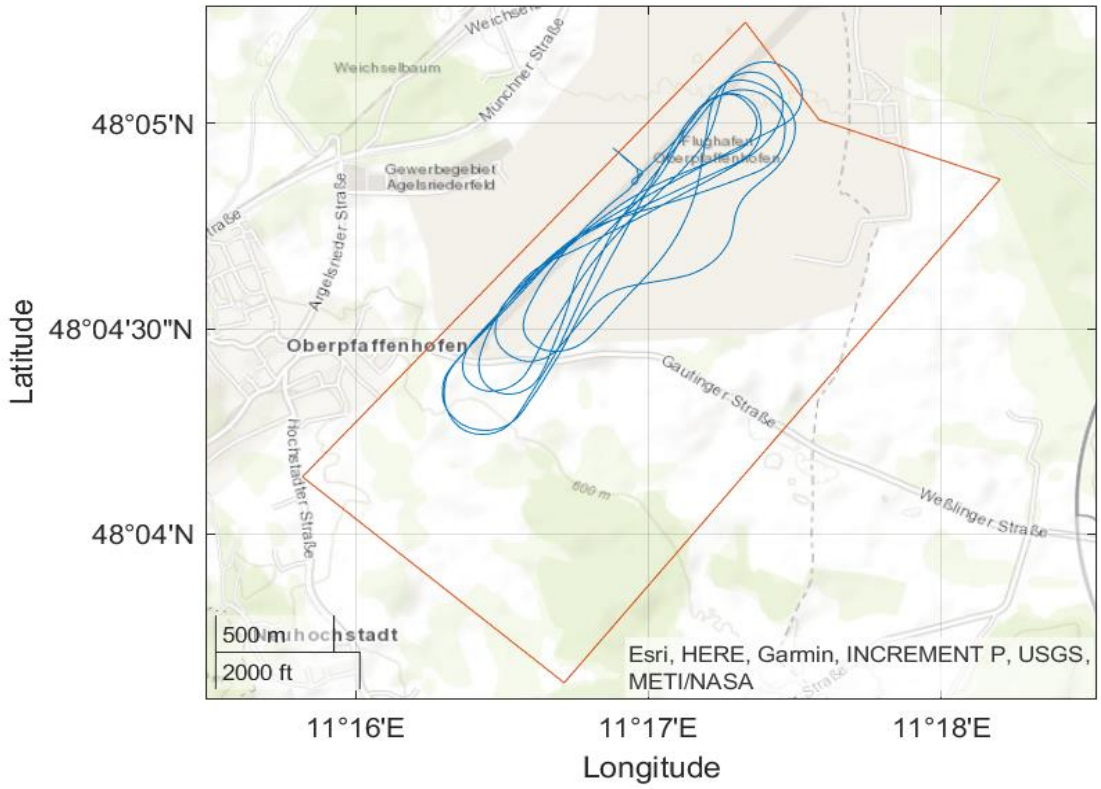

Flight data analysis

1. Flight test processing scripts

During initial phases of flight testing within the project, no on-field flight test data analysis was done. This was mainly due to high workload while on the test field. Consequently, the probability of immediately spotting problems with the aircraft or sensors was reduced, as data received via telemetry was limited. This was identified as a potential risk when multiple flights would be planned for a single day later on in the test campaign. If sensor problems are not identified during the visual inspection or via the telemetry, the test data recorded during the follow-up flight might become useless.

To counter this risk, a routine in MATLAB was developed for formatting, correcting, and analysing the raw flight test data. The main purpose of the routine was to conduct an automated preliminary flight data analysis right after the test flight with minimum intervention from the crew. The routine comprised of two steps: post-processing and analysis.

The post-processing step requires the raw log file (recorded at 200Hz) and aircraft setup file as inputs. The latter describes the parameters of the aircraft during the flight day, such as the centre of gravity position, take-off weight and sensor calibration values. Next, the post-processing step cleans up the raw log file from variables not related to flight physics, such as debug or sensor status variables. It is followed by trimming the flight log to 5 minutes before and after touchdown to reduce the file size. Finally, standard atmosphere variables for the day are assembled. As a result, a single file with a "timetable" variable is created.

The flight data analysis step further inspects the processed log file. Any of the following functionalities can be selected for the automated analysis:

2. Filtering and resampling

By default, most of the variables are passed through a peak filter and Spencer smoothing filter. Resampling is done only to speed up some of the functions listed below.

3. Sensor position error correction

The air-data probe and main IMU sensors are corrected for position errors.

4. Generating force and moment coefficients
5. Flight segmentation

The flight test trajectories always comprised of turn and straight legs, during which actual test manoeuvres were done. Therefore, it was convenient to have the straight legs automatically extracted. This is done by looking at the smoothed turn rate variable. After the segmentation, a summary of each leg is stored within a table including averages of airspeed, bank angle and other parameters for the segment. Therefore, a single leg can easily be chosen for a more detailed analysis without having to look at the complete flight.

6. Flight envelope display

Flight envelope is displayed together with flight data points marked within. This provides a quick overview about the moments during the flight that might have been outside the allowed flight envelope but were not noticed live via the available telemetry.

7. Flight test report generation

After the analysis, a Preliminary Flight Test Report can automatically be generated. The report includes trajectories, altitude and airspeed graphs, sensor error triggers, flight segment descriptions. It provides a quick overview of the flight and ideally can be already used during debriefing.

Similar and more advanced routines to the one described above have already been developed by Sobron ("ALAN Scripts")[1], Seher-Weiss ("FitlabGui")[2] and Bazzocchi[3].

The example of a flight test report that was automatically generated after the FT7 flight is seen in section X.

8. Lift curve analysis

To check for consistency in between the previous flight test campaigns, preliminary analysis of the FT7 was done.

Lift curve was investigated for clean configuration. Steady-level flight points were extracted from FT7 and compared to steady-level flight points and steady turn points from FT5 (*Figure 2.67*). Furthermore, theoretical estimation of the lift curve was added.

[1] Alejandro Sobron. “On Subscale Flight Testing: Applications in Aircraft Conceptual Design”. PhD thesis. Linköping University, 2018. ISBN : 9789176852200.

[2] Susanne Seher-weiss. FitlabGui - A MATLAB Tool for Flight Data Analysis and Parameter. Tech. rep. December 2015. 2016.

[3] Sean Bazzocchi. “UAV Flight Dynamics : Design and Development of a Framework for Flight Data Processing and Analysis”. Master. Politecnic University of Turin, 2018.

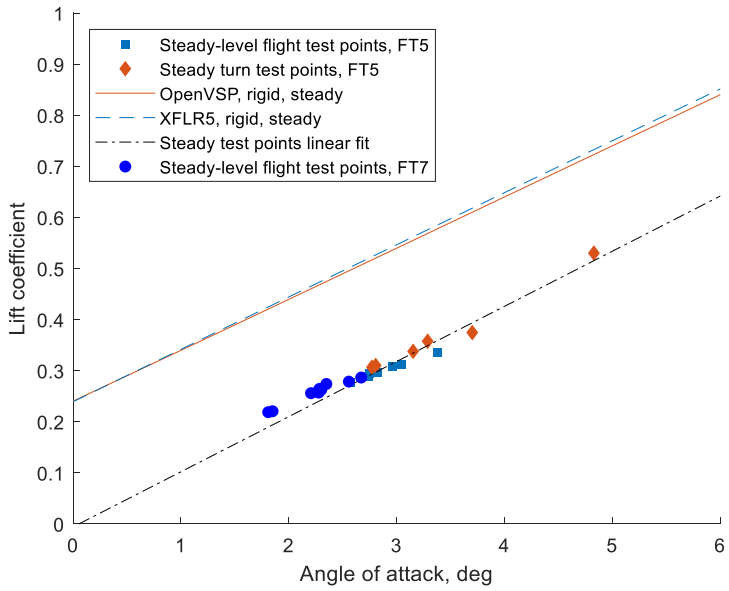

Figure 2.67 - Lift comparison (theoretical and in-flight data).

The following was noted:

- Lift curve as measured in-flight did not correspond to the theoretical estimations made by XFLR5 and OpenVSP software. An almost constant lift coefficient offset of around 0.2 can be observed which results in 35-45% lift loss in the 2-4deg angle of attack region.
- FT5 and FT7 data do align in the same trend.

The differences in between FT5 flight test data and theoretical estimations were already noticed before. However, initially it was assumed that maybe there are some errors in measurement of the angle of attack. After checking the alignment of the angle of attack probe, this suggestion was declined.

The reason for not achieving the estimated lift is being further investigated. Two potential cases are being checked:

- Loss of lift due to gaps in between the flaps and
- Wing flow separation due to bad turbulator design.

Unsteady lift coefficient curves from pushover-pull-up manoeuvres from FT5 were also compared (*Figure 2.68*).

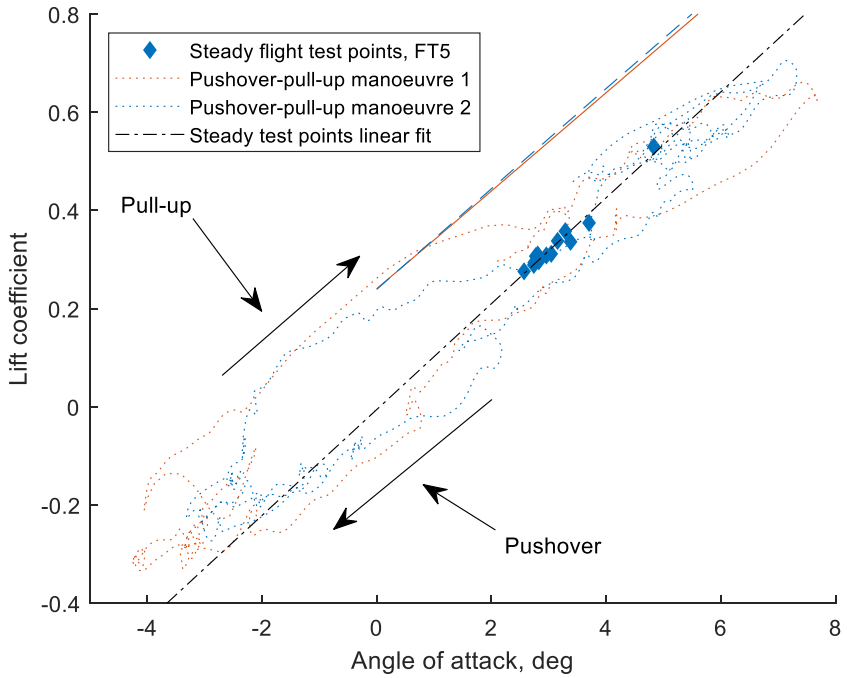

Figure 2.68 -Change of lift coefficient during pushover-pull-up manoeuvres.

It was noted that the lift coefficient values during the pull-up do match the theoretical predictions, while during pushover they fit in the same offset as the steady state manoeuvres. This could be an indication that the flow is indeed separated on a big part of the wing already at low angles of attack and it gets reattached during a pull-up.

3. Take-off data analysis

To better understand the bad take-off performance of the aircraft, detailed analysis of each take-off was done. Relevant data was plotted (*Figure 2.69* is an example from FT2) and specific take-off run points extracted. These points were summarised in *Table 1*.

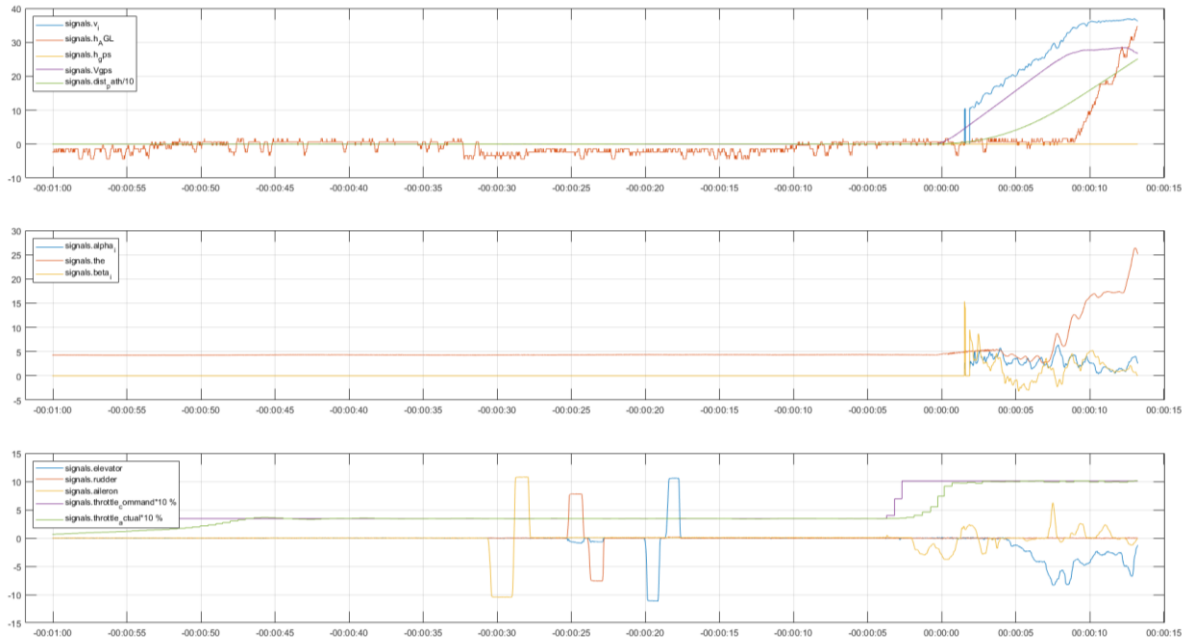

Figure 2.69 - Take-off data from Flight Test 2.

Table 1 - Take-off data summary. Values are averages from FT1, FT3, FT5, FT6, FT7. FT2 and FT4 were excluded due to high wind.

Nr	Description	Time, s	Distance, m	Airspeed, m/s	GPS Speed, m/s	Altitude (AGL), m	Throttle (command), %	Throttle (actual), %
1	Throttle up	-3.0	0.0	0.0	0.0	0	57	34
2	Start moving	0.0	0.3	0.0	0.5	0	100	83
3	Reach stall speed	4.4	43.0	18.0	16.5	0.8	100	100
4	Reach theoretical take-off speed	6.6	91.0	24.0	23.2	0.2	100	100
5	Take-off point (5m AGL)	10.7	198.2	33.9	31.9	5.3	100	100
6	Take-off finished (13m AGL)	12.8	267.8	36.7	35.1	13.4	100	100

What can be noted in the take-off data is that the lift-off airspeed, taken at 5m AGL is way higher than the design airspeed (34m/s vs 24m/s, or 42% higher). This might point to the same loss-of-lift problem as discussed in previous section.

4. Progress with flight testing

Multiple flight attempts were made since the first project flight in April, 2021. But with exceptionally bad weather this summer and technical issues while already in the airport, no flights took place in the period May-August.

For example, during flight preparations in July, a problem with the engine was discovered. It took the whole month to perform multiple tests with both engine units (spare and in-use), as well as to check the whole wiring. It was found that the control cable, going to the engine control unit, was broken. This meant that the engine sometimes would start going full-throttle and the pilot would not be able to control, neither shut the engine down. This was seen as hazardous risk and updates on the RXMUX software were made to eliminate the risk.

5. Comparison of built and theoretical airfoil geometry

To make sure that the wing is built as designed, another check was done to compare the theoretical and built airfoils.

The wing was scanned with the 3D scanner and compared to the CAD model (*Figure 2.70*). Most of the compared geometry matches the CAD model within 0.5mm.

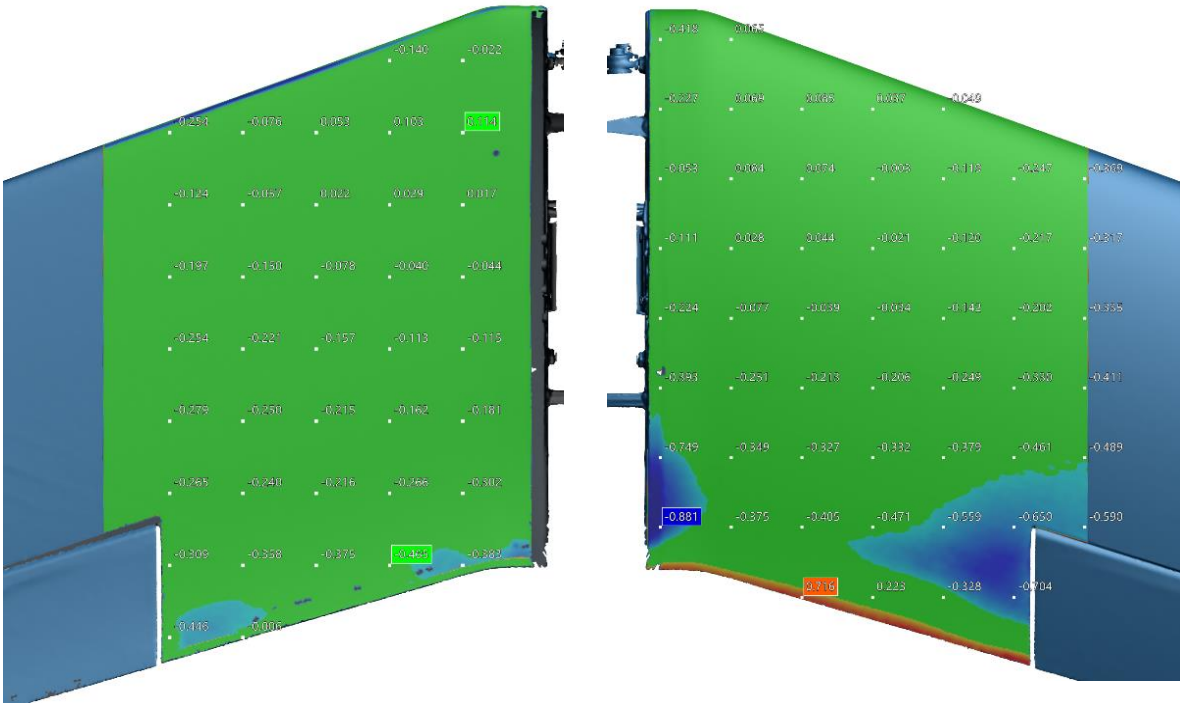

Figure 2.70 - Comparison in between the scanned wing and the CAD model (bottom surface left and top surface right). The built wing mostly matches the CAD within 0.5mm.

Furthermore, the airfoil shape was extracted at the root section. Then it was compared to the theoretical airfoil. After the comparison it was concluded that the airfoil matched the original one very well (*Figure 2.71*).

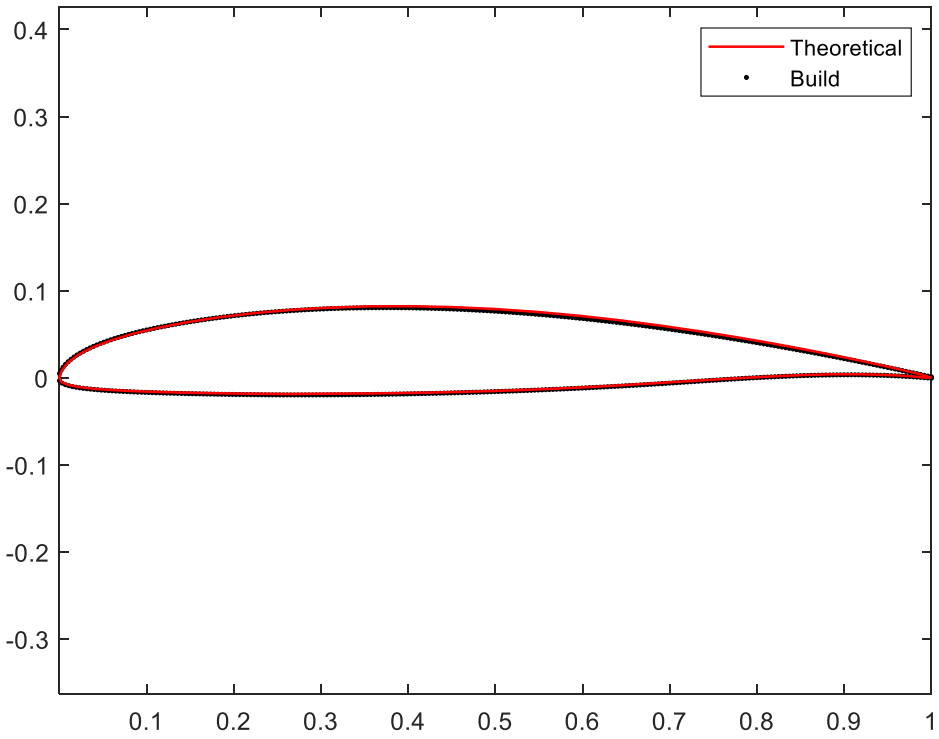

Figure 2.71 - Airfoil comparison in between the built and theoretical geometry.

6. Wing deformation measurement

A video-based wing deformation measurement system has been in development since May. The system will be used to gather further data for drag-reduction missions later.

The system uses two video cameras, mounted in the tail area of the aircraft (*Figure 2.72*). Tracking algorithms are applied to track flap hinges. This results in pixel coordinates of the hinges, which are later transferred into the 3D metric space.

The system is still in development until end of the year.

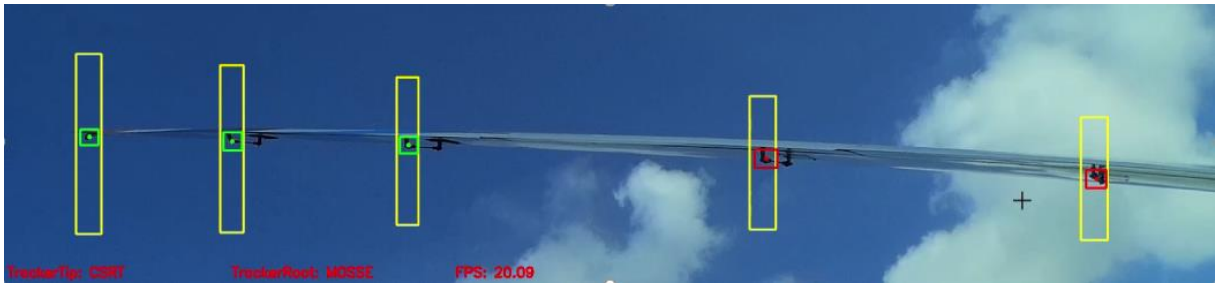

Figure 2.72 - A screenshot of wing deformation measurements in-flight.

Update and Validation of the -0 wing flight mechanical model

Structural Dynamics

The structural dynamics of a flexible aircraft can be divided into rigid body and flexible body dynamics. The rigid body dynamics basically describe the manoeuvre characteristics of the aircraft. In contrast, the flexible body dynamics represent the aircraft motion due to the flexibility of its structure. While the rigid body dynamics are described in nonlinear form, the equation of the flexible body dynamics is considered to be linear. A detailed FE model serves as basis for the structural model of the aircraft. The process of generating the FE model and its condensed version is described below. Subsequently, the EOM representing the rigid and flexible body dynamics are defined for the condensed model.

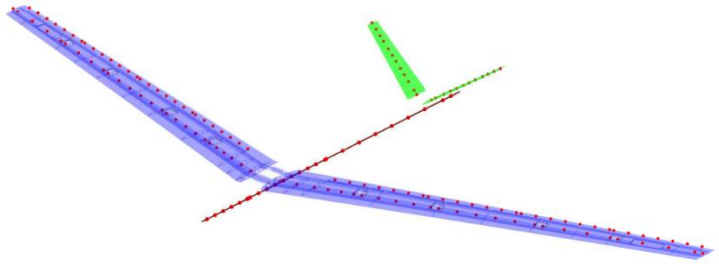

Figure 4: Full FE model of the FLEXOP demonstrator aircraft [9]

Finite Element Model

The aircraft structural FE model comprises the wing, fuselage and empennage and is shown in Figure 4. The FE software used here is MSC.NASTRAN. The wing is represented by a high-fidelity FE model comprising beam, surface and solid elements. Rigid body interpolation elements are added at predefined locations throughout the wing to facilitate the required model reduction. Further-more, the wing mass model is density-based as opposed to a lumped mass model. The fuselage structure is modelled using beam elements. The equivalent beam stiffnesses are obtained utilizing the cross sections of the fuselage hull at different sections and the lay-up of the hull. The mass is then lumped at the two beam nodes. The V-tail empennage FE model is shell-element-based comprising of the main structural load-bearing entities – the upper and lower skins, structural rubs, spars and the non-structural masses. Similar to the wing FE model, a density-based mass representation is used for the empennage as well.

Given that the FE model of the wing is of very high-fidelity (more than 600000 nodes), a Guyan reduction, also called condensation, is performed reducing the mass and stiffness matrix to less than 200 nodes in the condensed model.

Equations of Motion

The condensed model features rigid body and flexible modes, which are described by the EOM. These are based on an equilibrium of forces and moments. They describe the behaviour of the aircraft due to external loads originating from the aerodynamics and thrust. For simplification, the following assumptions are made.

- As the earth rotation can be neglected, the inertial reference system is earth fixed.

- Gravity is constant over the airframe.
- The deformations of the airframe are considered to be small which allows the use of linear elastic theory defined by Hooke's law.
- Due to small deformations of the aircraft structure, the aircraft mass moment of inertia J_b remains unchanged.

- As the structural deformations are small, loads act on the undeformed airframe.
- The eigenvectors of the modal analysis are orthogonal, because of which the total structural deformation can be written as a linear combination of the modal deflections.
- The rigid body and flexible body EOM are considered to be decoupled.

Rigid Body Dynamics

For the derivation of the nonlinear flight mechanical EOM, the aircraft is considered as a rigid body with a constant mass m_b and constant mass moment of inertia J_b. Therefore, the aircraft rigid body motion is described by the Newton-Euler EOM

$$\begin{bmatrix} m_b(\dot{V}_b + \Omega_b \times V_b - T_{be} g_e) \\ J_b \dot{\Omega}_b + \Omega_b \times (J_b \Omega_b) \end{bmatrix} = \underbrace{\Phi_{gb}^T P_g^{\text{ext}}(t)}_{P_b^{\text{ext}}(t)} = \begin{bmatrix} F \\ M \end{bmatrix}, \quad (1)$$

In Equation (1) the translational and angular velocity of the aircraft with respect to the body frame of reference are given by V_b and $_b$. The vector g_e represents the gravitational acceleration, which is transformed with T_{be} from the earth-fixed to the body-fixed frame of reference. The external loads vector

$$P_g^{\text{ext}}(t) = P_g^{\text{eng}}(t) + P_g^{\text{aero}}(t) \qquad (2)$$

includes the loads acting on the aircraft structure. Here the loads due to the engine thrust $P_g^{eng}(t)$ and the aerodynamic loads $P_g^{aero}(t)$ are considered. By means of the matrix Φ_{gb}^T the external loads are transformed into the rigid body frame.

Flexible Body Dynamics

As the displacements due to the aircraft flexibility are assumed to be small, linear elastic theory is applied to define the flexible body motion. Therefore the correlation between external loads $P_g^{ext}(t)$ and the generalized coordinates u_f representing the modal deformation of the structure is given by the differential equation

$$M_{ff}\ddot{u}_f + B_{ff}\dot{u}_f + K_{ff}u_f = \underbrace{\Phi_{gf}^T P_g^{\text{ext}}(t)}_{P_f^{\text{ext}}(t)}. \qquad (3)$$

The matrices M_{ff} , B_{ff} and K_{ff} depict the modal masses, dampings and stiffnesses. The modal matrix $_{gf}$ contains the eigenvectors of the structural modes sorted by frequency. Typically, higher frequencies have a smaller contribution to the overall system performance. Consequently, modal truncation can be applied to reduce the DOF significantly by considering only the most relevant eigenmodes.

Aerodynamics

The aerodynamic loads represent the major external loads acting on the aircraft structure. Their calculation is based on the VLM for steady aerodynamics and the DLM for unsteady aerodynamics. Both methods are based on a panel model, which is described in the following section.

Panel Model

The lifting surfaces are discretised by several trapezoidal-shaped panels, known as aerodynamic boxes as shown in Figure 5. Of note is the panel model for the fuselage. The wetted areas of the fuselage are projected onto a T-cruciform shaped panel model. Although this is a vast simplification, the fuselage aerodynamics are modelled quite accurately with respect to higher-order CFD simulations.

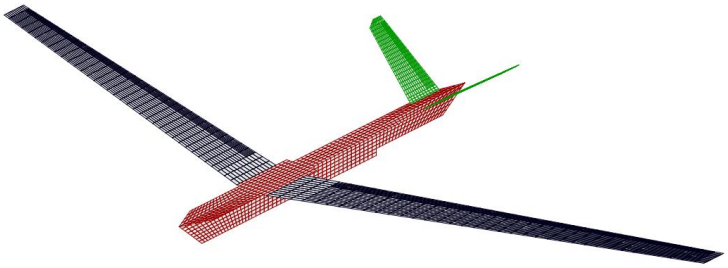

Figure 5: Aerodynamic boxes of the FLEXOP demonstrator aircraft [9]

Steady Aerodynamics— The VLM is used to model steady aerodynamics. As can be seen in Figure 6a, each aerodynamic box of the panel model possesses a horseshoe vortex at point l on the quarter-chord line. Due to the Helmholtz theo-rem the vortex is shed downstream to infinity at the side edges of the box. For each aerodynamic box the Pistolesi Theorem needs to be met, stating that there is no perpendicular flow through the control point j at the three-quarter-chord line.

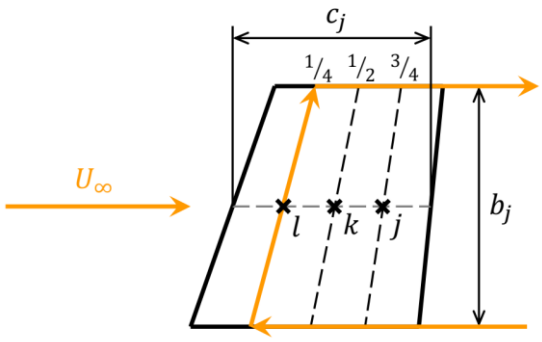

(a) Top view

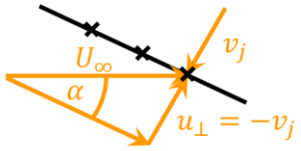

(b) Side view

Figure 6: Schematic drawing of an aerodynamic box [9]

Therefore the induced velocity at the control point needs to equalize the perpendicular component of the incoming flow, like shown in Figure 6b. By means of the Biot-Savart law the induced velocities v_j due to the circulation strengths $_j$ of the horseshoe vortices can be determined by

$$v_j = A_{jj}\Gamma_j. \qquad (4)$$

The matrix A_{jj} describes the contribution of all vortices to the induced velocities of the aerodynamic boxes. Inverting A_{jj} and multiplying with $2=c_j$, where c_j is the chord length of the respective aerodynamic box, leads to the aerodynamic influence coefficient (AIC) matrix Q_{jj}. In the steady aerodynamic case it is considered constant. The pressure coefficient c_{pj} of a panel is then determined by

$$\Delta c_{pj} = Q_{jj} w_j, \qquad (5)$$

where wj = is the velocity vj normalized with the flight speed U_∞. It is assumed to be equal to the angle of attack $_j$ of a panel, i.e. w_j = sin(w_j), as only small angles are considered. The downwash w_j comprises different aerodynamic contributions. It is affected by a rigid body motion of the aircraft
With

$$w_{jb_1} = \frac{c_r}{2U_\infty} D_{jk,2} \Phi_{ka} T_{ab} \begin{bmatrix} V_b \\ \Omega_b \end{bmatrix}. \qquad (6)$$

The vector $[V_b^T\ \Omega_b^T]^T$ contains the rigid body velocities V_b and angular rates $\Omega_b$and is transformed to the aerodynamic centre by means of T_{ab}. Subsequently, the respective motion of each panel reference point k is calculated by multiplying Φ_{ka} The resulting contribution to the downwash is then determined by multiplication with the matrix $D_{jk;2}$ and factorisation with $c_r/2U_\infty$, where c_r depicts the reference chord length. Further details on the determination of the contributions of the downwash can be found in Ref. 10. Under the assumption of small angles Equation (6) can be rearranged to

$$\begin{aligned} w_{jb_1} &= \frac{c_r}{2} D_{jk,2} \Phi_{ka} \begin{bmatrix} \cos\alpha_a \cos\beta_a \\ \tan\beta_a \\ \sin\alpha_a \\ p_a/U_\infty \\ q_a/U_\infty \\ r_a/U_\infty \end{bmatrix} \\ &\approx \frac{c_r}{2} D_{jk,2} \Phi_{ka} \begin{bmatrix} 1 \\ \beta_a \\ \alpha_a \\ p_a/U_\infty \\ q_a/U_\infty \\ r_a/U_\infty \end{bmatrix}. \end{aligned} \qquad (7)$$

It can be seen that, besides the angular rates p_a, q_a and r_a, the downwash is affected by the sideslip angle $_a$ and the angle of attack $_a$. The "1" in the vector represents a constant contribution to the downwash. This gives the opportunity to add the downwash caused by effects like camber and twist by adaptation of the first column of Φ_{ka}. As a first step, it is updated based on a steady computational fluid dynamics (CFD) calculation. The deflection of the control surfaces u_x is taken into account by changes in the downwash

$$w_{jx_0} = D_{jk,1}\Phi_{kx}u_x. \qquad (8)$$

The matrix Φ_{ka} links control surface deflections to the corresponding aerodynamic boxes. The differentiation matrix $D_{jk,1}$ then relates a displacement of the panel reference point k to the downwash w_j. Besides, the control surface deflection rate alters the lift, which can be accounted for by

$$w_{jx_1} = \frac{c_r}{2U_\infty} D_{jk,2}\Phi_{kx}\dot{u}_x. \qquad (9)$$

As depicted in Figure (3) the structural dynamics are affected by the aerodynamic loads P_g^{aero}. These can be expressed in terms of w_j as

$$P_g^{\text{aero}} = q_\infty T_{kg}^T S_{kj} Q_{jj} w_j + q_\infty T_{ag}^T S_r c_D, \qquad (19)$$

where the second term represents the aerodynamic drag loads with reference area S_r and the transformation matrix from the mean aerodynamic centre to the structural grid T_{ag}^T. Matrix S_{kj} depicts an integration relating the pressure in the aerodynamic boxes at point j with the forces at the aerodynamic grid points k. The forces at the aerodynamic grid points k are then interpolated onto the structural grid points via the transpose of the spline matrix T_{kg}. The splining model of the wing is exemplary shown in Figure 7.

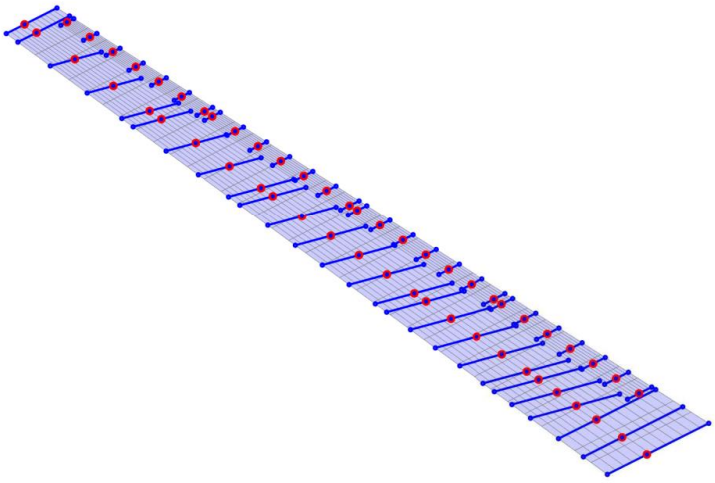

Figure 7: Splining between the aerodynamic model and structural model of the right wing [9]

Multiplying with the dynamic pressure q_∞ then leads to the aerodynamic loads acting on the structure. To distinguish between the distributions of the aerodynamic loads to the rigid and flexible body dynamics, Equation (19) is multiplied by Φ_{gb}^T and Φ_{gf}^T leading to

$$\begin{bmatrix} P_b^{\text{aero}} \\ P_f^{\text{aero}} \end{bmatrix} = \begin{bmatrix} \Phi_{gb}^T \\ \Phi_{gf}^T \end{bmatrix} P_g^{\text{aero}}. \qquad (20)$$

Due to aerodynamic loads the aircraft structure performs rigid body and flexible body motions which, in turn, affect the aircraft aerodynamics. Therefore the aeroelastic model is considered a loop between structural dynamics and aerodynamics.

Performed Manoeuvres

The parameter estimation process strongly depends on the performed manoeuvres in flight, as they define how well the characteristics of the aircraft can be determined. In order to define suitable excitation signals, a priori knowledge on the model is used. However, this is conflicting as the accuracy of the examined model determines the quality of the model parameters to be estimated. Nevertheless, under the assumption, that the chosen modelling process provides realistic results, this approach is considered applicable.

Flight Mechanical Manoeuvres

The first goal is to update the flight mechanical model. Therefore all contributions resulting from the aircraft flexibility are neglected. Besides, unsteady aerodynamic effects are ignored, as their contribution to the flight mechanical model is assumed to be small. As a result, for the aerodynamic load P_b^{aero} on the right-hand side of the rigid body equation of motion (1) it is only accounted for the downwash w_{jb1}, w_{jx0} and w_{jx1} yielding to

$$\begin{aligned} P_b^{\text{aero}} =& q_\infty \underbrace{\Phi_{gb}^T T_{kg}^T S_{kj} Q_{jj} \frac{c_r}{2} D_{jk,2} \Phi_{ka}}_{DQ_{h,b1}} \begin{bmatrix} 1 \\ \beta_a \\ \alpha_a \\ p_a/U_\infty \\ q_a/U_\infty \\ r_a/U_\infty \end{bmatrix} \\ &+ q_\infty \underbrace{\Phi_{gb}^T T_{kg}^T S_{kj} Q_{jj} D_{jk,1} \Phi_{kx}}_{DQ_{h,x0}} u_x \\ &+ q_\infty \underbrace{\Phi_{gb}^T T_{kg}^T S_{kj} Q_{jj} \frac{c_r}{2U_\infty} D_{jk,2} \Phi_{kx}}_{DQ_{h,x1}} \dot{u}_x. \end{aligned} \tag{21}$$

It is assumed, that the correlation between the control surfaces and the aerodynamic load given by the matrices DQ_{h,x_0} and DQ_{h,x_1} is accurately predicted by the proposed model. The focus is on an update of the rigid body contribution gathered in matrix DQ_{h,b_1}. It is a 6x6-matrix with the entries

$$Dh_{b1} = \begin{bmatrix} 0 & 0 & 0 & 0 & 0 & 0 \\ 0 & f_{y\beta} & 0 & f_{yp} & 0 & f_{yr} \\ f_{z0} & 0 & f_{z\alpha} & 0 & f_{zq} & 0 \\ 0 & m_{x\beta} & 0 & m_{xp} & 0 & m_{xr} \\ m_{y0} & 0 & m_{y\alpha} & 0 & m_{yq} & 0 \\ 0 & m_{z\beta} & 0 & m_{zp} & 0 & m_{zr} \end{bmatrix}. \tag{22}$$

There are 15 parameters, that are to be estimated. As can be seen the parameters related to forces in x-direction are neglected, due to the mentioned constraints of the model. Many more entries are equal to zero or considered too small to have a significant influence on the parameter estimation. The remaining parameters can be associated with either a longitudinal or a lateral aircraft motion.

In Table 2 the performed manoeuvres, separated in longitudinal and lateral, are listed with the parameters, that mainly contribute to the aircraft motion.

Table 2: Performed manoeuvres for the parameter estimation [11]

Longitudinal	
Steady level flight:	$f_{z0}, f_{z\alpha}, m_{y0}, m_{y\alpha}$
Pushover-pullup:	$f_{z0}, f_{z\alpha}, f_{zq}$
Short period:	$f_{z\alpha}, f_{zq}, m_{y\alpha}, m_{yq}$
Phugoid:	$f_{z0}, f_{z\alpha}, f_{zq}, m_{y0}, m_{y\alpha}, m_{yq}$
Lateral	
Steady sideslip:	$f_{y\beta}, m_{z\beta}$
Dutch-roll:	$f_{y\beta}, f_{yr}, m_{x\beta}, m_{xr}, m_{z\beta}, m_{zr}$
Bank-to-bank:	f_{yp}, m_{xp}, m_{zp}

The definition of the excitation signals for the short period, phugoid and dutch-roll mode are determined based on an a priori analysis of the initial model. The phugoid is excited by an elevator pulse, that is chosen to last 2 seconds with an amplitude of approximately 3°. This elevator deflection was found to be appropriate to excite the phugoid mode of the aircraft. The dutch-roll mode can be excited by a doublet on the rudder. The amplitude is chosen to be around 3°, while the half time length $\Delta t_{doublet}$ of the doublet is calculated with the dutch-roll frequency $\omega_{dutch-roll}$ by the rule of thumb

$$\Delta t_{\text{doublet}} \approx \frac{2.3}{\omega_{\text{dutch-roll}}} \qquad (23)$$

to be 1.22 seconds. The dutch-roll frequency $\omega_{dutch-roll}$ is determined from the simulation in advance of the flight test. Equivalently, the short period mode can be observed by exciting the elevator with a doublet. Equation (23) gives a $\Delta t_{doublet}$ of 0.24 seconds with the pre-determined frequency of the short-period $\omega_{short-period}$. The amplitude is chosen to be around 6°.

The steady level flight, pushover-pullup, steady sideslip and bank-to-bank manoeuvres were flown manually by the pilot.

Update of the Rigid Body Model

When it comes to updating an aircraft model or rather specific model parameters, a suitable process needs to be set up. On the one hand a model structure must be given including parameters to be estimated and on the other hand an optimization algorithm to find the somewhat best model parameters needs to be given. There exist different optimization algorithms to estimate model parameters, like the output error method (OEM), the filter error method (FEM) and more. Within the scope of this paper the output error method based on maximum likelihood estimation is chosen.

Output Error Method

In Figure 12 the basic procedure of the OEM is shown.

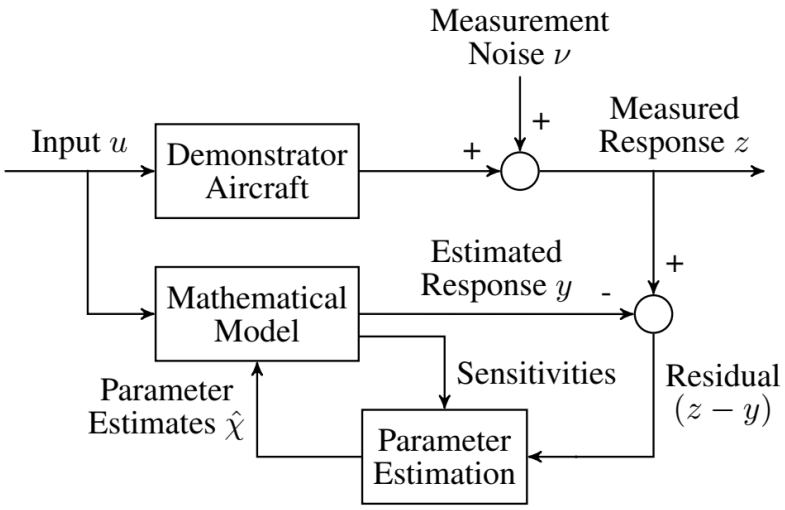

Figure 12: Concept of the output error method [25]

The upper path represents the flight test, where the outcome is the measured inputs and outputs. The OEM assumes, that the outputs are affected by measurement noise. Process noise, however, is neglected. Subsequently, the inputs are fed into the mathematical model to conduct a simulation of the considered flight test manoeuvre. Based on the difference between the flight test measurements and the simulation outputs, the parameters of the mathematical model are updated by means of an optimisation.

It is assumed, that the model equations are given in the form of

$$\begin{aligned} \dot{x}(t) &= f(x(t), u(t), \chi),\ x(t_0) = x_0 \\ y(t) &= g(x(t), u(t), \chi) \\ z(t_k) &= y(t_k) + \nu(t_k). \end{aligned} \tag{24}$$

The first two equations describe the proposed mathematical model. They dependent on the desired parameters χ. The last equation provides the relation between the discrete flight test measurements z and the output of the measurement equation y at a time instant t_k. They exclusively differ in the measurement noise ν. The noise process is considered stochastic and is characterized by Gaussian white noise with zero mean. Its definition is

$$\begin{aligned} E\{\nu(t_k)\} &= 0 \\ E\{\nu(t_k)\nu(t_l)^T\} &= R\delta_{kl}. \end{aligned} \tag{25}$$

The second expression of Equation \ref{eq:gwn} suggests that the noise process white noise, as it is time independent. Simultaneously the amplitude depends on chance defined by a Gaussian distribution with covariance matrix R it describes Gaussian noise. As a result the measurement vector $z(t_k)$ with dimension n_z is affected by Gaussian white noise and therefore its values are assumed to be Gaussian distributed with a probability density function

$$p(z(t_k)|\chi) = \frac{1}{(2\pi)^{(n_z/2)} sqrt|R|} \exp\left(-\frac{1}{2}(z(t_k) - y(t_k))^T R^{-1}(z(t_k) - y(t_k))\right). \quad (26)$$

With respect to Equation (24) the expected value of $z(t_k)$ is assumed to be $E\{z(t_k)\} = y(t_k)$ for the model parameters χ. For a set of N measurements the likelihood function becomes

$$p(z(t_1), ..., z(t_N)|\chi) = \prod_{k=1}^{N} p(z(t_k)|\chi) = [(2\pi)^{n_z}|R|]^{-N/2} \exp\left(-\frac{1}{2}\sum_{k=1}^{N}(z(t_k) - y(t_k))^T R^{-1}(z(t_k) - y(t_k))\right). \quad (27)$$

Goal of the maximum likelihood method (MLM) is to identify the model parameters χ, which maximise the probability defined by Equation (27). The optimal solution is the maximum likelihood estimate obtained as

$$\hat{\chi}_{ML} = \arg\left\{\max_{\chi} p(z|\chi)\right\} = \arg\left\{\min_{\chi}(-\ln p(z|\chi))\right\}. \quad (28)$$

For greater ease of handling the negative logarithm of the likelihood function $p(z|\chi)$ is considered, which simplifies Equation (27) to the cost function

$$J(\chi, R) = \frac{1}{2}\sum_{k=1}^{N}\left((z(t_k) - y(t_k))^T R^{-1}(z(t_k) - y(t_k))\right) + \frac{N}{2}\ln(|R|) + \frac{Nn_z}{2}\ln(2\pi). \quad (29)$$

At this point it is assumed, that the covariance matrix R is unknown a priori. As R depends on the model parameters χ and vice versa, the relaxation strategy is used to find the optimal solution of the redefined likelihood function (29) in two steps. Firstly, for a given parameter vector χ the maximum likelihood estimate of R is obtained by setting the partial derivative $\partial J(\chi, R)/\partial R$$ to zero. This yields

$$R = \frac{1}{N}\sum_{k=1}^{N}(z(t_k) - y(t_k))(z(t_k) - y(t_k))^T. \qquad (30)$$

Secondly, substituting (30) in (29) provides

$$J(\chi) = \frac{1}{2}n_z N + \frac{N}{2}\ln(|R|) + \frac{Nn_z}{2}\ln(2\pi). \qquad (31)$$

Apart from ln(|R|) all terms in Equation (31) are independent from the model parameters χ. The cost function therefore reduces to

$$J(\chi) = \det(R). \qquad (32)$$

Equation (32) is solved iteratively for the optimal model parameter χ by means of a Gauss-Newton algorithm.

Two-Step Method

By means of the two-step method (TSM) the model parameters can be determined. The TSM divides the state and parameter estimation problem in a flight path reconstruction and a parameter identification part. The flight path reconstruction is used to accurately reconstruct the time history of the aircraft states during the manoeuvre and besides allows the determination of potential instrumentation errors. As some sensor readings, like the angle of attack and the airspeed, are prone to be inaccurate, the measurements are improved based on past, present and future data and the flight mechanical equations. Subsequently, the identification of the model parameters follows.

The success of the TSM depends on the aircraft to be tested, the aircraft instrumentation, the excitation signals, the mathematical model selected for identification and the chosen algorithm for the analysis and adaption of the model.

Flight Path Reconstruction

The flight path reconstruction is based on a non-linear state-space system consisting of flight mechanical state and measurement equations. The considered inputs are the translational accelerations a_{bm} and the rotational rates Ω_{bm} measured in flight by an IMU placed in the fuselage. The states are the velocity vector V_b, the Euler angles ϕ, θ and ψ and the altitude h. The resulting state equations are given by

$$\dot{V}_b = a_b - (\Omega_{b,m} - \Delta\Omega_b) \times V_b + T_{be}g_e \qquad (33)$$

$$\begin{bmatrix}\dot{\phi}\\ \dot{\theta}\\ \dot{\psi}\end{bmatrix} = \begin{bmatrix}1 & \sin\phi\tan\theta & \cos\phi\tan\theta\\ 0 & \cos\phi & -\sin\phi\\ 0 & \frac{\sin\phi}{\sin\theta} & \frac{\cos\phi}{\sin\theta}\end{bmatrix}(\Omega_{b,m} - \Delta\Omega_b) \qquad (34)$$

$$\dot{h} = [0 \quad 0 \quad -1]\,T_{be}^{-1}V_b. \qquad (35)$$

Starting point of the state equations is the equilibrium of forces of the rigid-body equation of motion. Solving Equation (1) for $\dot{V}_b$ leads to Equation (33), where Ω_b is replaced by its flight test measurement Ω_{bm} including a potential sensor bias $\Delta\Omega_b$. The translational acceleration a_b is given with respect to the center of gravity. It is determined by

$$a_b = a_{b,m} - \dot{\Omega}_b \times d_s - \Omega_b \times (\Omega_b \times d_s) - \Delta a_b. \qquad (36)$$

The acceleration measurement $a_{b,m}$ needs to be corrected for the coriolis and the centrifugal force caused by the offset between the acceleration sensor position and the center of gravity d_s. A potential sensor bias is covered by Δa_b. Additional state equations of the Euler angles ϕ, θ and ψ are considered through Equation (34). The remaining state equation is given by Equation (35). The inverse of T_{be} transforms the velocity V_b to the Earth-fixed frame of reference. Extracting only the element, which contributes to the z-direction, and changing the sign leads to the derivative of the altitude $\dot{h}$.

The outputs or reconstructed instrumentation measurements are the true airspeed $U_{\infty,r}$, the angle of attack α_r, the sideslip angle β_r, the Euler angles ϕ_r, θ_r and ψ_r and the altitude h_r. The corresponding measurement equations are given by

$$U_{\infty,r} = \|V_b\|_2 \qquad (37)$$

$$\alpha_r = K_\alpha \tan^{-1}\left(\frac{V_{nb,z}}{V_{nb,x}}\right) + \Delta\alpha \qquad (38)$$

$$\beta_r = K_\beta \sin^{-1}\left(\frac{V_{nb,y}}{|V_{nb}|}\right) + \Delta\beta \qquad (39)$$

$$\phi_r = \phi \qquad (40)$$

$$\theta_r = \theta \qquad (41)$$

$$\psi_r = \psi \qquad (42)$$

$$h_r = h. \qquad (43)$$

As the α and β measurements of the noseboom are sensitive to errors, the scaling and bias variables K_α, $\Delta\alpha$, K_β and $\Delta\beta$ are introduced. The velocity vector V_{nb} at the noseboom is determined by

$$V_{nb} = V_b + (\Omega_{b,m} - \Delta\Omega_b) \times d_{nb}, \qquad (44)$$

where d_{nb} is the distance between the aircraft CG and the noseboom. In theory the difference between the flight test measurements and the reconstructed measurements in (37)-(43) with respect to the OEM is only coming from the process noise ν.

The unknown parameters $\Delta\Omega_b$, Δa_b, K_α, $\Delta\alpha$, K_β, $\Delta\beta$ as well as the initial states V_{b0}, $[\phi_0\ \theta_0\ \psi_0]^T$, h_0 in Equations (33)-(35) are determined based on the introduced OEM algorithm. The residual (z-y) to be minimized is the difference between the flight test measurements and their reconstructed counterpart in Equations (37)-(43).

The FPR is performed for each considered manoeuvre type separately. Figures 13 and 14 depict the FPR exemplary for a pushover-pullup manoeuvre (POPU) and for a sideslip manoeuvre (SL) in comparison with the measured flight test data (FTD).

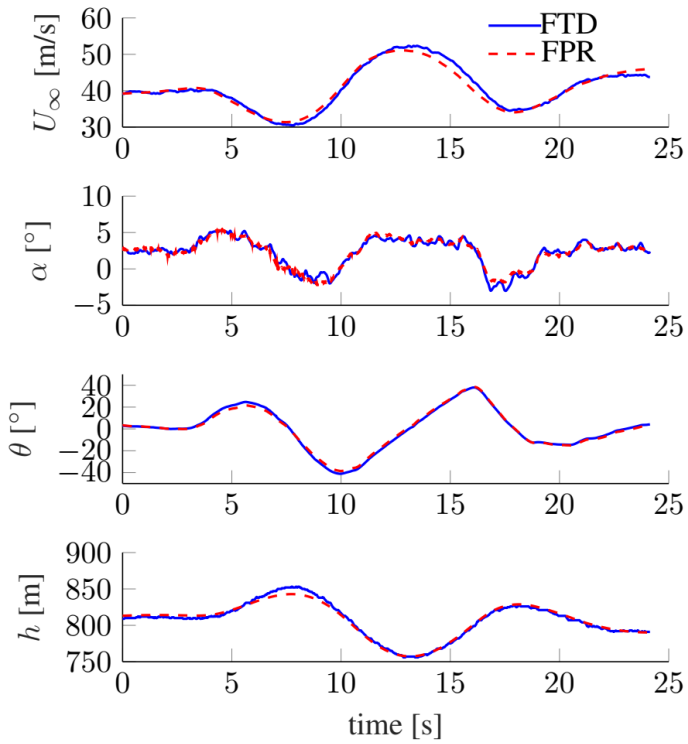

Figure 13: Comparison of reconstructed and flight test measurements (POPU)

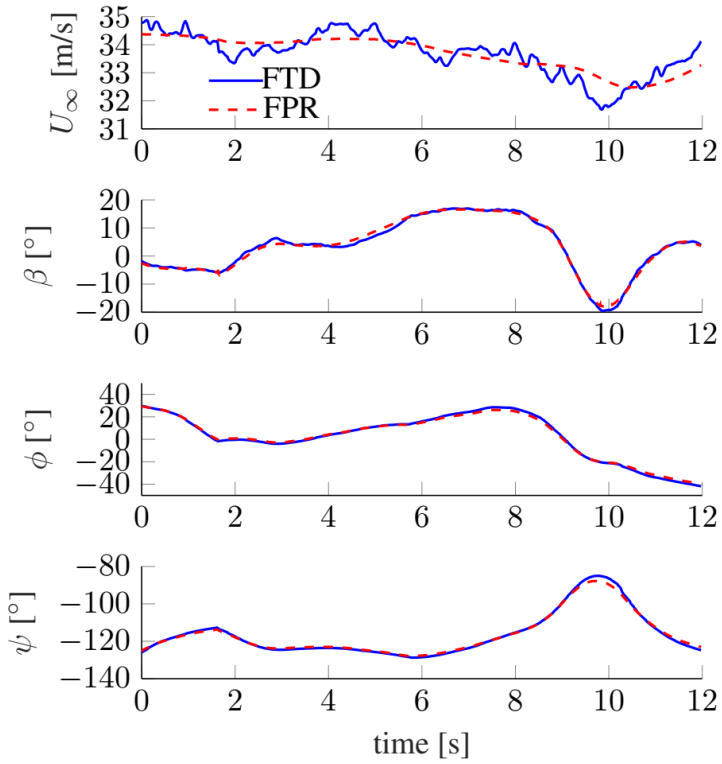

Figure 14: Comparison of reconstructed and flight test measurements (SL)

Only the measurement variables that play a major role for the manoeuvres are shown. For the POPU manoeuvre it can be seen, that α changes dynamically, while the remaining measurements are rather smooth. Nevertheless, the reconstructed α follows very closely the measurement.

The sideslip manoeuvre is not performed at a constant β as intended. However, it still offers the opportunity for updating lateral model parameters. The FPR follows the trends of the observations very well. An exception is the reconstructed true airspeed U_∞ which follows the trend of the measurement, but does not change as dynamically. As this behaviour is not observed for the additional measurements, it is valid to say the true airspeed is more strongly affected by disturbance.

Parameter Estimation

The parameter estimation is the second step of the two step method. The control surface deflections commanded during the various flight test manoeuvres are fed in the rigid body equation of motion (1). As mentioned before the parameters of the matrix $DQ_{h,b1}$ defined in Equation (21) are to be estimated. Based on the comparison between the outputs of the flight test z and the simulation y the model parameters are updated like described in the section “Output Error Method”.

The parameters corresponding to the longitudinal and lateral motion respectively are updated in separate steps. At first, the lateral manoeuvres are used to improve the matrix $DQ_{h,b1}$ with respect to the parameters $f_{y\beta}$, f_{yp}, f_{yr}, $m_{x\beta}$, m_{xp}, m_{xr}, $m_{z\beta}$, m_{zp} and m_{zr}. Subsequently, the longitudinal parameters f_{z0}, $f_{z\alpha}$, f_{zq}, m_{y0}, $m_{y\alpha}$ and m_{yq} are updated with the matrix $DQ_{h,b1}$ coming from the

previous step. The final step is to redo the lateral update. This approach is chosen, because the longitudinal manoeuvres also feature lateral contributions and vice versa. Therefore, a strict separation of the manoeuvres is not possible.

At the end, the OEM leads to the parameters summarized in Tables (3) and (4).

Table 3: Initial and final longitudinal parameters

Parameter	Initial	Final
f_{z0}:	-0.601	-0.484
$f_{z\alpha}$:	-15.12	-15.19
f_{zq}:	-7.41	-0.056
m_{y0}:	0.067	-0.02
$m_{y\alpha}$:	-1.63	-2.19
m_{yq}:	-13.58	-5.94

Table 4: Initial and final lateral parameters

Parameter	Initial	Final
$f_{y\beta}$:	-0.621	-0.661
f_{yp}:	-0.321	-2.35
f_{yr}:	2.52	3.41
$m_{x\beta}$:	-0.382	-2.08
m_{xp}:	-109.9	-126.4
m_{xr}:	1.28	32.61
$m_{z\beta}$:	0.464	0.48
m_{zp}:	0.294	-3.95
m_{zr}:	-4.02	-4.05

Of note is that the f_{z0} contributing to the lift with respect to camber and drag was lightly overestimated with the CFD calculations mentioned before. For corresponding moment coefficient m_{y0}, however, undergoes a relatively big change and switches sign. The $f_{z\alpha}$ and $f_{y\beta}$ value does not change much, which proves the strength of the VLM/DLM modelling approach. Some final parameter values differ strongly from their initial values. It is still under investigation to what extent the simplified modelling of the x-forces plays a role.

When the pushover-pullup (POPU) manoeuvre is performed with the model featuring the estimated parameters (PE), one can recognize a strong similarity with the reconstructed flight test data (FPR). Figure 15 depicts the trend of some of the observation variables affected by a longitudinal motion.

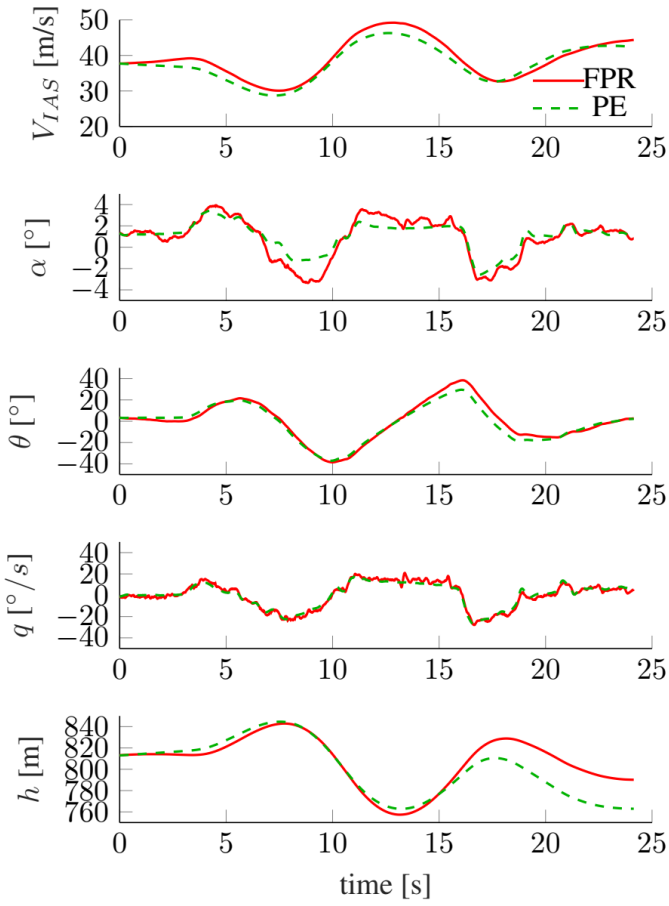

Figure 15: Comparison between reconstructed and simulated measurements (POPU)

The difference between the reconstructed and simulated angle of attack α possibly reveals the sensitivity to external disturbances. However, especially the pitch rate q matches very well between both data sets.

The measurements of the sideslip manoeuvre exhibited in Figure 16 proves, that the set of estimated parameters of the model fits well with the flight test data.

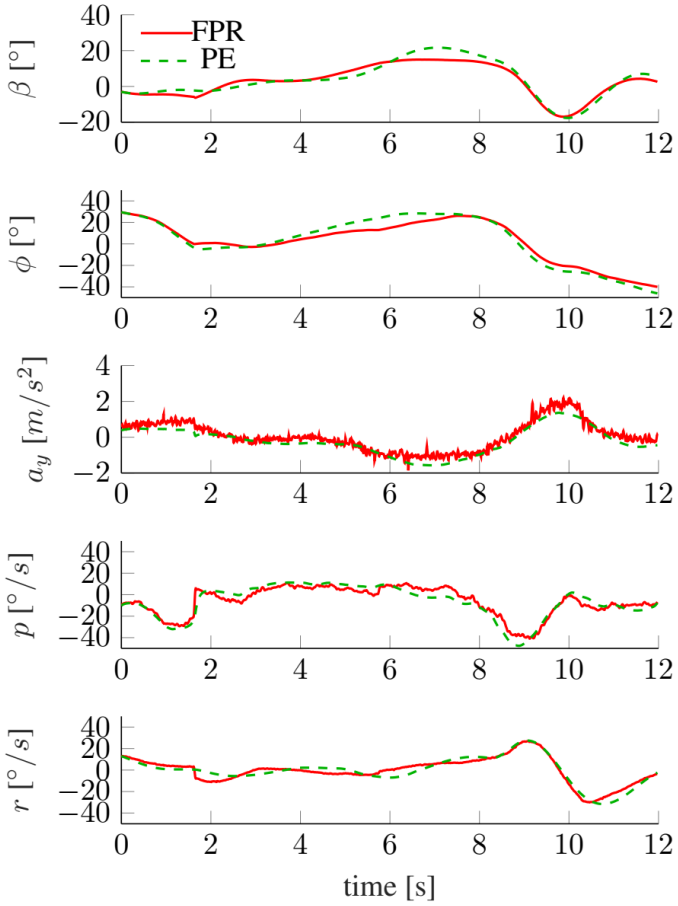

Figure 16: Comparison between reconstructed and simulated measurements (SL)

2.3.3 Deviations, their reason, impact on the project and corrective actions

The biggest deviation came from not being able to fix the aircraft's ground controllability in a timely manner. This mainly was due to two reasons: there were restrictions imposed on access to the workshops at TUM and the Airport due to Corona and the problem appeared to be way more difficult to solve than was initially anticipated. The many iterations, implementation of which only started in June, could only help bit by bit. In addition, not having a workshop at the airport, this proved time-costly to try new concepts out.

Due to the landing gear problems, it was decided not to risk the aircraft and not attempt to conduct test flights as was planned before. Therefore, the first flight test campaign had to be postponed until the controllability of the aircraft is sufficient and it can be made sure that the aircraft will not be destroyed due to ground controllability problems.

After solving the landing geaproblemst up to acceptable status a flight test on April 2021 could be conducted. During this test we had an unexpected low voltage warning. The cause could be solved afterwards during ground tests. Unfortunatly more technical problems, especially not starting or controllable engine prohibited further test flights so far.

Figure 2.73. Another close call due to the inadequate steering on the ground. The demonstrator stopped shortly before the taxiway lamp.

In order to mitigate the risk posed to the project by a delayed -3-wing design due to delays in the development of the multi-disciplinary design loop, a study was conducted that investigated the feasibility to equip an existing -0- or -2-wing with the hardware necessary to serve as a -3-wing substitute. The -0- and -2-wing was considered, because their skin layup is considered strong enough to make a redesign practical. The feasibility investigation focused on the feasibility of attaching and actuating a total of eight flaps at each wing, for that number of flaps was considered sufficient to allow shape control and load alleviation, while still feasible to integrate into an existing wing. The following questions were addressed, for they were considered the most important:

1. How can the total of four additional servos per wing be fixed?
2. How can the total of four additional servos per wing be powered?
3. How can the total of four additional flaps per wing be produced?
4. How can the total of four additional flaps per wing be attached to the respective wing?

In order to answer aforementioned questions, the structural and electrical information available about the -0- and -2-wing are compiled. Both, the -0-wing and the -2-wing have an internal structure that is able to withstand the flight loads within the envelope. The wing skins are made up of 30 and more layers of CFRP-material and an internal structure. The existing wiring consists of four 3-wire cable bundles for powering and controlling the servos as well as two CAN-bus cables. Of the two CAN-bus cables only one is in use while the other serves as preinstalled spare part. The setup is shown in the following pictures.

Figure 2.74: Inner part of a wing showing the inner structure and cabling before the attachment of servos and sensors.

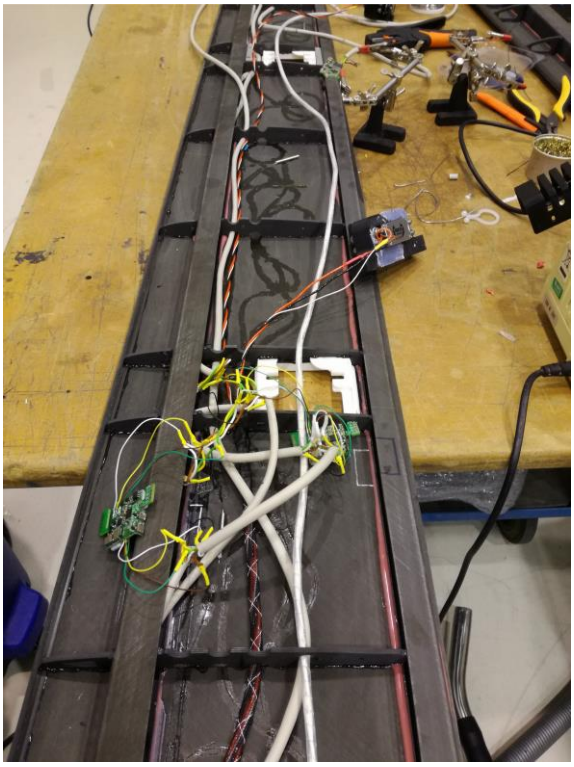

Figure 2.75: Outer part of a wing showing the inner structure and attached sensors and servos.

Based upon the information aforementioned, the following considerations were made:

1. The additionally required servos can either be attached externally or internally, because the skin is considered strong enough to attach additional servos on the outside as well as to withstand the damage caused by the cutting of holes for internal installation. The old servos, should not be moved.
2. Several possibilities for the powering of the additional servos are imaginable, the following are considered:
    a. Using the existing wiring only:
        i. Servos that are controlled using CAN-bus could be powered and controlled using the spare CAN-bus cable if the power consumption can be supported by the installed CAN-bus cable.
        ii. Servos that are controlled using CAN-bus could be powered by Y-cables that are spliced from the existing cables supplying the existing servos.
        iii. Standard servos that are controlled by the use of PWM-signals could be powered by Y-cables that are spliced from the existing cables supplying the existing servos and the necessary PWM-signal routed over the existing spare CAN-bus cable that is repurposed for that application.
    b. New wiring could be routed in the following places:
        i. Within in the leading edge, would make holes in the main spar necessary.
        ii. Between the rear spar and the flaps.
        iii. In the area between the two wing spars.
3. New flaps could be produced by either cutting existing flaps in half. This procedure, however, is considered very difficult because new hard-points for the hinges and servo horns have to be attached. Another approach would be the production of new flaps from a mold.

4. For the attachment of flaps new hinges have to be implemented. It is deemed feasible to attach the hinges on the rear (i.e. outer) side of the rear-spar. It is questionable, however, if this approach also works out for the most outer flaps. Here an opening of the wing structure could be both necessary and feasible.

Based on aforementioned considerations the retrofit of either a -0- or -2-wing is considered feasible. For a conclusive judgement, however, further detailed designs and installation routines have to be investigated which is currently done in a master thesis.

2.4 Explanation of the work carried per WP- Work Package 4

In order to demonstrate the benefits of including the Flight Phase Adaptive Aero-Servo-Elastic Aircraft Design Methods (FliPASED) in an integrated aircraft design, it is planned to demonstrate the performance claims in a scale-up task. As baseline reference for this scale-up task a High-Fidelity Flexible Aircraft Benchmark will be defined in coordination with the industrial advisory board and used as the reference during the project. The resulting derivative aircraft will have a more flexible wing, with tailoring modifications in the wing structure designed for lower safety factor, which is enabled by advanced avionics and flight control architecture, leading to better gust response at lower structural weight.

The two main objectives of the scale up task are:

1. The demonstration of the applicability of the collaborative design process to a (full-scale) passenger aircraft
2. The quantification of the benefits of integrated aircraft and controls design in terms of structural weight reduction and aircraft over-all performance parameters.

2.4.1 Objectives and activities

Within FliPASED the focus lies on including control design as a primary discipline in a collaborative design workflow/MDA/MDO.

Some previous experience within DLR included already a comprehensive load process (Klimmek, et al., 2017) Digital-X and Victoria (Görtz, et al., 2016; Görtz, et al., 2020) and preliminary steps have been taken to consider active control systems within the design cycle (Ilic, et al., 2020).

The efforts within the Filpased project seek to focus on inclusion of the control part, while deemphasizing the aerodynamic part.

In FliPASED the aerodynamics will consist mainly of low fidelity aerodynamics and methods based on potential flow theory. Hence, transsonic effects like shocks and wave drag will not be considered in the scale up task. This is a conscious choice in order to avoid overlap with other projects and to allow quick calculation times. Furthermore, the choice of an MDO architecture plays a secondary role.

This distinguishes the approach in FliPASED to other efforts which mainly focus on aero-structural optimization (Kenway, et al., 2014). In the future the findings of FliPASED may be integrated in MDO workflows with more realistic aerodynamic properties.

FliPASED wants to demonstrate the benefits of including active control technologies early in the design rather than an afterthought.

Scale up objective function

The overall objective function for the scale up task will be based on evaluation of mission criteria, such as range or blockfuel. This way two primary design goals can be addressed.

The first goal is to minimize the aerodynamic drag. Specifically, the induced drag is addressed by high aspect ratio wing designs. However, the resulting slender wing structures tend to be very flexible and defueling the wing tanks change the mass distribution and in turn the shape of the wing. To counteract the detrimental effect on the induced aerodynamic drag, active wing shape control deflects the control surfaces to restore a drag optimal lift distribution for the changing wing mass.

The second goal is to minimize the structural weight. This can be achieved by employing active load alleviation control laws to minimize design loads for manoeuvres as well as gusts and turbulence in combination with passive methods for load alleviation such as aeroelastic tailoring.

Furthermore, the aforementioned high aspect ratio wings are more prone to an adverse fluid structure interaction called flutter. Conventionally, this is addressed by increasing the wing stiffness or placing additional mass in suitable locations. The employment of active flutter suppression allows to relax these stiffness requirements and therefore save weight.

To assess the benefits of the mentioned active control technologies, the mission is analyzed at multiple points of the mission, i.e. different mass cases due to defueling. The conjecture is that inclusion of active control theory in the design phase leads to very different wing designs and large overall fuel savings.

2.4.2 Starting point and approach

The workflow that is setup in WP2, initially addresses the design of wings for the demonstrator. The objective there is to maximize the difference between open loop and closed loop performance of the individual control functions in order to assess and validate their benefits by flight test. Fuel burn and minimal weight are not primary design objectives.

For the scale up task, a passenger aircraft is considered. The design objectives have been described in the previous section. Apart from the differing objective functions, the most notable difference to the demonstrator workflow, is that the structure is now sized by the loads, i.e. the employed control functions have a direct impact on the overall weight of the structure. The changed stiffness and mass properties therefore make a convergence loop necessary.

Figure 2.76 shows an early version of the envisaged scale up workflow. The XDSM diagram shows a convergence loop including structural sizing, controller design of the various functions and the loads analysis of the closed loop aircraft.

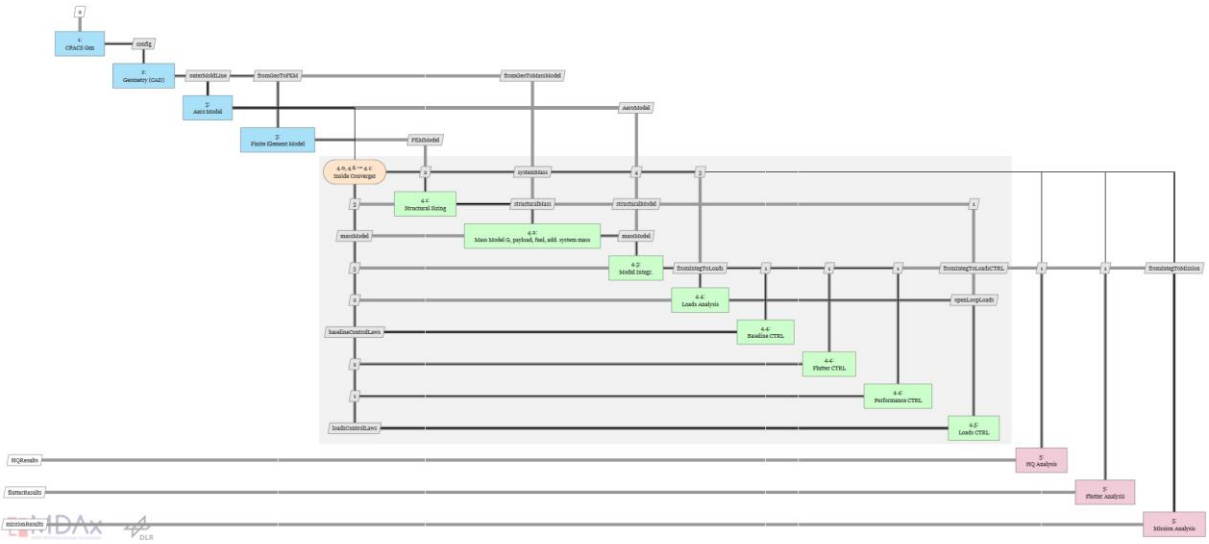

Figure 2.76 XDSM diagram of the scale up workflow

A further complication arises, as the CATIA based structural model generation is targeted towards the demonstrator wing. It will be investigated how this model generation process can be adapted to a transport aircraft wing. As contingency, an alternative model generation module (CPACS-MONA) is available at DLR's Institute of Aeroelasticity. This module has been used in several MDO workflows before.

2.4.3 Efforts and achieved results, name involved contractors

So far different reference aircraft models have been evaluated based on their suitability for the scale up task.

XRF1: Airbus eXternal Research Forum Model (A330 like)

The XRF1 Model is a multidisciplinary aircraft model which is intended to further development and validation of flight physics and broader multidisciplinary technologies by the external research community. The XRF1 model can be released to research establishments under the terms and conditions of a Framework Non Disclosure Agreement (FNDA). The DLR used this model in several MDO related projects and the FP7 EU project Smart Fixed Wing Aircraft. A parameterization in CPACS format is available and could be used.

Figure 2.77 Airbus XRF1 FEM model

The pros and cons of using the XRF1 as a reference model are summarized below.

Pros:

- experience at many research establishments
- mature dynamic model
- has been used also in FLEXOP

Cons:

- NDA required
- rules about IT security apply
- restrictions for publication apply

CRM: NASA Common Research Model (B777 like)

The Common Research Model of NASA would be another choice for a reference aircraft model. The pros and cons related to this model are summarized in the following.

Pros:

- free to use CAD
- structural model available at DLR-AE (FERMAT config)
- aero loft suitable for high fidelity CFD

Cons:

- no CPACS available
- not much experience with this configuration in the concortium
- Boeing/NASA model

D150: DLR 150Pax Model (A320 like)

The D150 configuration was developed within the DLR project VAMP (Zill, et al., 2012). It is comparable to the Airbus A320-200. Data published by the manufacturer, for example on the Airbus website, and input data to the preliminary design program PrADO for the application example Airbus A320, are used for the D150 configuration (Klimmek, 2016). Its geometry is shown in Figure 2.78.

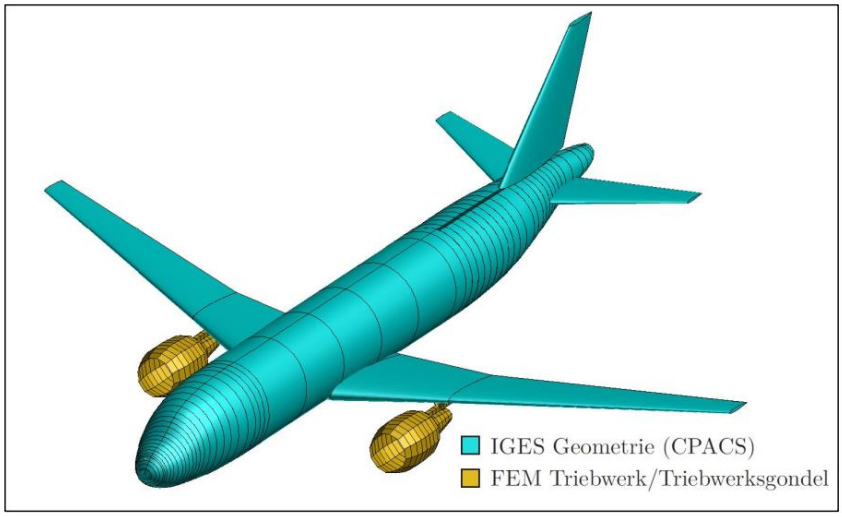

Figure 2.78 IGES-geometry of the D150-configuration

Table 2. lists the general parameters of the D150 configuration. The cruise speed V_C and cruise Mach number M_C are set to the maximum operational speeds V_{MO} and M_{MO}. The values for V_{MO} and M_{MO} for the Airbus A320 can be found in the EASA Type-Certificate Data Sheet (Frank, et al., 2012). The dive speed V_D can be calculated using the diagram of worksheet LTH BM 32 100-05 of the Luftfahrttechnischen Handbuch (LTH), and the dive Mach number $M_D = M_C + 0.07$ from the Acceptable Means of Compliance AMC 25.335(b)(2) of CS25.

The three airfoil profiles used for the four profile sections, with which the planform geometry is built, originate from the geometry of the DLR-F6 configuration. The DLR-F6 configuration is similar to the

geometry of the Airbus A320 and was developed in the 1980s as a publicly-available geometry for aerodynamic studies.

Table 2 Main parameters of the D150-configuration

Wing	
Surface area	122.3 m^2
Span	33.91 m
Reference chord	4.19 m
Aspect ratio	9.4
Taper ratio	0.246
Sweep angle at 25% chord line	24.94°
HTP	
Area	30.98 m^2
Span	12.45 m
Aspect ratio	5.0
Taper ratio	0.33
Sweep angle at 25% chord line	28.0°
VTP	
Area	21.51 m^2
Span	5.87 m
Aspect ratio	1.6
Taper ratio	0.35
Sweep angle at 25% chord line	35.0°
Operational empty weight (OEM)	40638 kg
Maximum zero-fuel weight (MZFM)	60500 kg
Maximum take-off weight (MTOM)	72500 kg
Cruise Mach number	0.78
Cruise speed / Mach number	180 m/s EAS, Mach 0.82
Dive speed / Mach number	209 m/s EAS, Mach 0.89

Maximum flight level	12500 m

The pros and cons of using the D150 are as follows.

Pros:

- DLR owned configuration
- CPACS available
- experience from multiple other projects
- no publication issues
- more relevant for industry

Cons:

- short/medium range aircraft
- potentially less benefits to demonstrate
- aero loft not suitable for CFD

Reference Model Choice

The consortium has decided to use the D150 aircraft model for the scale-up work package. Next steps will be made regarding the parameterization of the already existing D150 CPACS dataset. The parameterization will enable the evaluation of the benefits of a high aspect ratio configuration of the D150 in comparison with the conventional configuration as already available in the baseline CPACS dataset.

Disciplinary Modules for the Scale-Up Workflow

The efforts regarding the scale up workflow concentrated on development and integration of methods for the performance and misson evaluation. One major goal of the project is to reduce the detrimental effects of high aspect ratio wings on flutter stability and structural loads due their increased flexibility by means of active control. The main driver for high aspect ratio wings is the reduction of induce drag.

Thefore, an implementation and validation of a Vortex Lattice Method which is able to predict induced drag has bee worked on. This is an essential modelling aspect for the adaptive wing shape control. The implementation contains a near field and a far field (Trefftz plane) drag evaluation. Validation against existing tools and implementations of other partners have been conducted.

To test the implementation, an optimization to minimize induced drag has been conducted using 16 spanwise distributed flaps along the span of the demonstrator aircraft. The drag improvements achieved for the -0 wing by control surface deflections are shown in the following table.

CD Improvement	20 m/s	30 m/s	40 m/s	45 m/s	50 m/s	60 m/s
-0 wing	3.76%	2,97%	3,98%	5,36 %	7,21%	11,69%

Figure 2.79 table with induced drag improvments with wing shape control

The corresponding flap deflections and resulting lift distributions of the wing shape control are depicted in Figure 2.80.

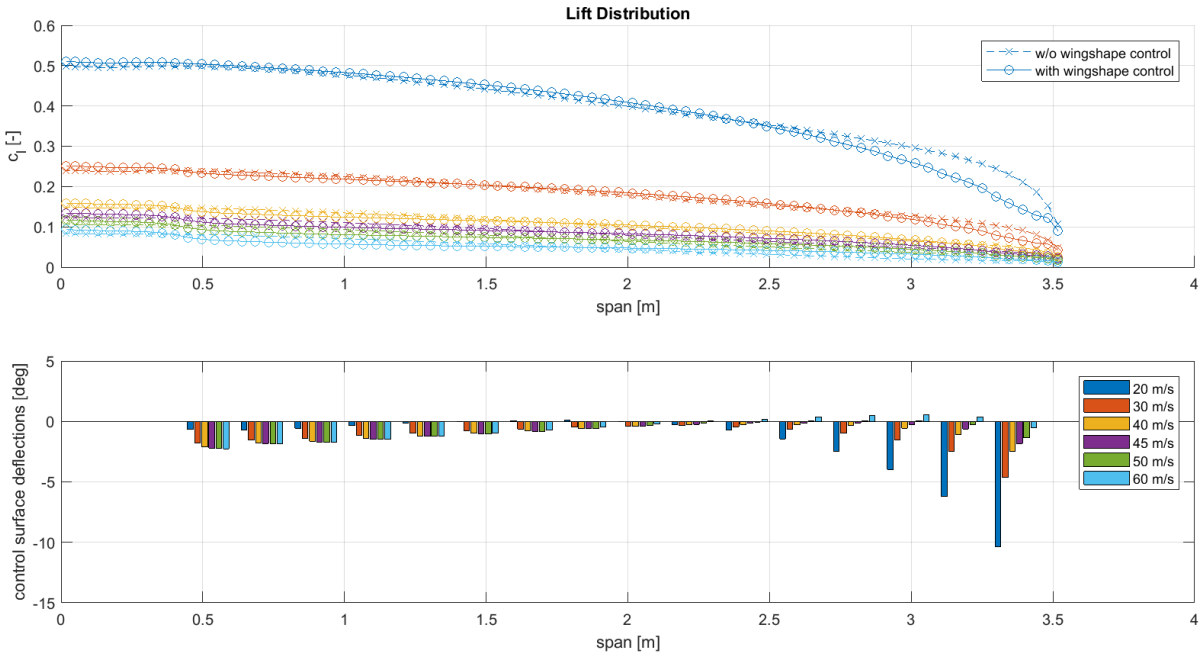

Figure 2.80 lift distributions with and without wingshape control and the corresponding flap deflections for a speed range between 20 m/s and 60 m/s

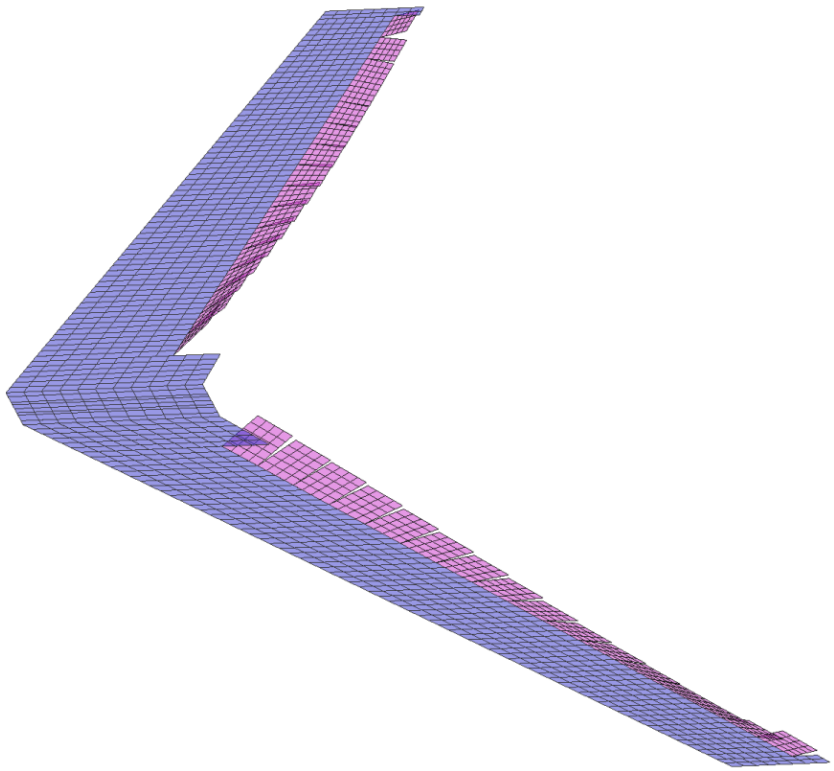

Figure 2.81 optimized flap deflection for a 16 flap -0 wing configuration @ 50m/s (control deflections 20x exaggerated)

Bibliography

Fialho I. [et al.] Gain-Scheduled Lateral Control of the F-14 Aircraft During Powered Approach Landing [Journal] // AIAA Journal of guidance, control and dynamics. - 2000. - Bd. 23. - S. 450-458.

Frank Edward H. und Lyle Jim Type-Certificate Data Sheet No. EASA.A.064 for Airbus A318-A319-A320-A321 [Buch]. - [s.l.] : European Aviation Safety Agency, 2012.

Frank Edward H. und Lyle. Jim SBus Specification B.O // SBus Specification B.O. - 1990. - \url{http://www.bitsavers.org/pdf/sun/sparc/800-5922-10_SBus_Specification_B.0_Dec90.pdf}.

Görtz S. [et al.] Collaborative Multi-Level MDO Process Development and Application to Long-Range Transport Aircraft [Konferenz] // 30th International Congress of the Aeronautical Sciences, Daejeon, South Korea, September 25-30. 2016. - 2016.

Görtz Stefan [et al.] Overview of Collaborative Multi-Fidelity Multidisciplinary Design Optimization Activities in the DLR Project VicToria [Konferenz] // AIAA AVIATION 2020 FORUM. - [s.l.] : American Institute of Aeronautics and Astronautics, 2020.

Ilic Caslav [et al.] Cybermatrix Protocol: A Novel Approach to Highly Collaborative and Computationally Intensive Multidisciplinary Aircraft Optimization [Konferenz] // AIAA AVIATION 2020 FORUM. - [s.l.] : American Institute of Aeronautics and Astronautics, 2020.

JETI model s. R. O. EX Bus communication protocol // EX Bus communication protocol. - 2013. - \url{http://www.bitsavers.org/pdf/sun/sparc/800-5922-10_SBus_Specification_B.0_Dec90.pdf}.

Kenway Gaetan K. W. und Martins Joaquim R. R. A. Multipoint High-Fidelity Aerostructural Optimization of a Transport Aircraft Configuration [Journal] // Journal of Aircraft. - [s.l.] : American Institute of Aeronautics and Astronautics (AIAA), 1 2014. - Bd. 51. - S. 144–160.

Klimmek Thomas [et al.] Loads Analysis and Structural Optimization - A Parameterized and Integrated Process [Konferenz] // 1st European Workshop on MDO for Industrial Applications in Aeronautics - Challenges and Expectations, 24.-25. Okt. 2017, Braunschweig. - 2017.

Klimmek Thomas Statische aeroelastische Anforderungen beim multidisziplinären Strukturentwurf von Transportflugzeugflügeln [Bericht] : Ph.D. dissertation / DLR - Institut für Aeroelastik. - 2016.

Meirovitch L. Fundamentals of vibrations [Buch]. - [s.l.] : McGraw-Hill, 2001.

Schmidt D. K. Modern Flight Dynamics [Buch]. - [s.l.] : McGraw-Hill, 2012.

Zill Thomas, Ciampa Pier Davide und Nagel Björn Multidisciplinary design optimization in a collaborative distributed aircraft design system [Konferenz] // 50th AIAA Aerospace Sciences Meeting including the New Horizons Forum and Aerospace Exposition. - 2012. - S. 553.

2.5 Explanation of the work carried per WP- Work Package 5

2.5.1 Objectives and activities

• Project Coordination

• Evaluation of collaborative tools and their best practices

• Management of exploitation and dissemination of project results

2.5.2 Starting point and approach

The consortium is made up of four beneficiaries. Three of them (SZTAKI, TUM, DLR) have been involved in our previous coordinated project (FLEXOP) and with the fourth one (ONERA) we have had several common H2020 projects already (VISION). The previous cooperations imply a smooth project implementation on the management side.

2.5.3 Efforts and achieved results, name involved contractors

Task 5.1: Project Management (SZTAKI)

The main activities of the Management Team were:

• Ensured achievements of overall project schedule and objectives by

o Constant monitoring of project achievements against the work plan – there was a notable delay in project implementation due to the outbreak of Covid-19 epidemics (see section Deviations, their reason, impact on the project and corrective actions)

o Identification of risks and definition of risk mitigation measures through the Risk Reigster

o Solving any technical, financial, administrative or contractual issues or conflicts between partners, when needed

• Handled and distributed the funds according to the rules agreed within the consortium – pre-financing was distributed according to the Consortium Agreement.

1	SZTAKI	800 156,25
2	TUM	926 531,25
3	DLR	706 121,25
4	ONERA	451 875,00

• Maintained regular contact with the partner organisations

• Established a scientific and industrial advisory group

The Scientific Advisory Group (SAG) was confirmed by the Steering Committe in the first month of the Project for the purpose of offering advice and support on a wide range of Project-relevant issues. Members of the SAG are internationally recognised experts in the field of the Project.

Prof. Peter Seiler, Faculty of Electrical Engineering & Computer Science, University of Michigan
Daniel Ossmann from Munich University of Applied Sciences

Roeland de Breuker from Technical University of Delft.

The Industrial Advisory Group (IAG) includes key experts from the FLiPASED domains representing the key OEMs from Europe. Members were confirmed by the Steering Committe in the first month of the Project

Sebastien Blanc A350XWB loads and aeroelastics Designated Expert and Airbus - Active Adaptive Wing Leader, Airbus Commercial Aircraft
Carlo Aquilini, Airbus Defence and Space
Colo Ludovic (Aero-Structural design directorate) From Dassult- Aviation
Olivier Cantinaud (Technical Systems Directorate, Flight Dynamics Department) From DassultAviation

• Managed risk and settle any disputes within the consortium

• Organised the management team meetings, consortium meetings and meetings with scientific advisory group

Kick-off meeting: of the project has taken place at (and hosted by) SZTAKI on 12-13th September 2019. All 4 of the partners and the members of the Scientific and the Industrial Advisory Group got together for the first time. The meeting started with presentations of each partner and followed by project presentations. Steering committee meeting was also held where the members of the Management Support Team and the Scientific and the Industrial Advisory Group as well as the WP Leaders were elected.

1st Progress Meeting: of the project was planned to be held on the 19-20th of March in Münich but it was postponed and replaced by several thematic (and WP specialized) online meetings due to the emerging COVID situation.

The actual first progress meeting was organized on the 13-16th of November 2020 (Friday-Monday) where the progress of tasks was discussed and rescheduled in detail. See the recovery plan in section Deviation.

See the meeting folder with relevant presentations and minutes:

https://dms.sztaki.hu/nextcloud/s/s8n79K4HJPMTQbp/download

weekly webexes were held by the coordinator – usually dedicated to a WP or a relevant deliverable – 52 meetings until the end of the period

WP/deliverable webexes were also organized by the coordinator or by different partner organisations whenever needed by the workflow – several meetings dedicated to Fligt Testing and flight test data processing (3), to D1.2 Toolchain workshop, but also to Flutter Evasive Action, to MDO and also to different deliverables.

See the meeting folder with relevant presentations and minutes for all the meetings:

https://dms.sztaki.hu/nextcloud/s/s8n79K4HJPMTQbp

1st Review Meeting: of the Project was held on the 9th of June 2021. The rehearsal day was organised two day prior to the Review on the 7th of June. Due to COVID related restrictions both events were held online. The reinforcement of Risk Management with effective risk mitigation mesasures and the feasible rescheduling of the project was requested by the Reviewer and the Project Officer. An intermediate check to be conducted at the end of 2021/beginning of 2022 was found necessary by both parties.

See the meeting folder with relevant presentations:
https://dms.sztaki.hu/nextcloud/f/442490

• Reported to and chaired steering committee on the consortium meetings. Steering committee meetings were held together with other online meetings.

• Reviewed and validated the project reports to ensure consistency with the project tasks (especially in the case of reviewing the different project implementation concepts and deliverables)

• Submitted reports and other deliverables to the Commission – 12 deliverables submitted between M1-M24.

• Transmitted documents and information connected with the Project to and between the Work Package Leaders and the partner concerned

• Prepared and updated the schedules of the whole project (for the rescheduling of the project please see section Deviation.

• Ethical, social and gender issues encountered during the project life will be monitored. It includes activities for preparing the gender issues plan and support to the other partners for applying the plan. (During Grant Preparation phase a separate deliverable was introduced to the project in a new WP called EPQ - Requirement No. 1 – the deliverable was submitted in due time). Referring to the Horizon Europe requirements SZTAKI has already developed its Gender Equality Plan and stareted its first related activities by setting up the internal council (implementing the plan) and by organising the first gender workshops within the institute.

A Project Handbook defining procedures, templates and methods for the assessment of project achievements was issued in the beginning of the project. It was also submitted as a deliverable.

After submitting the 24 Month progress report the next progress report will be the Final Report – this will be submitted as a WP5 deliverable and will be lebaorated simultaneously with the 2nd Periodic Report.

The organisation of the workshops with the scientific advisory group were and will be financially supported.

The travel expenses of the scientific advisory group are financially covered by WP5 – their participation on the Kick-off meeting was already paid by WP5 (coordinator). Other meetings with IAG and SAG members were held online thus had no related travel cost.

Task 5.2: Collaboration tools, methods and practices (SZTAKI)

Common problem in multidisciplinary projects is the lack of understanding between partners due to their background and expertise, which leads to conservative designs or creates miscommunication, risking delays, costly re-designs or redundant solutions for the same problem by multiple stakeholders. We planned to tackle these issues by implementing collaborative project management solutions. After a thorough analysis of the different workflows and work groups we decided to use the following tools: Nextcloud for sharing, editing documents, defining tasks. Webex for online meetings. Overleaf and GIT for solving technical tasks.

The consortium established collaborative tools for project management (Nextcloud + Agantty), software development (Git), document editing (Overleaf). Moreover the collaborative work process also involves common hardware development tools - a common hardware-in-the-loop platform. The partner contributions within the common MDO toolchain are all implemented and tested using the RCE environment.

Task 5.3: Exploitation and Dissemination Management (SZTAKI)

This task includes:

• Observation of the evolving research and development trends as well as communication of the observances to the consortium members – follow-up done by the coordinator.

• Co-ordination of issues related to Intellectual Property Rights – this topic is regulated in the Consortium Agreement the partners have signed.

• Set-up of an Exploitation and Dissemination Plan; dissemination of results will be achieved by publications of individual partners. Furthermore a session organised in the most appropriate international congress will be organised to give a survey of the achievements within the project. Several publications have already been submitted by project partners. The Exploitation and Dissemintation Plan was submitted.

• In accordance with the dissemination plan the consortium members have to identify results with potential for patenting and publication activities must be aligned with patent application rules – this topic is regulated in the Consortium Agreement the partners have signed.

2.5.4 Deviations, their reason, impact on the project and corrective actions

See in section Deviations from Annex 1 (if applicable)

2.6 Impact

The primary impacts of the project are achieved with respect to the improved design environment comprising enhanced toolsets optimized for collaborative interactions within and across organizations, the validated datasets contribute to the community along the Open Research Data initiative and finally the best practices and standards for collaborative design environments as well as the design process itself. Latter will be derived from the collaborative process applied in the project itself. Since the developed tools are validated using a flight demonstrator, the targeted Technology Readiness Level of this activity is TRL5.

Through dissemination of validated data publicly, the project will provide a rare opportunity to generate great impact on the flexible aircraft research community as flight test data are very sparsely available due to confidentiality reasons. Subsequent impact will be achieved through the application of the enhanced design process on new aircraft development activities, leading to significant improvements in development and certification costs, providing continuous progress towards improved structural and aerodynamic efficiency. This technological progress has an impact on airline operating costs through fuel savings, leading also to the environmental goals set out in the ACARE goals and Flightpath 2050.

Similar to the Udacity Autonomous Vehicle initiative and Baidu Apollo open source projects, which aims to become "the Android of the auto industry." we plan to share the design methodology and interfaces openly for the aircraft design process. As Infoworld described, “Apollo enables Tier 1 providers, vehicle makers, and start-ups to build their own autonomous vehicles without the burden of reinventing the wheel.” We envision a similar proposition to the aircraft industry, by providing a baseline methodology and modular

benchmark setup for SMEs, start-ups and companies which are traditionally not connected with the aerospace industry to make their tools and methods compatible with aviation needs.

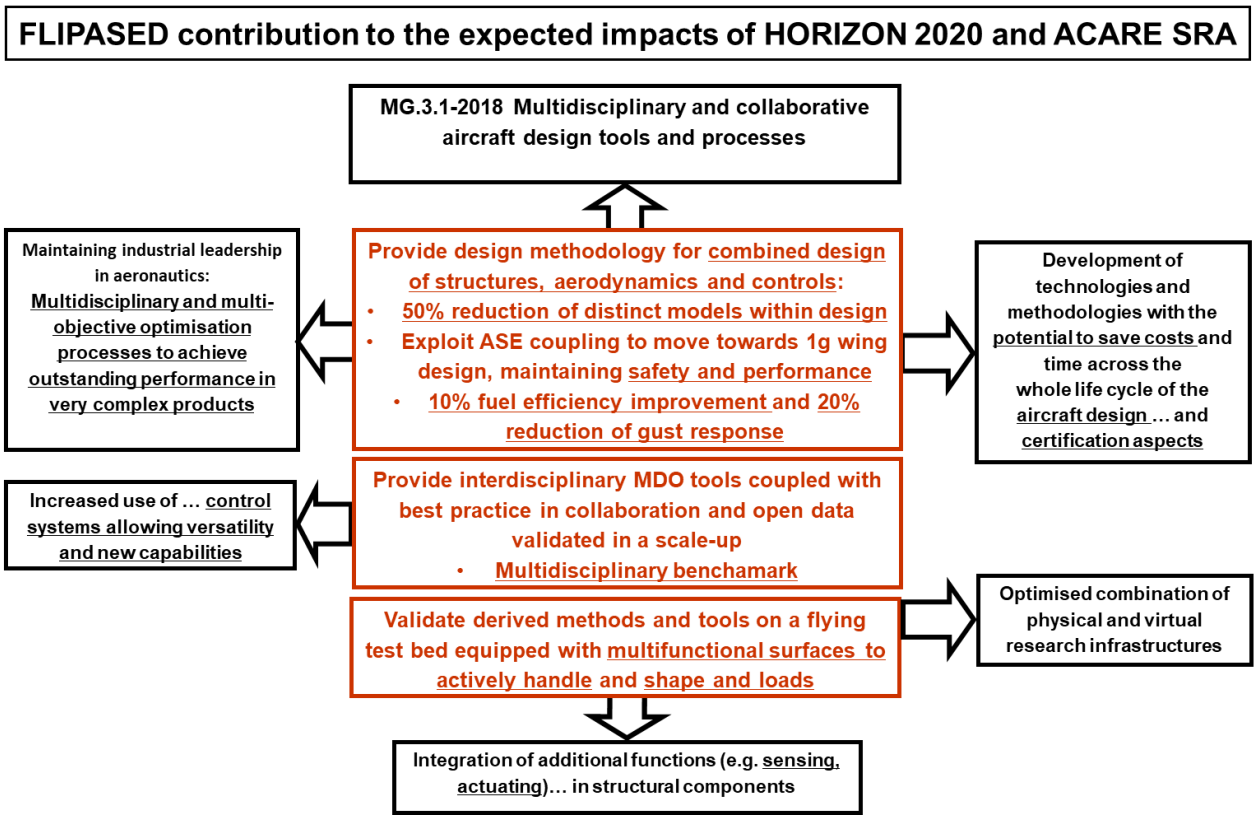

Figure 2.82 Contribution to expected impacts of H2020 and ACARE SRE

With respect to further research, the project will develop simulation, visualization and testing capabilities that provide a legacy for future research activities. The developed design tools will work across disciplines to produce integrated wing structures, including the inherent sensing and actuation layout, with aeroelastic tailoring and aeroelastic control. They will be implemented so as to reduce the number of design iterations, reducing the design effort and time for future design tasks. An inherent capability will be provided by the low cost flight demonstrator which is aligned with the underlying design models and validation data. For future research this will provide a platform for validation and experiments, based on open source tools for data management (Apache Spark and Flink), modelling (scikit-learn, numpy, scipy, Tensorflow, Keras, etc.) and visualization (Grafana, matplotlib, etc). Specific impacts are expected in the following areas:

- *Advanced multidisciplinary and collaborative capabilities for whole aircraft along its life cycle.* - Collaborative multi-disciplinary aspects will be enhanced on design, demonstration and scale-up level.
- *Significantly reduced aircraft design cycle and higher complexity decision trade-offs.* - Taking structures, control and aircraft overall design into the same MDO loop will make sure deeper trade-offs are exploited, and less compromises are taken during a/c design and operation.

- *Development of synergies on visualisation methods and big-data analytics.* - The collaboration among prominent Research Institutes and Universities with the large amount of generated data will fuel further collaboration beyond the consortium.
- *Increase the European innovation potential in Aeronautics and Air Transport (AAT) by a more balanced and integrated collaboration of industry, including SMEs and research providers*. - The developed tools and methods will aim at standardizing the interfaces between teams, which will have great impact on the possibilities of collaboration between industry, academia and SMEs.

Overall, the topic is expected to have significant impact on Flightpath 2050, namely towards "maintaining global leadership*" (not to lag behind X-56, 777X and other US programs, and to be ahead of Brazil who is also active in flexible wing shape and structure control)* as well as "protecting the environment" *(fuel efficiency is one key aspect, while more optimal structure/active control allows longer lifespan due to less fatigue load – hence less impact on the environment)* challenges.

3 Update of the plan for exploitation and dissemination of result plan (Technical Report 2)

Not Applicable - Exploitation and Dissemination Plan has just been submitted.

4 Update of the data management plan (if applicable)

Not Applicable – first version of Data Management Plan was submitted.

5 Follow-up of recommendations and comments from previous review(s) (if applicable)

Not applicable – Mid-Term review has been organized 3 month ago. The recommendations were followed:

The reinforcement of Risk Management with effective risk mitigation mesasures and the feasible rescheduling of the project was requested by the Reviewer and the Project Officer. An intermediate check to be conducted at the end of 2021/beginning of 2022 was found necessary by both parties.

6 Deviations from Annex 1 (if applicable)

At the start of the project the schedule for deliverables was revised due to conflicts with other project schedules.

The consortium is not on time with several tasks, namely with the MDO toolchain integration within RCE environment and the flight test campaigns. These are traced back to two root causes:

- Due to flight safety aspects of the demonstrator the landing gear and pilot procedures must be revised and redesigned, this led to number of taxi tests and a lengthy procedure to clear the demonstrator for further flight testing, while also part of the roof at the workshop of TUM had collapsed, what also rendered work in the lab impossible,
- These tasks and the collaborative work process were significantly delayed due to the covid situation, when work from home office was possible, but common brainstorming sessions with partners at the same location could not be organized and access to advanced IT infrastructure was also impossible.

6.1 Tasks

The tasks within WP1, WP2 and WP3 have been carefully revised to recover as much time as possible in a contingency plan. These modifications include a more streamlined -3 wing design and manufacturing plan, while executing the flight testing and wing manufacturing in parallel. These steps are the following:

Analysis and Design

1. Demonstrator single workflow (FLEXOP re-design in RCE)
2. Run sensitivity study on single parameter perturbation→establish tool performance
3. Performance assesment of OL vs. CL (GLA, MLA, drag reduction CLAW)
4. Predict performance gain of (-0: 4 flaps and -3: 8 flaps)
5. Scale-up: D150 baseline MDO iterations (MLA, GLA, drag, flex) – possibility to run D150 with more flaps
6. Validate the tool predictions
7. Conclusion and recommendations for standardization

Flight Testing

1. -2 sys I.D. and W.P. nav
2. -1 flight + OMA
3. -1 flutter test
4. -0 modifications → -3 (8f)
5. -0 flight test (GLA, MLA, drag) on/off to establish baseline
6. -3 static test and GVT
7. -3 flight test (GLA, MLA, drag) on/off to validate tools

It is worth mentioning the goal of the consortium to conduct concentrated 2 weeks long test campaign at Cochstedt Airport (DLR facility). The team and equipment are prepared for this test but we have not received flight approval from the German Aviation Authorities due to new approval process by EASA regulations.

Performance gains analysis:

Pre-defined mission (8 horserace circles with increasing speed – 35 m/s vs 70 m/s wing shape are different, constant 1.5 vs 2.5 G circle also mimic different loading)

Turns → MLA on/off → benefits are visible and quantifiable

GLA 1 round on / 1 round off at the same atmospheric conditions

Simulation/analysis predictions on -0 and -3 vs. Flight test of -0 and -3 to validate the tools

Direct comparison and validation requires:

Simulation assesment to see the targets in term of performance gains

Root bending moment and thrust measurement

MLA, GLA and performance (drag red.) CLAW design and implementation

Analysis of simulated vs. actual peak and mean responses

Reconstruction of wind and flexible a/c response (using air data and wing shape estimation)

Scale-up:

- Pre defined standard mission
- MDO toolchain with several convergent iterations (including loads convergence)
- Performance assessment of MLA, GLA, perf CLAW on/off
- Hi-Fid Simulation vs. Tool predictions on benefits

Direct comparison and validation requires:

- Establish the D150 baseline with our tools
- Integrate the loads convergence loop in MDO
- Run MDO on standard D150 with no control
- Run MDO with control using possibly modified D150 (more flaps)
- Drag model

6.2 Use of resources

The consortium submitted tables for the 20-month periodic report and these numbers are repeated here. Due to the COVID related lack of resources we have not been able to update these tables 4 months after the periodic report.

SZTAKI:

SZTAKI	Costs incurred in the first 20M	Costs estimated for the 1st period (20M)- based on project plan	Costs estimated for the whole project (40M)- based on project plan	%

Personnel costs	223 256,8	250 000,0	511 000,0	44%
Subcontracting				
Other direct costs	17 308,7	118 000,0	342 500,0	5%
travel	3 402,8	18 000,0	42 500,0	8%
equipment	8 726,5	20 000,0	50 000,0	17%
other goods & services	5 179,4	80 000,0	250 000,0	2%
Indirect costs	60 141,4	92 000,0	213 375,0	28%
Total	300 706,9	460 000,0	1 066 875,0	28%

SZTAKI	Staff effort per WP (hours)	Staff effort planned for the period (M1-M20)	Staff effort planned for the whole project (40M)	**%**
WP1	3 238,0	2 866,7	5 733,3	56%
WP2	3 249,0	2 508,3	5 016,7	65%
WP3	3 083,0	2 150,0	4 300,0	72%
WP4		358,3	716,7	0%
WP5	2 964,0	2 580,0	5 160,0	57%
total	12 534,0	10 463,3	20 926,7	60%

Actual PM rate	Planned PM rate
2 553,1	3 500,0

SZTAKI

justification of the deviation in

- equipment

Procurement of several equipment already happened (HIL related), but depreciation cost for only a few months was booked for the project, since a depreciation period of 36 months is mandatory according to Hungarian law. Purchase of other equipment (air data computer) is underway, but more strict procurement laws in Hungary (transparency declaration) delays the purchases, since the law departments have to be involved.

- other goods and services

Purchase of goods and services is significantly under the plans, since the intention was to instrument the wing with fibrebrag sensors, but the wing detailed design have not started yet and the fibrebrag purchase could not be completed without the detailed plans.

- "overspending" of hours in WP3

There was significantly more effort required to test and develop custom avionics components (both software and hardware) during the covid lockdown since development environments have to be modified to work from home office. Extra effort was spent on augmenting test and development platforms with tools allowing remote work.

- difference between actual and planned PM rate

Work, especially in WP3 is done by young students instead of experienced researchers, what drove the PM rate down. It was not possible to plan with these young employees at the time of the proposal, since they are employed just only a few years ago.

HUF EUR exchange rate was 310 at the time of the proposal and now it is 350.

TUM:

TUM	Costs incurred in the first 20M	Costs estimated for the 1st period (20M)- based on project plan	Costs estimated for the whole project (40M)- based on project plan	%
Personnel costs	387 183,4	329 150,0	658 300,0	59%
Subcontracting	0,0	0,0	0,0	
Other direct costs	14 010,0	40 000,0	330 000,0	4%
travel	888,0	15 000,0	30 000,0	3%
equipment	13 122,0	25 000,0	50 000,0	26%
other goods & services	0,0	0,0	250 000,0	0%
Indirect costs	96 440,5	92 287,5	247 075,0	39%
Total	482 202,5	461 437,5	1 235 375,0	39%

TUM	Staff effort per WP (hours)	Staff effort planned for the period (M1-M20)	Staff effort planned for the whole project (40M)	%
WP1	3 441,0	1 505,0	2 007,0	171%
WP2	1 377,0	1 612,0	3 225,0	43%
WP3	5 689,0	4 658,0	9 316,0	61%
WP4	0,0	156,0	1 720,0	0%

WP5	0,0	0,0	0,0	
total	10 507,0	8 791,0	16 268,0	65%

Actual PM rate	Planned PM rate
5 281,5	5 800,0

As not as many flight tests could take place due to the corona situation in 2020 equipment cost are lower than planned at the current project state. The other goods and services budget is for the manufacturing and systems/sensors of the -3 wing. As the production has not started yet there are also no spending so far. TUM spend more man hours than initially planned in WP1. The reasons for that are that on the one hand that we mainly use junior staff (PhD students and students) which need more time than senior staff but are therefore cheaper. This is also the reason why the actual PM rate is lower than the planned PM rate. On the other hand the effort of setting up a collaborative work process with this complexity with all requirements, interfaces, models and tools was more time consuming than anticipated. Nevertheless the major contribution from TUM for WP1 is already done by now.

DLR:

DLR	Costs incurred in the first 20M	Costs estimated for the 1st period (20M)- based on project plan	Costs estimated for the whole project (40M)- based on project plan	%
Personnel costs	260 252,2	337 598,0	675 196,0	39%
Subcontracting	0,0	0,0		
Other direct costs	6 441,3	39 000,0	78 000,0	8%
travel	2 343,2	16 000,0	32 000,0	7%
equipment				
other goods & services	4 098,1	23 000,0	46 000,0	9%
Indirect costs	66 673,4	94 149,5	188 299,0	35%
Total	333 366,9	470 747,5	941 495,0	35%

DLR	Staff effort per WP (hours)	Staff effort planned for the period (M1-M20)	Staff effort planned for the whole project (40M)	%
WP1	954,5	910,2	1 820,3	52%
WP2	3 043,2	2 021,0	4 042,0	75%
WP3	1 279,0	1 720,0	3 440,0	37%
WP4	125,0	1 576,7	3 153,3	4%
WP5	0,0	0,0	0,0	
total	5 401,7	6 227,8	12 455,6	43%

Actual PM rate	Planned PM rate
6 905,7	7770

Actual PM rate slightly lower than planned PM rate:

Currently, the project is run with junior staff. As the projects progresses more senior grade colleagues will join in, resulting in an increased PM rate

Staff effort consumption:

WP4 has just started so the low number of hours worked on WP4 is no deviation from project plan. Also using 75 % of WP2 hours is in line with planning as most of DLR's contributions are already implemented in this WP.

Underspending of Other Direct Cost

Apart from the COVID related underspending of travel costs the other costs are also in line with planning. Other goods and services category cover mostly the costs of ground testing like static tests and the GVT which are planned for later in the project.

ONERA:

	Costs incurred in the first 20M	Costs estimated for the 1st period (20M)- based on project plan	Costs estimated for the whole project (40M)- based on project plan	%
Personnel costs	93 746,7	232 000,0	464 000,0	20%

Subcontracting	0,0	0,0	0,0	
Other direct costs	3 209,7	9 000,0	18 000,0	18%
travel	3 209,7		18 000,0	18%
equipment	0,0	0,0	0,0	
other goods & services	0,0	0,0	0,0	
Indirect costs	24 239,1	60 250,0	120 500,0	20%
Total	121 195,5	301 250,0	602 500,0	20%

	Staff effort per WP (hours)	Staff effort planned for the period (M1-M20)	Staff effort planned for the whole project (40M)	%
WP1	454,0	186,0	372,0	122%
WP2	1 000,0	1 550,0	3 100,0	32%
WP3	261,0	1 550,0	3 100,0	8%
WP4	0,0	0,0	310,0	0%
WP5	0,0	0,0	0,0	
total	1 715,0	3 286,0	6 882,0	25%

Actual PM rate	Planned PM rate
6 793,2	8 000,0

The overconsumption of hours in WP1:

Long discussions to clearly separate the work in between partners (social disctancing made these discussions even longer)

Pandemic issues made the availability of the data slower

Setting up the MDO work plan was actually more teious than expected and the involvement in the technical path slowed down

We expect to accelerate our implication in the coming year to recover the underspending.

6.2.1 Unforeseen subcontracting (if applicable)

Not applicable

6.2.2 Unforeseen use of in kind contribution from third party against payment or free of charges (if applicable)

Not applicable

7 Risk Register

ID	WP	Description	Potential Impact	Mitigation action(s)	Related deliverable(s)	Risk Owner	Potential Program Impact (current)	Probability (current)	Risk rating
R1	1,4	The experimental results of the scaled demonstrator are not applicable for scaling-up the results.	The industrial relevance of the project will be compromised. Limitations of the tools for demonstrator will be established and the applicability of the methodology will be established. The direct relationship between experiment and scale-up will be relaxed and more generic tool related recommendations will be established for the scale-up.	The flight vehicle and its wings will be designed as a scaled down version of a commercial aircraft concept in WP1 to have the most commonality. The required fidelity scaling laws will be used during scale-up, while highlighting the applicability of the results.	D4.2, D4.3	Thiemo Kier	Minor	Likely	Medium
R2	1,2,3	The control surface and sensor equation models on the re-designed “advanced	The methodology of MDO design and the oveall architecture will be still valid, just the	A higher fidelity FEM model will be applied for the aeroelastic	D3.9,	Muhammad Meddaikar	Minor	Unlikely	Low

		wing" differ significantly between GVT and initial mathematical models during the optimal movables and sensor selection tasks.	individual building blocks including more precise modelling, more robust control design will be built into subsequent applications of the tools.	modelling, which are also updated by the ground vibration test results. As the final step, the overall aeroelastic model parameters are retuned based on flight test data.					
R3	1,2	The parametric modelling is too high dimensional for rapid MDO design based evaluation of the aircraft configuration.	The iterative MDO process fails to execute, leading t inconclusive results. The scaled-back / reduced version will not provide sufficient performance advantage w.r.t. the baseline.	The parametric modelling is too high dimensional for rapid MDO design based evaluation of the aircraft configuration.	D2.4	All (B. Vanek)	Major	Highly likely	Medium
R4	2,3	The all movable control design results in too complex and/or high order controllers for implementation.	The complexity of the overall MDO loop will increase - materializing in R3. In case the speed of design is not significantly high, the real world implementation and industrial relevance	The control performance objectives will be refined and the controllers derived for a lower order model. The resulting controllers will be thoroughly tested with the high fidelity	D2.1, D2.3	Charles P. Vassal	Major	Unlikely	Low

			(related also to certification) might suffer.	model before implementation.					
R5	3	The demonstrator will suffer a catastrophic in-flight failure.	The flight test campaign will be set back by several months. The second fuselage and backup wings have to be used.	The air vehicle will be equipped with an emergency recovery parachute system to minimize the risk of loss of an airframe.	D3.3, D3.6, D3.11, D3.12,	Christian Rossler	Major	Likely	Medium
R6	1,2	Wing shape control results in too low elastic deformation authority for drag reduction in case of the original FLEXOP -1 wings.	The team already assessed the drag reduction potential and proposed to extend the flight envelope - at high speeds (+60 m/s) the benefits starts to increase significantly.	This issue will be addressed in the re-resign of FLEXOP -1 wing with a particular focus on the structural reinforcements and control surface effectiveness	D3.6, D3.11	Balint Vanek	Minor	Unlikely	Medium
R7	3	Unfavourable weather conditions delay the flight test campaign.	The already delayed flight test campaign will suffer even more delays.	The project will file for an extension in extremely serious case	D3.3, D3.6, D3.11, D3.12,	Christian Rossler	Major	Likely	High
R8	1	Collaborative work process will not be able to gather sufficiently standardized,	The tools will not live on at the consortium partners as standalone modules for future exploitation	The benchmark status of the individual components and the overall methodology	D1.7, D4.2	Balint Vanek	Major	Likely	Low

		independent tools and relations for wider user base	and the impact of the project, especially towards industry, will be reduced.	will be emphasized					
R9	2	Analytical redundancy based methods will not be suitable for integration with the rest of the tools.	Fault detection, identification and reconfiguration methods will not be an integral part of the MDO process. What might have impact on certification aspects of the overall methodology and the resulting conceptual design (leading to overly optimistic perf. claims).	The design iterations in MDO could be started from different baseline configurations, special cases will be defined to address the analytical redundancy based methods	D1.7, D2.2, D4.3	Balint Vanek	Negligible	Unlikely	Low
R10	3	The flight test will not provide sufficiently high amount of data for DataScience related tasks.	Data Science based methods will not be trained and/or evaluated on real datasets leading to lower overall project impact.	The basic tools and the data processing pipeline will be set-up and shared, the use cases will be demonstrated with the available data	D2.5	Christian Rossler	Minor	Unlikely	Low

R11	5	Low amount of scientific publications due to lack of conferences (COVID related cancellations)	The main results of the project will be documented in technical reports instead of peer-reviewed publications.	More journal papers will be submitted and potentially after the project closure the papers will be accepted with proper acknowledgement of the EU funding.	D5.5	Virág Bodor	Major	Likely	High
R12	5	Further delay due to COVID impact (4th wave)	More restrictions applied to travel, office work and field testing.	Re-scheduling of tasks, milestones and deliverables. Re-focusing the project tasks on items possible to execute from home office instead of airfields and labs.	D5.8, D5.9	Virág Bodor	Major	Highly likely	High
R13	1	MDO process developed for the demonstrator not applicable for scale-up	The scale-up aircraft requires an inner convergence loop for loads sizing, which is not present at the demonstrator level - inner convergence	The problem is already tracked and special emphasis will be made to have the DLR MONA tool to self-contain this problem.	D4.1, D4.3	Balint Vanek	Extreme	Unlikely	High

			loops might increase execution time and convergence properties.						
R14	1	RCE infrastructure with cross institution execution might run into delays	The tools of partners run at their local servers with the corresponding software licenses, while DLR's main RCE server schedules the tasks. DLR already started work on moving this server to the 'demilitarized zone' but progress is slow.	The whole RCE framework with all components might be run from a single server inside DLR, with special care on softvare license needs.	D1.7, D4.2	Thiemo Kier	Major	Likely	Medium
R15	3	Work in the lab or tests cant be conducted due to Corona situation	The already delayed flight test campaign will suffer even more delays. The manufacturing or the -3 wing could be delayed	Improove efficiency of flight tests, e availability of test crew and ground testing and training	D3.2, D3.5, D3.6, D3.7, D3.9, D3.10, D3.11	Christian Rossler	Major	Likely	Medium
R16	2,3	Input for advanced wing design comes too late	The detailed design, manufacturing and testing of the advanced -3 wing	Plan B established with using an existing wing and retrofitting changed	D3.5, D3.7, D3.9, D3.10	Christian Rossler	Major	Highly likely	High

			could not be finished withing the timeframe of the project.	flap geometry, actuators and sensors.					
R17	4	Runtimes of the individual tools of the scale up process are too long	not enough parametric full runs of the toolchain can be executed to achieve meaningful results	Employ simpler tools to shorten runtimes, while monitoring the impact on the accuracy of the results.	D4.3	Thiemo Kier	Major	Likely	High

8 Dissemination and Exploitation of Results

8.1 Scientific publications

Authors / Speaker	Partner	Title	Conference / Journal	state	Place	DOI
Matthias Wüstenhagen ; Özge Süelözgen ; Lukas Ackermann; Julius Bartaševicius	DLR, TUM	Validation and Update of an Aeroservoelastic Model based on Flight Test Data	AeroConf 2021 (IEEE)			
Balint Patartics, Gyorgy Liptak, Tamas Luspay, Peter Seiler, Bela Takarics and Balint Vanek	SZTAKI	Application of Structured Robust Synthesis for Flexible Aircraft Flutter Suppression	IEEE Transaction on Control System Technology Journal:	accepted		
Béla Takarics and Balint Vanek	SZTAKI	Robust Control Design for the FLEXOP Demonstrator Aircraft via Tensor Product Models	Asian Journal on Control	accepted		
Bauer, P ; Anastasopoulos, L ; Sendner, F-M ; Hornung, M ; Vanek, B	SZTAKI, TUM,	Identification and Modeling of the Airbrake of an Experimental Unmanned Aircraft	JOURNAL OF INTELLIGENT & ROBOTIC SYSTEMS			
Réka Dóra Mocsányi, Béla Takarics, Aditya	SZTAKI	Grid-Based and Polytopic Linear	Fluids	accepted		

Kotikalpudi, Bálint Vanek		Parameter-Varying Modeling of Aeroelastic Aircraft with Parametric Control Surface Design				
Réka Dóra Mocsányi, Béla Takarics, Bálint Vanek	SZTAKI	Grid and Polytopic LPV Modeling of Aeroelastic Aircraft for Co-design	IFAC PapersOnline	accepted		
Réka Dóra Mocsányi, Béla Takarics, Bálint Vanek	SZTAKI	Control-oriented Aircraft Modelling and Analysis Framework for Educational Purposes	2021 IFAC Workshop on Aerospace Control Education	submitted		
Thiemo Kier	DLR	An Integral Flexible Aircraft Model for Optimal Control Surface Scheduling of Manoeuvre Load Alleviation and Wing Shape Control Functions	Category: Dynamics Specialists: Innovative Control Strategies for Next-Generation Gust and Maneuver Load Alleviation Systems AIAA SciTech 2022	submitted		
Matthias Wüstenhagen	DLR	Synthesis of a Multiple-Model Adaptive Gust Load Alleviation Controller for a Flexible Flutter Demonstrator	Category: Dynamics Specialists: Innovative Control Strategies for Next-Generation	submitted		

			Gust and Maneuver Load Alleviation Systems AIAA SciTech 2022			
Balint Patartics, Yagiz Kumtepe, Bela Takarics, Balint Vanek	SZTAKI	On the necessity of flexible modelling in fault detection and isolation for flexible aircraft	Modeling, Estimation and Control Conference (MECC) 2021 October 24-27. 2021 Austin, Texas, USA	submitted		
Tamás Baár, Tamás Luspay,	SZTAKI	Robust Minimum Gain Lemma	Conference on Decesion and Control (CDC) 2021. Submitted, not yet accepted	submitted		
Özge Süelözgen	DLR	A Novel Updating Algorithm for Linearized State-Space Models of an Unmanned Flexible Aircraft Using Flight Test Data (submitted draft paper)	SciTech 2022 (AIAA) San Diego, CA (USA)	3-7.01.2022		
Julius Bartasevicius, Mirko Hornung	TUM	Design and testing of an in-flight thrust measurement system for a pylon-mounted miniature jet engine	Category : Flight Testing	submitted		

Julius Bartasevicius, Sebastian J. Koeberle, Daniel Teubl, Christian Roessler, Mirko Hornung	TUM	Flight Testing of 65kg FLEXOP Subscale Demonstrator	ICAS	accepted		

8.2 Dissemination and communication activities

The consortium partners have engaged in limited amount of direct peer-to-peer type of dissemination and communication activities due to COVID.

Some highlights are the opening of the new TUM Campus, where numerous politicians and media have seen the FLiPASED demonstrator (Figure 8.1). Another occasion is an exhibit coupled with a Ministerial delegation visit in Budapest at the Budapest University of Technology and Economics, where three ministers from Hungary, and numerous other guests have seen the Hardware-in-the-loop platform of the demonstrator.

The consortium members are also active in social media, mostly Linkedin, where a number of posts have received more than 1000 views.

Opening of the new department building by (from left) Dean Prof. Mirko Hornung, Bavaria's Minister President Dr. Markus Söder and TUM President Prof. Thomas F. Hofmann

Image: TUM/Fabian Vogl

CAMPUS NEWS, PRESIDENT | 14.07.2021 READING TIME: 3 MIN

TUM opens new department building

Minister President Söder: "The largest aerospace faculty in Europe"

The Technical University of Munich (TUM) continues its robust growth, opening a new building for the Department of Aerospace and Geodesy in Ottobrunn on Monday. The building will be the future core of TUM activities at its Ottobrunn site southeast of Munich. The objective is to create Europe's most important university research and teaching center for aerospace and aviation, said university President Thomas F. Hofmann.

Figure 8.1 News about Opening of the new department building by (from left) Dean Prof. Mirko Hornung, Bavaria's Minister President Dr. Markus Söder and TUM President Prof. Thomas F. Hofmann

8.3 Intellectual property rights resulting from the project

The project developed no IPR uptil the Mid-Term Report.